

# Design of a High Speed Planing Hull with a Cambered Step and Surface Piercing Hydrofoils

by

Leon Alexander Faison

Bachelor of Science in Electrical Engineering,  
Christian Brothers University, 2007

Submitted to the Department of Mechanical Engineering  
in Partial Fulfillment of the Requirements for the Degrees of

Naval Engineer and Master of Science in Mechanical Engineering  
at the  
Massachusetts Institute of Technology  
June 2014

© 2014 Leon Alexander Faison. All rights reserved.

The author hereby grants to MIT permission to reproduce and to distribute publicly paper and  
electronic copies of this thesis document in whole or in part in any  
medium now known or hereafter created.

Signature of Author

Leon Alexander Faison

Department of Mechanical Engineering

May 9, 2014

Certified by

Chrysostomos Chrysostomidis, Director of MIT Sea Grant

Doherty Professor of Ocean Science and Engineering

Professor of Mechanical and Ocean Engineering

Thesis Supervisor

Certified by

Stefano Brizzolara, Assistant Director for Research at MIT Sea Grant

Research Scientist, Department of Mechanical Engineering

Thesis Advisor

Accepted by

David E. Hardt

Ralph E. and Eloise F. Cross Professor of Mechanical Engineering

Chairman, Departmental Committee on Graduate Students

Report Documentation Page		Form Approved OMB No. 0704-0188
Public reporting burden for the collection of information is estimated to average 1 hour per response, including the time for reviewing instructions, searching existing data sources, gathering and maintaining the data needed, and completing and reviewing the collection of information. Send comments regarding this burden estimate or any other aspect of this collection of information, including suggestions for reducing this burden, to Washington Headquarters Services, Directorate for Information Operations and Reports, 1215 Jefferson Davis Highway, Suite 1204, Arlington VA 22202-4302. Respondents should be aware that notwithstanding any other provision of law, no person shall be subject to a penalty for failing to comply with a collection of information if it does not display a currently valid OMB control number.		
1. REPORT DATE <b>09 MAY 2014</b>	2. REPORT TYPE	3. DATES COVERED
4. TITLE AND SUBTITLE <b>Design of a High Speed Planing Hull with a Cambered Step and Surface Piercing Hydrofoils</b>		5a. CONTRACT NUMBER
		5b. GRANT NUMBER
		5c. PROGRAM ELEMENT NUMBER
6. AUTHOR(S) <b>Leon Faison</b>		5d. PROJECT NUMBER
		5e. TASK NUMBER
		5f. WORK UNIT NUMBER
7. PERFORMING ORGANIZATION NAME(S) AND ADDRESS(ES) <b>Massachusetts Institute of Technology, 77 Massachusetts Avenue BLDG 11-120, Cambridge, MA, 02139</b>		8. PERFORMING ORGANIZATION REPORT NUMBER
9. SPONSORING/MONITORING AGENCY NAME(S) AND ADDRESS(ES)		10. SPONSOR/MONITOR'S ACRONYM(S)
		11. SPONSOR/MONITOR'S REPORT NUMBER(S)
12. DISTRIBUTION/AVAILABILITY STATEMENT <b>Approved for public release; distribution unlimited.</b>		
13. SUPPLEMENTARY NOTES		

## 14. ABSTRACT

Design of a high speed planing hull is analyzed by implementing a cambered step and stern, surface piercing hydrofoils, commonly known as a Dynaplane hull. This configuration combines the drag reduction benefits of a stepped hull with a fully ventilated afterbody by using a stern stabilizer. The largest obstacle with this design is maintaining trim control and stability at high speeds. There has been limited research on the Dynaplane design since Eugene Clement first conducted tow tank tests in the David Taylor Model Basin (DTMB) in the 1960s. Modern experimental methods such as computational fluid dynamics (CFD) allow the designer to run multiple simulations at once while testing a variety of parametric variables. The analysis will combine theoretical, empirical, and computational methods to determine the hydrodynamic characteristics of the design and develop a new Dynaplane configuration that allows for speeds in excess of 50 knots. The design approach begins with using a reference hull named Model 5631 from a small systematic series of resistance tests at the DTMB. This modeled hull is based on the U.S. Coast Guard 47 ft Motor Lifeboat which is a hard chine, deep V planing hull. Clement's Dynaplane design process was followed with exception of the stern stabilizer recommendation. Instead, a surface piercing super cavitating (SPSC) hydrofoil designed by Dr. Stefano Brizzolara was used. These designs further improve upon the powering requirements of a conventional planing hull by effectively increasing the lift to drag ratio. A commercially available CFD software program called Star-CCM+ is used for the computational portion. The computational model is first validated using results from the Model 5631 tow tank tests. Three series of CFD tests were then conducted on the new Dynaplane design; which include developing wake geometry predictions for a swept back stepped hull, and then varying the trim angle and longitudinal center of gravity. These tests were run at an  $F_n V = 5$  in a calm sea state. Results from the analysis demonstrate the benefits of a fully ventilated afterbody using the SPSC hydrofoils and predict the hydrodynamic behavior for the new design. Also, the results extend the range of application of Clement's Dynaplane design to hulls with 20 degree deadrise. This thesis gives naval architects design guidance for such a hullform and demonstrates the potential of CFD as a tool for analyzing these parametric variables.

## 15. SUBJECT TERMS

## 16. SECURITY CLASSIFICATION OF:

a. REPORT

**unclassified**

b. ABSTRACT

**unclassified**

c. THIS PAGE

**unclassified**17. LIMITATION OF  
ABSTRACT18. NUMBER  
OF PAGES**82**19a. NAME OF  
RESPONSIBLE PERSON

THIS PAGE IS INTENTIONALLY LEFT BLANK

# **Design of a High Speed Planing Hull with a Cambered Step and Surface Piercing Hydrofoils**

by

Leon Alexander Faison

Submitted to the Department of Mechanical Engineering  
on May 9, 2013 in Partial Fulfillment of the Requirements for the Degrees of  
Naval Engineer and Master of Science in Mechanical Engineering  
at the Massachusetts Institute of Technology

## **Abstract**

Design of a high speed planing hull is analyzed by implementing a cambered step and stern, surface piercing hydrofoils, commonly known as a Dynaplane hull. This configuration combines the drag reduction benefits of a stepped hull with a fully ventilated afterbody by using a stern stabilizer. The largest obstacle with this design is maintaining trim control and stability at high speeds. There has been limited research on the Dynaplane design since Eugene Clement first conducted tow tank tests in the David Taylor Model Basin (DTMB) in the 1960s. Modern experimental methods such as computational fluid dynamics (CFD) allow the designer to run multiple simulations at once while testing a variety of parametric variables. The analysis will combine theoretical, empirical, and computational methods to determine the hydrodynamic characteristics of the design and develop a new Dynaplane configuration that allows for speeds in excess of 50 knots. The design approach begins with using a reference hull named Model 5631 from a small systematic series of resistance tests at the DTMB. This modeled hull is based on the U.S. Coast Guard 47 ft Motor Lifeboat which is a hard chine, deep V planing hull. Clement's Dynaplane design process was followed with exception of the stern stabilizer recommendation. Instead, a surface piercing super cavitating (SPSC) hydrofoil designed by Dr. Stefano Brizzolara was used. These designs further improve upon the powering requirements of a conventional planing hull by effectively increasing the lift to drag ratio. A commercially available CFD software program called Star-CCM+ is used for the computational portion. The computational model is first validated using results from the Model 5631 tow tank tests. Three series of CFD tests were then conducted on the new Dynaplane design; which include developing wake geometry predictions for a swept back stepped hull, and then varying the trim angle and longitudinal center of gravity. These tests were run at an  $FnV=5$  in a calm sea state. Results from the analysis demonstrate the benefits of a fully ventilated afterbody using the SPSC hydrofoils and predict the hydrodynamic behavior for the new design. Also, the results extend the range of application of Clement's Dynaplane design to hulls with 20 degree deadrise. This thesis gives naval architects design guidance for such a hullform and demonstrates the potential of CFD as a tool for analyzing these parametric variables.

Thesis Supervisor: Chrysostomos Chrysostomidis

Title: Director, MIT Sea Grant; Doherty Professor of Ocean Science and Engineering

THIS PAGE IS INTENTIONALLY LEFT BLANK

## Acknowledgements

This thesis would not have been possible without the guidance and support of so many individuals and organizations who helped the author achieve its completion. The sincerest appreciation is expressed to the following:

- To my family and friends, for their love and support.
- To Dr. Stefano Brizzolara, for his enthusiasm, confidence, and guidance in the accomplishment of this research. Without his technical expertise, this thesis would not have been possible.
- To Dr. Chrysostomos Chrysostomidis, for giving me the opportunity to work with the bright minds within MIT's Sea Grant program.
- To the members of the Innovative Ship Design Lab, Luca Bonfiglio, Giuliano Vernengo, Zvi Sheingart, and Vasileios Georgiadis, who all provided contributing efforts and feedback on the research.
- To Dr. Donald L. Blount, for his practical experience, insight and technical knowledge on planing hulls.
- To CAPT Mark Thomas and CDR Jerod Ketcham, for setting the example of the U.S. Navy's Core Values and teaching the Naval Officers in the 2N Program about naval construction and engineering.
- Lastly, the author would like to thank the United States Navy for sponsoring his graduate studies at MIT.

## Table of Contents

Abstract	3
Acknowledgements	5
Table of Contents	6
List of Tables	7
List of Figures	8
Nomenclature	10
Chapter 1 – Introduction	11
1.1 Background	11
1.2 Planing Hull Dynamics	12
1.3 Motivation	16
1.4 Design Procedure	18
Chapter 2 – Numerical Model Validation	20
2.1 Hull Selection	20
2.2 Computational Engineering	21
2.3 CFD Validation	24
2.4 Performance Enhancements	29
Chapter 3 – The Dynaplane Configuration	31
3.1 Clement’s Dynaplane	31
3.2 Cambered Step Design	32
3.3 Afterbody and Stern Stabilizer Design	40
3.4 Wake Profile Comparison from Empirical and Computational Methods	46
3.5 Final Design	55
Chapter 4 – Hydrodynamic Analysis	56
4.1 Stability Concerns	56
4.2 Previous Methods for Predicting Dynamic Stability	57
4.3 Model 5631 Dynaplane Pitch and Heave Moment Considerations	60
4.4 Model 5631 Dynaplane Longitudinal Center of Gravity Analysis	68
4.5 Final Results Comparison to Reference Hull	72
Chapter 5 – Conclusions	73
5.1 Summary	73
5.2 Future Work	73
Appendix A: Spray Formation for Model 5631 Dynaplane	75
Appendix B: Empirical Resistance MATLAB Code	76
Bibliography	80



## List of Tables

Table 1: U.S. Coast Guard 47' MLB Model Variants .....	20
Table 2: Brizzolara and Federici's Drag Reduction Results .....	30
Table 3: Cambered Step Variant Generation .....	32
Table 4: Chosen Design Parameters for Dynaplane Configuration .....	32
Table 5: Application Limits for Savitsky and Morabito's Empirical Method .....	47
Table 6: Primary Characteristics for the Model 5631 Dynaplane Design .....	55
Table 7: Moment Contributions of Model 5631 Dynaplane .....	65
Table 8: Final Comparison of Reference Hull and new Dynaplane design .....	72

## List of Figures

Figure 1: Hullform Categories for Seagoing Vessels .....	12
Figure 2: Pressure Distribution on Flat Planing Surface .....	13
Figure 3: World War I British 55' Coastal Motor Boat .....	13
Figure 4: $R_T/W$ Comparison for Changing Deadrise and Stepped Hulls .....	14
Figure 5: Transport Efficiency, $E_T$ , for High Speed Vessels .....	15
Figure 6: Drag to Lift Ratios for Varying Deadrise on a Prismatic Planing Surface .....	18
Figure 7: Model 5631 Profile and Body Plan Views and Geometric Parameters .....	20
Figure 8: Illustration of Two-Phases Using VOF Model, a) Unsuitable Grid b) Suitable Grid ...	22
Figure 9: Mesh Density and VOF Discretization for CFD Model Domain.....	22
Figure 10: Prism Layer Mesh Illustration along Planing Surface.....	23
Figure 11: Virtual Tow Tank with Half Hull Arrangement.....	24
Figure 12: Resistance Validation Results for 375 lb Model 5631 .....	25
Figure 13: Trim Validation Results for 375 lb Model 5631 .....	25
Figure 14: Heave (Vertical Translation) Validation Results for 375 lb Model 5631 .....	26
Figure 15: Wetted Area Validation Results for 375 lb Model 5631 .....	26
Figure 16: Resistance Validation Results for 483 lb Model 5631 .....	27
Figure 17: Trim Validation Results for 483 lb Model 5631 .....	27
Figure 18: Heave (Vertical Translation) Validation Results for 483 lb Model 5631 .....	28
Figure 19: Pressure Coefficient and Volume Fraction of Water on 375lb Model 5631 .....	28
Figure 20: Reduced Wetted Surface Area Due to Spray Rails/Deflectors .....	29
Figure 21: High Speed (50 kts) Patrol Craft with 20 degree Deadrise .....	29
Figure 22: Wetted Area and Pressure Distribution Comparison for Stepless and Stepped Hulls	30
Figure 23: Comparison of Calculated and Experimental Results of $L/D$ for Johnson 3-Term Cambered Surface and a Flat Plate, $AR = 2.0$ .....	33
Figure 24: Swept Back Angles for Cambered Planing Surface, Plan View .....	34
Figure 25: Correction Value for Swept Back Angle to Lift and $L/D$ Ratio.....	35
Figure 26: $L/D$ Ratio Versus $C_{Lb0}$ Results for a Johnson 3-Term Profile, $AR = 2$ .....	36
Figure 27: $C_{L,d}$ Versus Aspect Ratio for a Johnson 3-Term Profile, $\tau=2.5$ deg .....	37
Figure 28: Center of Pressure Location Versus $C_{Lb0}$ for a Johnson 3-Term Profile, $\tau=2.5$ deg ..	37
Figure 29: Length Dimensions on Cambered Step .....	38
Figure 30: Camber Profile with Johnson 3-Term Equation, $Cl,d=0.236$ .....	39
Figure 31: Plan, Profile and Body Plan Views of Preliminary Cambered Step on Model 5631 ..	39
Figure 32: Dimensionless Resistance Versus Speed Curve for Dynaplane Configured Boat .....	40
Figure 33: Surface Piercing V Hydrofoil with a 30 degree Dihedral .....	41
Figure 34: 2D Profile Examples of Super Cavitating and Sub-Cavitating Hydrofoils .....	41
Figure 35: 2D Profiles of Super Cavitating Hydrofoils at Sub-Cavitating Speeds .....	42
Figure 36: 2D Profiles of Super Cavitating Hydrofoils at Cavitating Speeds .....	43
Figure 37: Ventilation Formation from CFD Simulation .....	44
Figure 38: Ventilation Formation from Cavitation Tunnel Tests .....	45
Figure 39: Design Draft for Tested Submerged Lengths of Brizzolara's Hydrofoil.....	45
Figure 40: Stepped Hull Afterbody Orientation with a Stern, Submerged Hydrofoil .....	46
Figure 41: Wetted Area for Parameter Calculation .....	47
Figure 42: Reference Longitudinal Axis for Wake Profile.....	47
Figure 43: Wake Profile Depictions, No Camber (top) vs Camber (bottom) .....	48

Figure 44: Flow Direction for Camber and No Camber .....	49
Figure 45: Wake Profile Comparison of Transverse Step vs Swept Back Step at Centerline, 3.5 deg Trim.....	49
Figure 46: Wake Profile Comparison of Transverse Step vs Swept Back Step at 1/4 Buttock, 3.5 deg Trim.....	50
Figure 47: Wake Profile for Swept Back Step (No Camber) at 3.5 deg Trim.....	50
Figure 48: Wake Profile for Cambered Step at 3.5 deg Trim.....	51
Figure 49: Wake Profile Comparison of Steps with Camber and No Camber at 3.5 deg Trim ...	52
Figure 50: Perspective View of Wake Profile from Cambered Step at 3.5 deg Trim .....	53
Figure 51: Bottom View of Wake Profile from Cambered Step at 3.5 deg Trim.....	53
Figure 52: Rendering of SPSC Hydrofoil Used.....	54
Figure 53: Vertical and Transverse Positioning of SPSC Hydrofoil's Design Draft .....	54
Figure 54: Plan, Profile, and Body Plan Views of Model 5631 Dynaplane Design.....	55
Figure 55: Planing Hull Dynamic Instabilities .....	56
Figure 56: Dynamic Instabilities for Model 5631 Dynaplane Configuration.....	57
Figure 57: Dynamic Transverse Instability (DTI) Regions .....	58
Figure 58: Trim versus Speed Curve for Predicting Bow Drop .....	59
Figure 59: Free Body Diagram of Model 5631 Dynaplane .....	60
Figure 60: Drag Force Component of Model 5631 Dynaplane, Run 1 .....	61
Figure 61: Heave (Z Translation) Monitor for Model 5631 Dynaplane, Run 1 .....	62
Figure 62: Pressure Coefficient and Volume Fraction of Water @ 3.5 deg Trim and $F_n V=5$ .....	62
Figure 63: Drag Force Component of Model 5631 Dynaplane, Run 2 .....	63
Figure 64: Heave (Z Translation) Monitor for Model 5631 Dynaplane, Run 2 .....	63
Figure 65: Drag Force Component of Model 5631 Dynaplane, Run 3 .....	64
Figure 66: Heave (Z Translation) Monitor for Model 5631 Dynaplane, Run 3 .....	64
Figure 67: Total Pitching Moment for CFD Runs 1-5.....	66
Figure 68: Depiction of the Four Sections Analyzed.....	67
Figure 69: All Contributing Forces to Pitching Moment for Model 5631 Dynaplane .....	67
Figure 70: Longitudinal Stability Margin, h, versus Trim Angle .....	68
Figure 71: Trim Monitor for Model 5631 Dynaplane, Run 6.....	69
Figure 72: Heave (Z Translation) Monitor for Model 5631 Dynaplane, Run 6 .....	69
Figure 73: Trim Monitor for Model 5631 Dynaplane, Run 11.....	70
Figure 74: Heave (Z Translation) Monitor for Model 5631 Dynaplane, Run 11 .....	71
Figure 75: Surface Contour Aft of the Cambered Step where SPSC Hydrofoils Enter Water.....	71

## Nomenclature

$\alpha$	Angle of attack
AR	Aspect ratio, $b^2/S$
$A_p$	Projected chine area
$B_{PX}$	Maximum beam over chines
$b$	Breadth of planing surface
$B_f$	Beam between hydrofoils
$\beta$	Deadrise angle
BOA	Beam overall
$C_D$	Drag coefficient, $D/(0.5\rho v^2 S)$
$C_L$	Lift coefficient
$C_{Lb0}$	Lift coefficient of flat plate
$C_{Lb\beta}$	Lift coefficient of hull with a given deadrise angle
$C_{L,d}$	Lift coefficient for a 2D cambered planing surface
$C_V$	Speed coefficient with respect to hull's beam, $v/\sqrt{gb}$
$c$	chord length of cambered curve
$\Delta$	Displacement of vessel
$D$	Drag Force
$Fn_L$	Froude number using length at waterline, $v/\sqrt{gLWL}$
$Fn_V$	Froude number using underwater volume, $v/\sqrt{g\nabla^{1/3}}$
$g$	acceleration due to gravity
$\gamma$	Angle between the spray root line and centerline
$L_c$	Length of wetted chine
$l_{cp}$	Distance from transom to center of pressure
$L_k$	Length of wetted keel
$L_p$	Length of project chine area
$l_r$	Length of cambered surface at the root or keel
$l_t$	Length of cambered surface at the tip
$l_m$	Mean wetted length of planing surface or Mean Hydrodynamic Chord (MHC)
LCG	Longitudinal distance from transom of the center of gravity
LOA	Length overall
LWL	Length along the waterline
$\phi$	Swept back angle between 50% chord line and a transverse line
Re	Reynolds number, $vL/\nu$
$R_T$	Total resistance
$\rho$	Density of fluid
$S$	Wetted area of cambered planing surface
$\theta$	Swept back angle between the trailing edge, or step, and a transverse line
$\tau$	Trim angle of planing hull
$v$	Velocity of fluid flow
$\nu$	Kinematic viscosity of fluid
$\nabla$	Underwater volume of planing hull
$W$	Weight of planing hull

## Chapter 1 – Introduction

### 1.1 Background

The desire for maximizing speed in a maritime vessel has been around since the advent of naval architecture. It was the thought in the mid-1800s that a vessel's hull speed could not be surpassed. Early naval architects considered a vessel's hull speed as the speed at which the wavelength of the wave generated by the bow is equal to the ship's length. Pioneers such as John I. Thornycroft, Charles D. Mosher, and Nathanael G. Herreshoff proved that a vessel could exceed its hull speed with efficient hull design and modern engine technology at the time. A commission in the 1860s was formed by the Institution of Naval Architects in England to identify the most efficient hull shape. Model tests conducted by William Froude provided a convention for predicting the behavior of full scale ships based on scaled models. This new dimensionless parameter or Froude number is the vessel's speed,  $v$ , divided by the square root of the gravity constant multiplied by the ship's length,  $L$ .

$$\text{Fn}L = \frac{v}{\sqrt{gL}}$$

There was now a testing parameter to be used for practical experimentation to determine efficient hull designs which could achieve high speeds. Most of the earlier examples of exceeding hull speed used round bilge hulls. Hard chine or flat bottom bottoms didn't begin to surface until the beginning of the 20<sup>th</sup> century with their first application being tested on seaplanes. During the 1930s and throughout World War II, many efforts were focused on planing technology. Institutions like the National Advisory Committee for Aeronautics (NACA) began extensive testing of this technology, first beginning with aircraft technology but later being incorporated in high speed marine vessels. The researchers of this period began to understand the effects of loading and powering for high performance planing vessels. These planing hulls depended largely on hydrodynamic forces as opposed to hydrostatic forces associated with displacement vessels. Researchers began to determine the need for the development of a more appropriate speed coefficient to study and compare these planing hulls. Two examples are shown in the equations below, the volumetric Froude number,  $\text{Fn}V$ , and a speed coefficient with respect to the hull's beam,  $C_v$ . Using dimensionless parameters based on a vessel's weight or beam was useful in predicting planing hull performance for a range of hull sizes and especially in model tests which predicted early hydrodynamic characteristics of planing hulls.

$$\text{Fn}V = \frac{v}{\sqrt{g\nabla^{\frac{1}{3}}}} ; C_v = \frac{v}{\sqrt{gB}}$$

Progression of propulsion and hull design technology saw a direct correlation with achieving high Froude numbers. In 1963, Daniel Savitsky completed and published a widely accepted paper called "Hydrodynamic Design of Planing Craft." His paper conducted an empirical approach for predicting the performance on a variety of simple prismatic planing hulls. The success and acceptance of his research sparked a sudden surge of model test data at the U.S. Navy's David Taylor Model Basin, DTMB, located in West Bethesda, MD. Planing hull technology owes much of its beginnings to those early researchers, Savitsky, Clement, Blount

and many others at the DTMB. The focus on improving powering in planing craft consisted of full scale hulls as well as experimental models. Performance of planing hulls not only included maximizing speed but it also focused on stability at speed. Empirical equations were developed based on those early series of model tests which are able to solve hull resistance and trim at a given speed, as well as vertical accelerations and stability in a given seaway.

## 1.2 Planing Hull Dynamics

With the accomplishment of exceeding hull speed, research then focused on understanding the dynamics of planing hulls and optimizing the geometry to develop an efficient design. A great illustration of the types of seagoing vessels associated with certain speeds ranges is shown in Figure 1. Once you move into the planing regime, hydrodynamic forces play an important role in the performance of the hull. In this chapter, we will analyze the dynamics specifically for planing hulls.

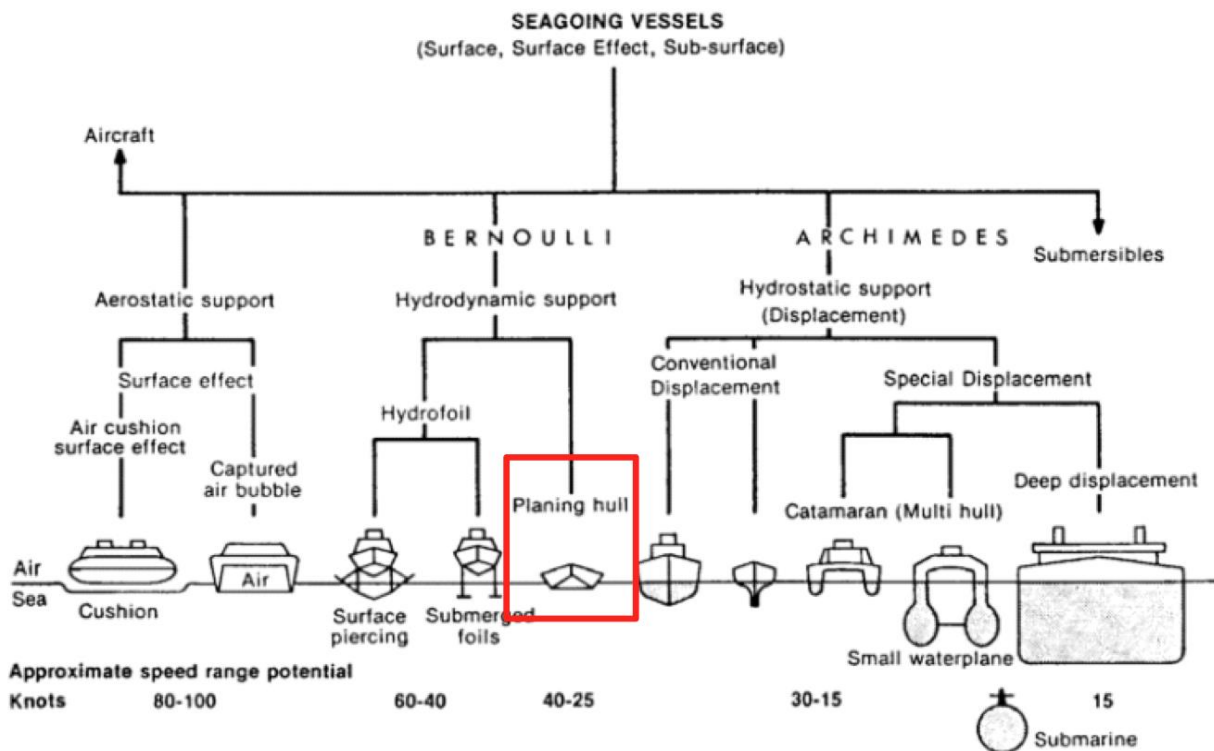
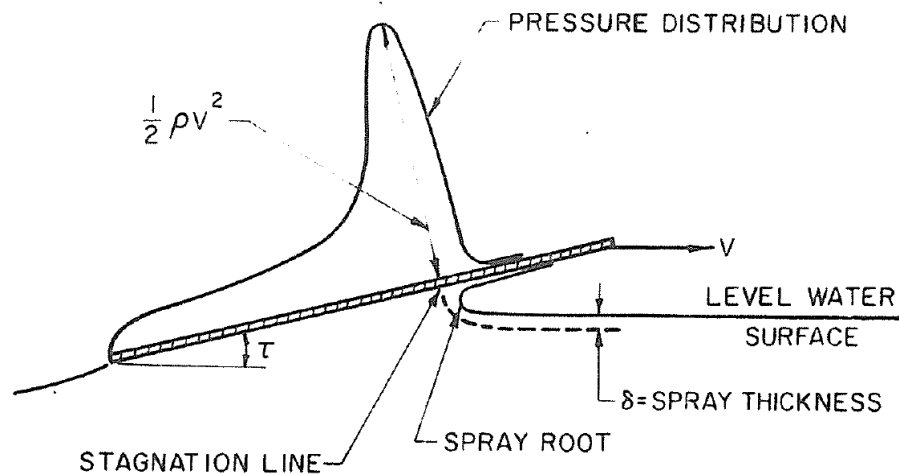


Figure 1: Hullform Categories for Seagoing Vessels

To better understand the dynamic forces of planing hulls, early researchers such as Savitsky, conducted series of tests with a flat plate, which is equivalent to a zero degree deadrise hull. From these tests, one was able to determine the fluid flow across such a hull and the dominant forces being applied. In Figure 2, the largest forces applied to the wetted area of that flat plate, or planing surface, are at the stagnation line. The stagnation line is where the local velocity of the flow field is essentially zero, and can also be described as where the flow separates into the water spray and the fluid flow moving aft along the hullform. This concentration of pressure provides majority of the hydrodynamic lift needed to enter the planing regime, but also contributes to majority of the drag. In this example, a flat plate is traveling through water, but from Figure 2 the

trim angle determines the magnitude of this pressure concentration. The idea behind the Dynaplane configuration is to take advantage of this concentration of pressure and design a lifting surface which possesses a high lift to drag ratio. This type of lifting surface can be likened to an aircraft wing, which is cambered; but first, the evolution of improving powering requirements starting from the flat plate will be discussed.



**Figure 2: Pressure Distribution on Flat Planing Surface**

The early seagoing vessels that exceeded their hull speeds were round bilge hulls. Compared to large displacement vessels, high speed round bilge hulls take advantage of a streamline design; but the hullform is still limited by the frictional resistance of the wetted area. Early solutions to this problem involved creating a stepped hull, as shown in Figure 3. The Thornycroft Company developed and built these boats for the British Royal Navy. The stepped hull takes advantage of reducing the wetted area, thus decreasing the resistance or drag on the hull.

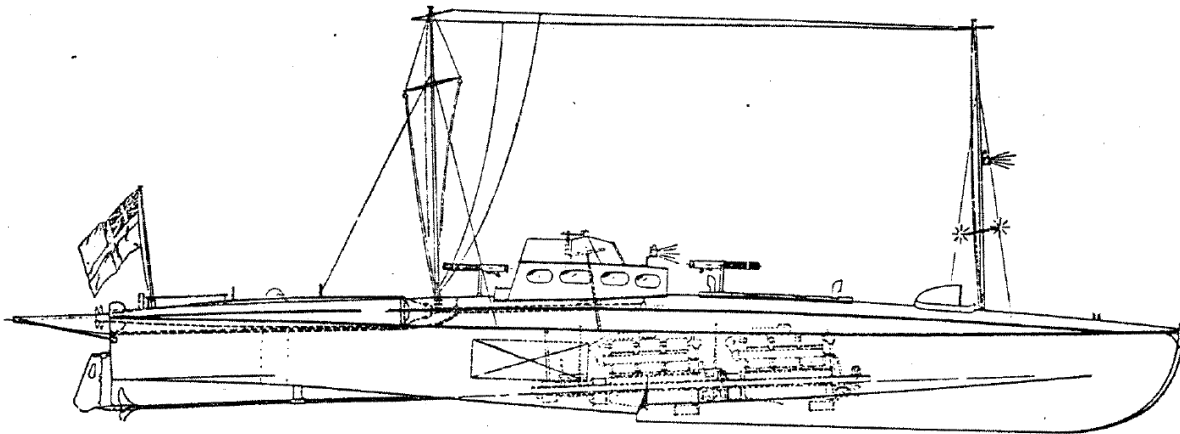


**Figure 3: World War I British 55' Coastal Motor Boat**

Further testing began to discover the reduction of wetted area can be achieved by diverting the water spray away from the hull. From this conclusion, the hard chine planing hull began numerous testing at the DTMB (Savitsky, 1964; Clement and Blount, 1963). These tests changed several hull parameters such as  $A_p$ ,  $L_p$ ,  $B_{pX}$ , and  $L_p/B_{pX}$ . One of the goals to the model series of



tests was to determine the effects of changing the wetted area and how to design the hull's geometry to ensure a minimum frictional resistance.

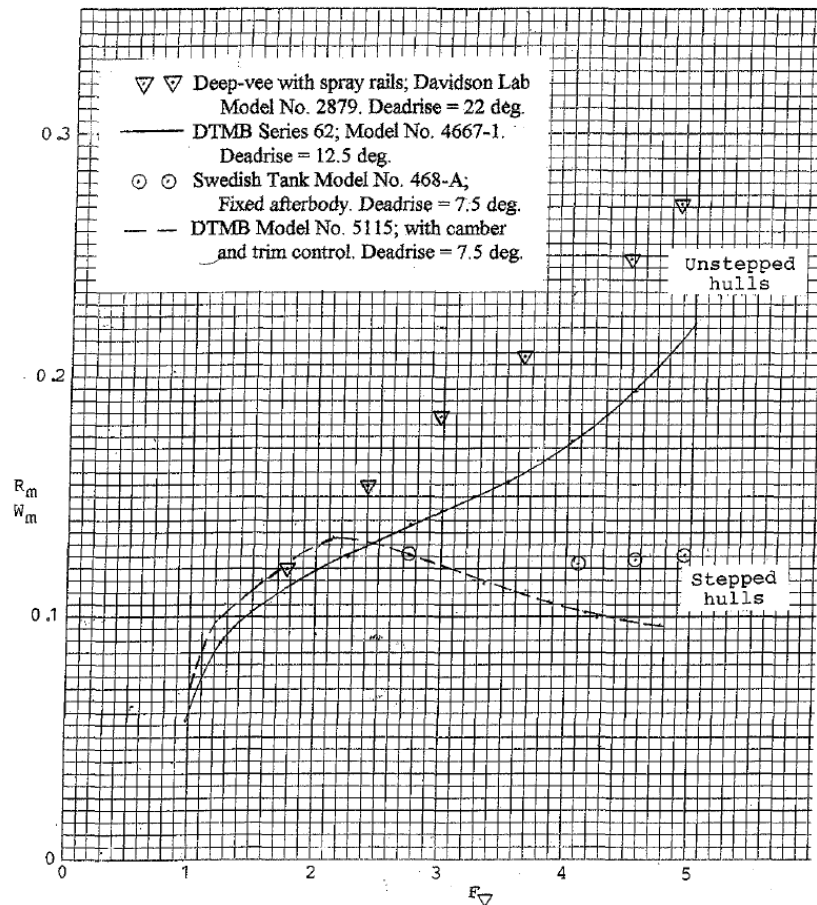


Figure 4:  $R_T/W$  Comparison for Changing Deadrise and Stepped Hulls

With the introduction of proven model test results and certain design features which improve the overall performance of planing hulls, further testing was demanded to expand the range of parameters as applications of planing hulls grew. For example, high speed vessels were needed in offshore operations, primarily for military purposes at first. A majority of the sponsorship of these series of model tests were funded by government organizations to be intended for military use. When encountering a given sea state while operating offshore or in a coastal region, hulls with a higher deadrise angle perform better, with improved ride quality as the impact of wave is reduced. However, there is a disadvantage with having a deep V hull; a higher deadrise angle causes more wetted area. Therefore, the problem of increased wetted area has returned. The concept of stepped hulls was applied to deep V hulls as well. In Figure 4, Clement compared hullforms with steps and without steps, in addition to three deadrise angles: 7.5, 12.5 and 22 degrees. The results from the figure below were conducted at DTMB, the Davidson Lab's tow tank, and a tow tank in Sweden. First, their results show a clear divergence between stepped hulls and unstepped hulls. Next, the added resistance by increasing the deadrise angle is also shown. It can be concluded from this figure that stepped hulls have approximately 50% reduction in total resistance. Also, a step with camber and aft lifting surface provides even further drag



reduction at high speeds. Stepped hulls start to show benefits at  $F_nV > 3$ ; however, more recent analysis shows that stepped hulls become more advantageous at  $F_nV > 5$ , shown in Figure 5. There will always be room for improvement in the performance of planing hulls especially when they're pushed to the maximum safe operating envelope.

As shown in Figure 1, high speed vessels are divided into more categories than just planing hulls. In order to better compare the performance characteristics of high speed vessels such as planing monohulls, surface effect ships, or catamarans, a parameter called a vessel's transport efficiency is introduced. This allows the designer to give a non-dimensional value to the vessels ability to efficiently carry fuel, cargo, and payload. The transport efficiency is a ratio of the overall propulsive efficiency,  $\eta$ , divided by the dimensionless bare hull resistance to weight ratio. Higher transport efficiency is desired and in Figure 5, various types of hullforms are analyzed.

$$E_T = \frac{\eta}{\left(\frac{R_T}{W}\right)_{BH}}$$

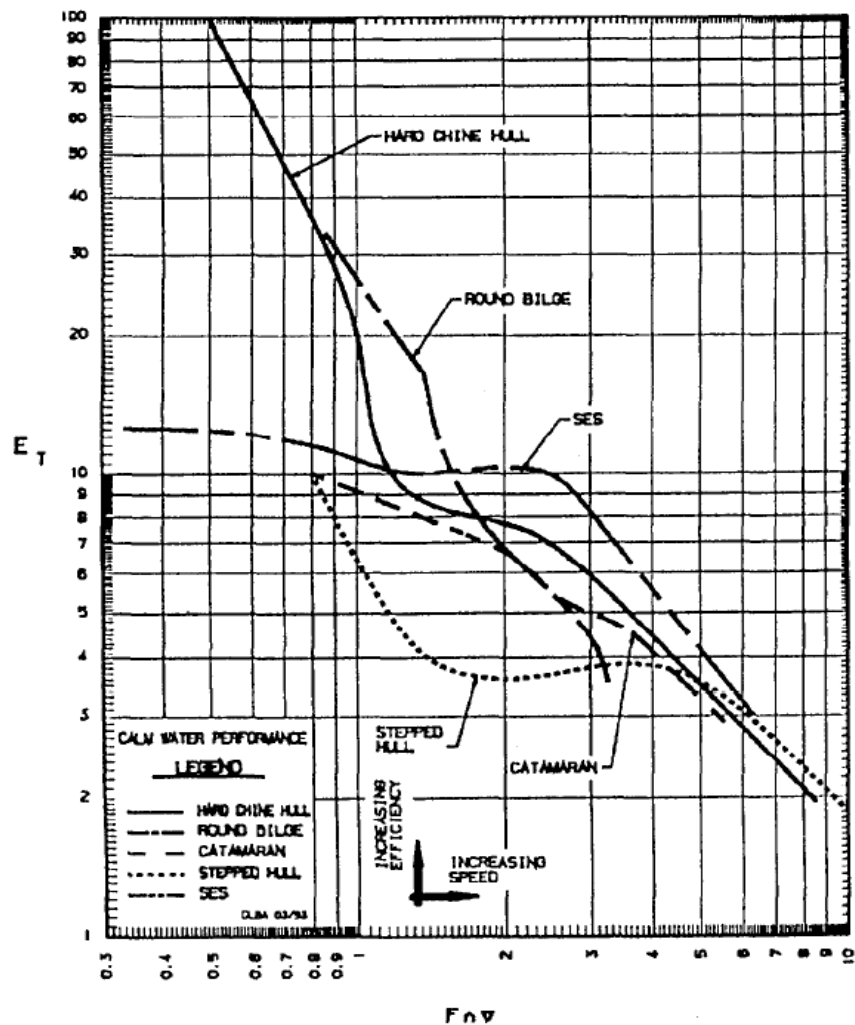


Figure 5: Transport Efficiency,  $E_T$ , for High Speed Vessels

It can be shown below that stepped hulls begin to perform better than other hullforms, such as hard chine hulls, SES and catamarans, at  $F_nV$  values greater than 5. For this reason, the incorporation of a stepped hull into Model 5631 powering improvements was necessary. The speed coefficient the hull was designed towards was  $F_nV = 5$ . For the purpose of this thesis and later studies, defining design requirements early allows for an overall efficient testing and evaluation procedure.

### 1.3 Motivation

The motivation for this thesis originates from reading published papers on planing hull technology and meeting the goals of MIT's iShip Lab, directed by Dr. Stefano Brizzolara. This thesis begins with a new design of a Dynaplane configured planing hull, and then explores the potential improvements for very high speed planing hulls, utilizing a fully ventilated afterbody, surface piercing hydrofoils, and a swept back stepped hull with a cambered planing surface. Savitsky expressed the importance of using model test data for the design of planing hulls utilizing the benefits of hydrofoils (Savitsky, 1964). Later this thesis uses a computational model to determine the advantages of these innovative design features.

Computational fluid dynamics (CFD) in numerical models gives the designer a wider range of possibilities than physical model testing. It is of particular importance to the author to understand and demonstrate the capabilities of CFD models and its potential in studying planing hull and hydrofoil technology. Many of the earlier model testing data, Series 62 and Series 64, are still used by designers today; and the methods used for predicting performance rely on empirical equations which have a limited range of applicability. This thesis attempts to show the clear advantages of CFD and the accuracy it can achieve in predicting key performance parameters for planing hulls. CFD allows the naval architect to test his design in potentially longer simulations that capture more data, all at a relatively low cost.

The cost of construction and risks involved with full scale tests has inhibited most of the advancement in technology of planing hulls. This leads to the majority of newly derived empirical and analytical methods being based on physical model testing in tow tanks. With the demand for more modern technology and improvement in the planing hull industry, the cost of construction of model and tow tank availability has also led to a downshift in improving technology. Savitsky and Morabito said, "[We] encourage the development of CFD since such a tool may be useful in extending the range of parametric variables at modest cost" (Savitsky and Morabito, 2009). It is not to say that physical model testing will be obsolete but the reliance and dependability of CFD models is demonstrated to be much more powerful in its capability. Computational modelling allows for real time simulation adjustments. Results can be produced for a wider range of parametric variables in less time because you can make adjustments to the model geometry and run those changes in a short period of time; whereas, a physical model requires a new model constructed for each iteration. CFD allows for more complex geometry and the possibility for longer simulations. A computational model doesn't come without any disadvantages. It is computationally expensive, meaning it requires several cores of processors to calculate each time step. Also, it requires basic knowledge of numerics and a level of expertise to operate the software and code. However, newer CFD tools, such as Star-CCM+, give the user a

graphical interface which is intuitive and allows for functionality similar to typical computer aided design (CAD) programs.

Besides the clear advantages and disadvantages for using a computational model for solving planing hull dynamics, the planing hull industry requires the level of accuracy and fidelity of each model to be sufficient. For this reason, this thesis validates the computational model used in the design and compares it with empirical prediction methods used widely throughout current research (Brizzolara and Serra, 2007). In their research, a RANSE solver was used to test a prismatic planing hull. Their results were then validated using experimental data and empirical methods. The numerical measurements were within 10% of experimental and empirical results. Later refinements of the numerical model implemented on systematic planing hull series (Brizzolara et al, 2009) and on real planing crafts with various types of appendages lead to an increase of the accuracy to the order of 3% on drag (Brizzolara and Villa, 2010). The accuracy and fidelity of their results prove that computational models can predict the proper physics of these types of fluid problems.

A goal of this thesis is to continue the discussion of using computational models for planing hull performance predictions. With results on a 20 degree deadrise hull validated in Brizzolara and Serra's analysis, the validation of further model tests is encouraged. In Chapter 3, the Star-CCM+ computational model will be validated using the experimental results from the small systematic series of model tests. These simulations also allow the designer to test changes in specific parameters to the hull, for example trim, LCG, and hull geometry. Additional motivation is encouraging the continued use of CFD modelling, so that it can be used to accurately predict performance of planing hulls with low levels of speculation or uncertainty.

At high speeds, planing hulls experience hydrodynamic lift along with the associated drag component. Proper balance between lift and drag must be achieved to establish an effective design. Lift to drag ratios in marine vessels, such as planing hulls, are quite different than their aircraft counterparts. A higher specific gravity in the medium causes increased drag with a nonlinear lift relationship. Also, variations in the hull's deadrise largely affect the lift that can be produced. Early model tests produced empirical equations for prismatic planing surfaces but modern, high speed planing hulls largely differ from the typical prismatic hull or flat plate used in those earlier model tests (Clement, 1966). In Clement's research, lift to drag ratios greater than 10 were desired for stepped hulls. However, certain hull parameters at speed such as trim and deadrise play an important role in achieving high lift to drag ratios. In Savitsky's "Hydrodynamic Design of Planing Hulls," the drag to lift ratios of planing hulls with variations in deadrise, trim and beam are analyzed. The results from this analysis are shown in Figure 6 below but in an inverse form, drag to lift.

A design goal of this thesis is to concentrate improving powering requirements from a more novel approach. Traditionally, planing hull design focused on optimizing the running trim to achieve the minimum amount of drag with maintaining a proper lift force. In Figure 6, for a flat plate to achieve the smallest drag to lift ratio, it must travel at a running trim of approximately 4 degrees. The novel approach presented in this thesis is to achieve reduced drag by increasing lift and reducing the wetted area as opposed to finding that optimum running trim angle.

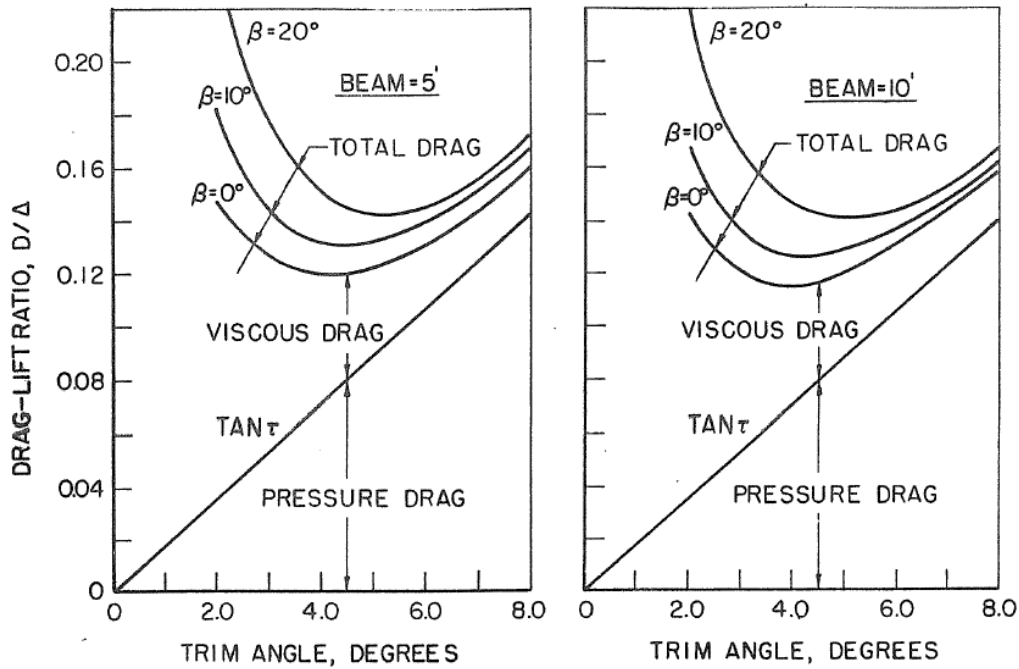


Figure 6: Drag to Lift Ratios for Varying Deadrise on a Prismatic Planing Surface

The inception of stepped hulls took advantage of this reduced wetted area and found that the pressure on the afterbody of planing hulls only accounted for less than 10% of total pressure on the planing surface. In Figure 2, it can be seen that the majority of this pressure on the planing surface is towards the front end at the stagnation line. The new Dynaplane design presented in this thesis takes advantage of the reduced wetted area from a step but incorporates a cambered surface to provide additional lift at a designed trim angle. Therefore, the benefits of this novel approach allow the designer to specify a running trim angle and then design a cambered lifting surface to provide the lift necessary to achieve high lift to drag ratios.

#### 1.4 Design Procedure

Testing a new design begins with the selection of a reference hull, then continuing with validation of model before the hydrodynamic analysis can start. Model 5631 was selected as the reference hull, which has a 20 degree deadrise, remaining constant throughout much of the wetted area. The newly developed numerical model requires validation in order to assure accuracy and fidelity of the hydrodynamic results. The model test data from a previous study was used to validate the model (Metcalf et al, 2005). In this analysis, attempts were made to take advantage of the Dynaplane configuration and improve upon the parent hull's performance. This conversion uses Clement's method described in detail in his paper, "A Configuration for a Stepped Planing Boat Having Minimum Drag (Dynaplane Boat)." As compared to a prismatic planing surface in Figure 6, the Dynaplane configured Model 5631 should be able to reduce drag by 20%. Once the Dynaplane design was completed, the hull was then run in the computational model at three trim angles, 3.5, 4.0, and 4.5 degrees, with the hull being allowed to freely heave. This resulted in the hull reaching a stable heave condition.

Further testing included three main groups of tests:

1. Five tests with different LCG locations at a given stable trim angle.  
[40%, 42%, 43%, 44%, and 46%]
2. Two different trim angle tests with fixing the heave position found at the designed trim of 3.5 degrees. [4.0 and 4.5 degrees]
3. Six tests with fixed trim and heave to determine the wake geometry of a swept back step and a cambered step.

All these tests provided experimental information in determining the hydrodynamic behavior of the Model 5631 Dynaplane configuration.

There are three overarching goals to this research. First, to explore the powering improvements of a planing hull through innovative design features, including a cambered step and stern, surface piercing hydrofoils. The design has several advantages over traditional planing hull designs, including the increase of the lift to drag ratio produced by the cambered lifting surface and the fully ventilated afterbody section by use of two stern hydrofoils. Second, the development of computational modeling, specifically CFD, in the study and design of high speed planing hulls. Savitsky, Morabito, and Blount have all encouraged the use and development of computational modeling in planing hull research. There is limited planing hull design using CFD codes. With continued research, validation, and accuracy demonstration, CFD models will become the industry standard in the design and eventual construction of these high speed vessels. Third, to provide a novel approach in determining the drag reduction of planing hulls by increasing the lift coefficient of the planing surface and reducing the wetted area. It is the primary purpose of MIT's iShip Lab to innovate and provide novel solutions to the marine design community.

## Chapter 2 – Numerical Model Validation

### 2.1 Hull Selection

In MIT's iShip Lab, it is our mission to promote innovation in the design of ships. For this thesis, a hard chine deep V planing hull was to be chosen. This thesis provides innovative solutions to improving power requirements; for example, drag reduction through a fully ventilated step and a new Dynaplane configuration. The resistance tests of a small systematic series for the U.S. Coast Guard's 47' MLB was available. It was attractive because it was a modern set of tests, conducted in 2005, and the model used was a seagoing vessel with a hard chine and deep V hull features that met the design requirements. Table 1 lists the characteristics of model variant 5631 and Figure 7 illustrates the hull lines of the model.

	<b>Model 5628 (Parent Hull)</b>	<b>Model 5631</b>
<b>LBP</b>	10 ft [3.05 m]	10 ft [3.05 m]
<b>B</b>	3.08 ft [0.939 m]	2.24 ft [0.683 m]
<b>T</b>	0.608 ft [0.185 m]	0.510 ft [0.155 m]
<b>L/B</b>	3.24	4.47
<b>B/T</b>	5.08	4.39
<b>Deadrise [deg]</b>	16.61	20
<b>Displacement</b>	375 lb [170 kg]	375 lb [170 kg]
<b>A<sub>p</sub></b>	25.88 ft <sup>2</sup> [2.4 m <sup>2</sup> ]	18.76 ft <sup>2</sup> [1.74 m <sup>2</sup> ]
<b>LCG [42%]</b>	4.2 ft [1.28 m]	4.2 ft [1.28 m]
<b>A<sub>p</sub>/V<sup>2/3</sup></b>	7.83	7.83

**Table 1: U.S. Coast Guard 47' MLB Model Variants**

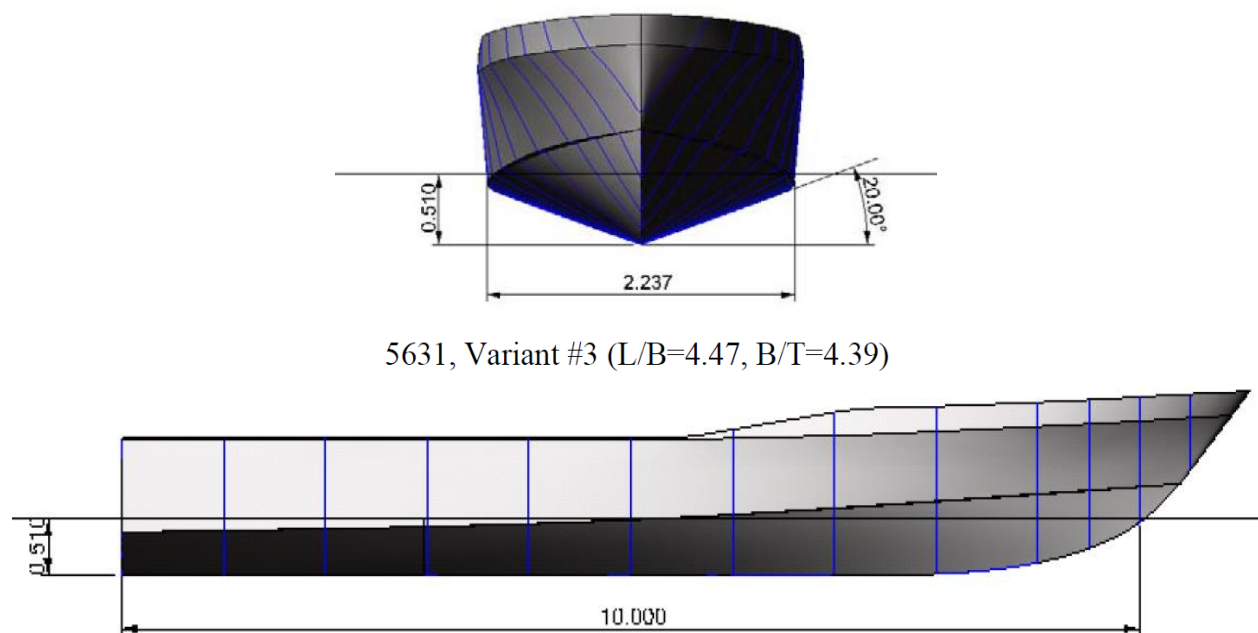


**Figure 7: Model 5631 Profile and Body Plan Views and Geometric Parameters**

## 2.2 Computational Engineering

The study of planing hulls has traditionally been an empirical science. This involves the testing of physical models, whether full scale or scaled versions. There are inherent inaccuracies when experimenting with physical models; for example, calibration of the test equipment and human error dealing with the measurements. These are just a few of the problems a researcher can face when model testing. Computational engineering entered the stage with a revolutionary way to solve complex fluid flow problems. The application of computational models, at first, found itself to be highly inaccurate because of unrealistic physics modelling. However within the past decade, robust solvers have been developed to allow the use of CFD to transition from a purely research tool to a design tool naval architects can use for final design (Brizzolara, 2012). CFD offers a relatively inexpensive and efficient method to produce results in less time than physical model testing. However, these models can be computationally expensive and require a level of knowledge of numerics that the designer may or may not possess.

CFD allows the naval architect to develop models and environments that match real world problems and systems. Since the early 1980s, numerical algorithms have been generated to solve the fluid flow problems in a complex nonlinear system. First, we must revisit the Navier-Stokes equations and explain the Reynolds' operators which are time-averaged solutions to solve the fluid flow problem in the Navier-Stokes equations based on the assumptions of turbulence (Newman, 1977). The decomposition of this equation developed by Osborne Reynolds approximates these time-averaged solutions for turbulent flows, known as the Reynolds-averaged Navier-Stokes equations (RANSE).

Navier Stokes equation, in Einstein notation:

$$\frac{\delta u_i}{\delta x_i} = 0$$

$$\frac{\delta u_i}{\delta t} + u_j \frac{\delta u_i}{\delta x_j} = f_i - \frac{1}{\rho} \frac{\delta p}{\delta x_i} + \nu \frac{\delta^2 u_i}{\delta x_j \delta x_j}$$

Reynolds operators incorporated into Navier Stokes equations, in Einstein notation:

$$\frac{\delta \bar{u}_i}{\delta x_i} = 0$$

$$\frac{\delta \bar{u}_i}{\delta t} + \bar{u}_j \frac{\delta \bar{u}_i}{\delta x_j} + \overline{u'_j \frac{\delta u'_i}{\delta x_j}} = \bar{f}_i - \frac{1}{\rho} \frac{\delta \bar{p}}{\delta x_i} + \nu \frac{\delta^2 \bar{u}_i}{\delta x_j \delta x_j}$$

Where

$$u(x, t) = \bar{u}(x) + u'(x, t)$$

Several RANSE solvers have been developed and are available for use in CFD code. Four commonly known numerical algorithms are PHOENICS, FLUENT, FLOW3D, and STAR-CD

(Versteeg and Malalasekera, 1995). All of these methods are based on a finite inertial reference frame. STAR-CCM+ implements these equations in its software to determine quantitatively the performance characteristics of the model. This program consists of several theoretical methodologies to calculate the fluid flow around a body, consisting of a RANSE VOF, or volume of fluid, multiphase model. This type of model allows for a domain to be established with space and time discretization. The advantage of CFD programs, such as STAR-CCM+, is that it allows the user to specify the domain, or inertial reference frame, for which the system will behave. Essentially, we are creating a virtual tow tank. As you can see in Figure 8, two grids are shown containing two phases. The grid on the left, a), is unsuitable because within each cell of the grid the two phases are not interacting appropriately; specifically they do not share the same velocity, pressure, and temperature fields. However, the grid on the right, b), appropriately illustrates the continuity between phases throughout each cell in the grid.

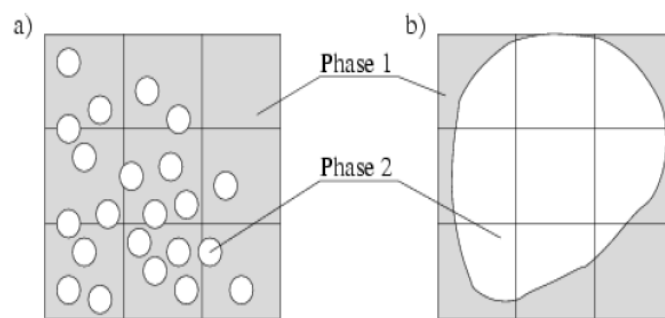


**Figure 8: Illustration of Two-Phases Using VOF Model, a) Unsuitable Grid b) Suitable Grid**

For our virtual tow tank, VOF becomes especially useful because it is ideal for small contact area between the two phases. Meaning, if we maintain a relatively smooth free surface throughout the virtual tow tank, then we can feel confident of the physics in the multiphase model. In Figure 9, the separation between two phases, water (red) and air (blue), is displayed. This spatial distribution between phases is calculated in the CFD software, which is known as the Volume Fraction value. Note the mesh density, which becomes important in capturing accurate fluid interaction between each cell as well as the free surface.

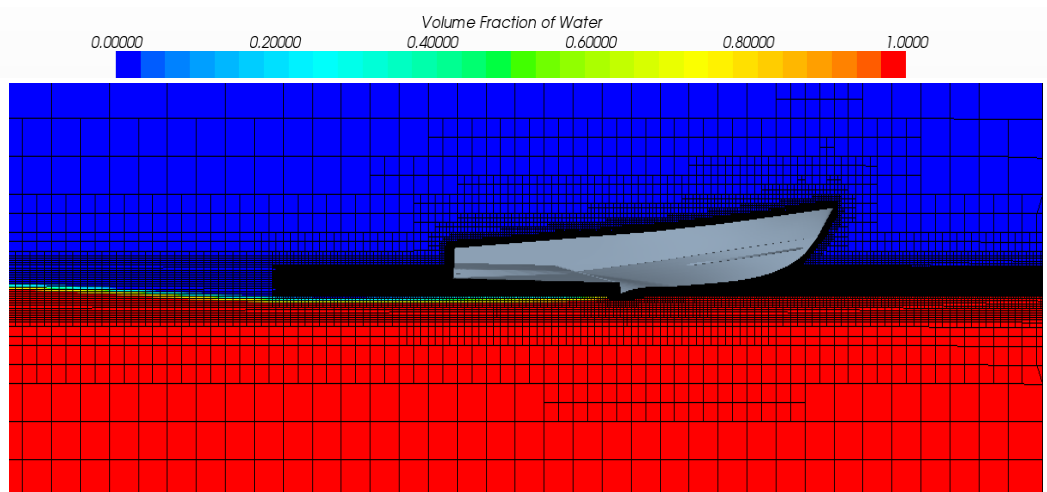


**Figure 9: Mesh Density and VOF Discretization for CFD Model Domain**



For testing models in virtual tow tanks, mesh density allows for proper velocity and pressure continuity, and the formation of the boundary layer. The space discretization is dictated by two factors, velocity of fluid flow and time. The velocity of fluid flow is defined by the designer or researcher depending on the experiment. The time is determined by the time it takes for the fluid, or material, to pass through each cell in the mesh. The software algorithms solve the RANS equations using an implicit unsteady approach. This requires an iterative process, in which the system is solved for each physical time-step. Within STAR-CCM+, the user is required to set the physical time-step. The accuracy of the time-step size is dependent on the velocity of the flow and cell size. The Courant number is a dimensionless parameter, shown by the equation below, which allows the researcher to understand the validity and accuracy of their mesh. Given a flow velocity,  $U$ ; time-step,  $\Delta t$ , and cell size,  $cs$ ; the Courant number can be calculated. The ratio must be less than or equal to 1 to ensure fidelity.

$$\text{Courant Number, } \frac{U \Delta t}{cs} \leq 1$$

STAR-CCM+ also allows for several parameters to be adjusted to refine the mesh. The model is placed in the inertial reference frame, whose size is determined to allow for fully developed physical fluid properties. The Dynamic Fluid Body Interaction feature is used in this model to allow the planing hull to freely move while interacting with the fluid around it. Mesh morphing also plays into this complex problem because as the model is free to move, the mesh must be allowed to change around the moving body. The morphing of each cell can become computationally expensive in the model if not properly adjusted and monitored. The boundary layer formation is accounted for by the Prism Layer Mesher, which is illustrated in Figure 10.

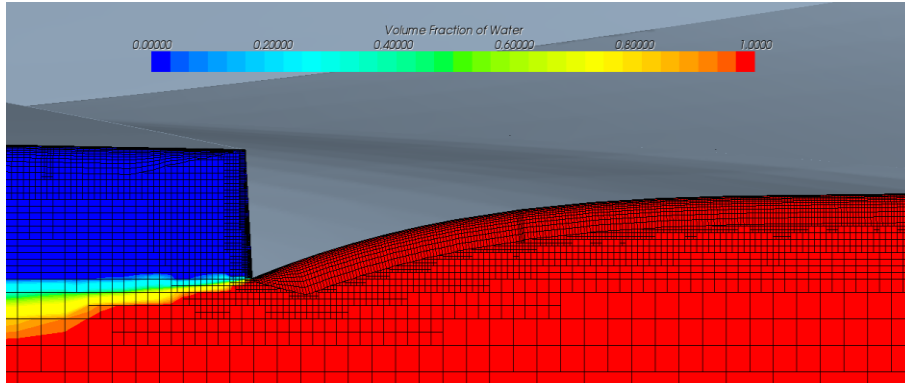


**Figure 10: Prism Layer Mesh Illustration along Planing Surface**

The overall domain is established by setting geometric constraints and then assigning those boundaries to become the flow inlet, pressure outlet, and symmetry planes. The flow inlet determines the direction from which the flow is acting and the velocity of that flow. The pressure outlet sees the oncoming flow and calculates the pressure fluctuations from the flow disturbances, whether that is a body or wall contribution. The symmetry planes allow for no reflective properties from the fluid flow. Next, the model is treated as a no-slip wall, from which physical properties can be monitored and later collected. After mesh generation and appropriate setting of initial conditions, the virtual tow tank can begin simulation. In the next section, the mesh resolution and domain created for this thesis are explained.

## 2.3 CFD Validation

The use of computational models when comparing them to reality requires a validation of existing experimental or theoretical results. For this thesis, the results from the U.S. Coast Guard model tests, specifically Model 5631, are used to validate the CFD model to be used in follow-on design and research. Furthermore, the Savitsky Method (Savitsky, 1964) will also be used to validate the resistance and trim calculation using a MATLAB script, given in Appendix A. First, the parameters of the computational model must be defined. A 3D computer aided design (CAD) model of variant 5631 was acquired from the test facility. Using Rhino 3D, a commercially available CAD software program, Model 5631 was rendered and imported into STAR-CCM+. The virtual tow tank parameters are 14m x 6m x 8m (LxWxH), to allow for proper formation of the fluid flow. The mesh resolution was then determined by the computational resources available. Using the MIT iShip High Performance Computing (HPC) cluster, 32 to 64 core processors could be allocated for running each simulation. In an effort not to burden the HPC, a 60,000 to 100,000 cell per core guideline was set.

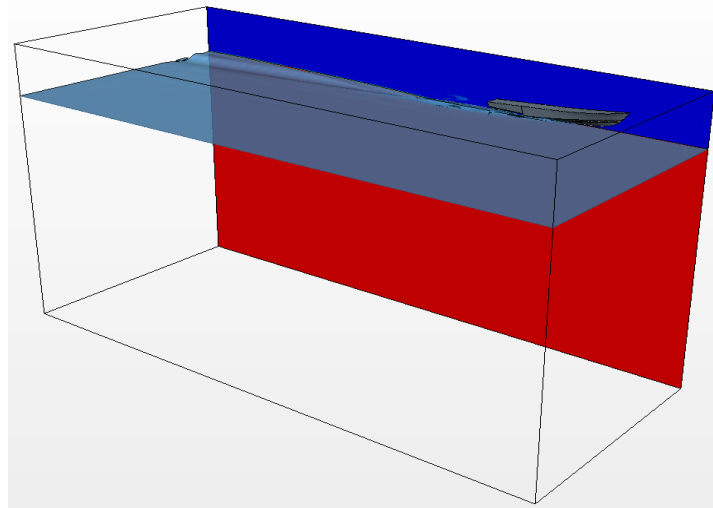


**Figure 11: Virtual Tow Tank with Half Hull Arrangement**

To further reduce computational time, the virtual tow tank used a half hull approach. Knowing that the planing hull is symmetric, and accounting for the symmetry plane benefits, the inertial reference frame was cut in half, as demonstrated in Figure 11. Lastly, post processing of the simulation can monitor particular values of many different parameters, such as velocity and pressure; as well as the ability to capture scenes, both static and dynamic in nature. These scenes allow for the display of streamlines, animation, velocity and pressure fields, and plots of parameters chosen to monitor, Figure 11 is an example of one those scenes. CFD validation begins with the resistance, trim, and heave calculation of Model 5631, displacing 375lb and 483lb starting at five speed values, 48, 54, 58, 64, and 68 knots. These speeds are in full scale to give the reader an understanding of the very high speeds that are desired. A wetted area calculation was validated using only the 375lb weight. The very high speed nature of the new Dynaplane design requires using the upper range of available model test data. These speed values are maintained from the original set of tests. The simulations were run in calm seas allowing the hull to freely heave and pitch.

### 375 lb Model 5631 STAR-CCM+ Validation

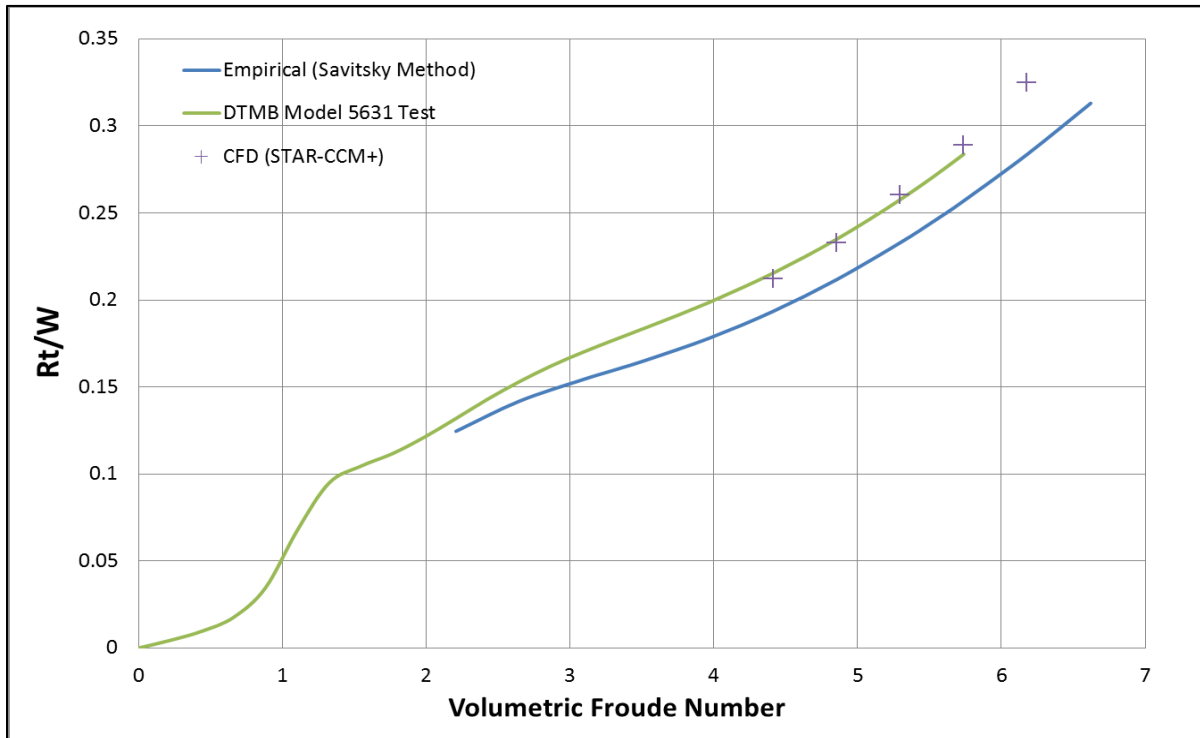


Figure 12: Resistance Validation Results for 375 lb Model 5631

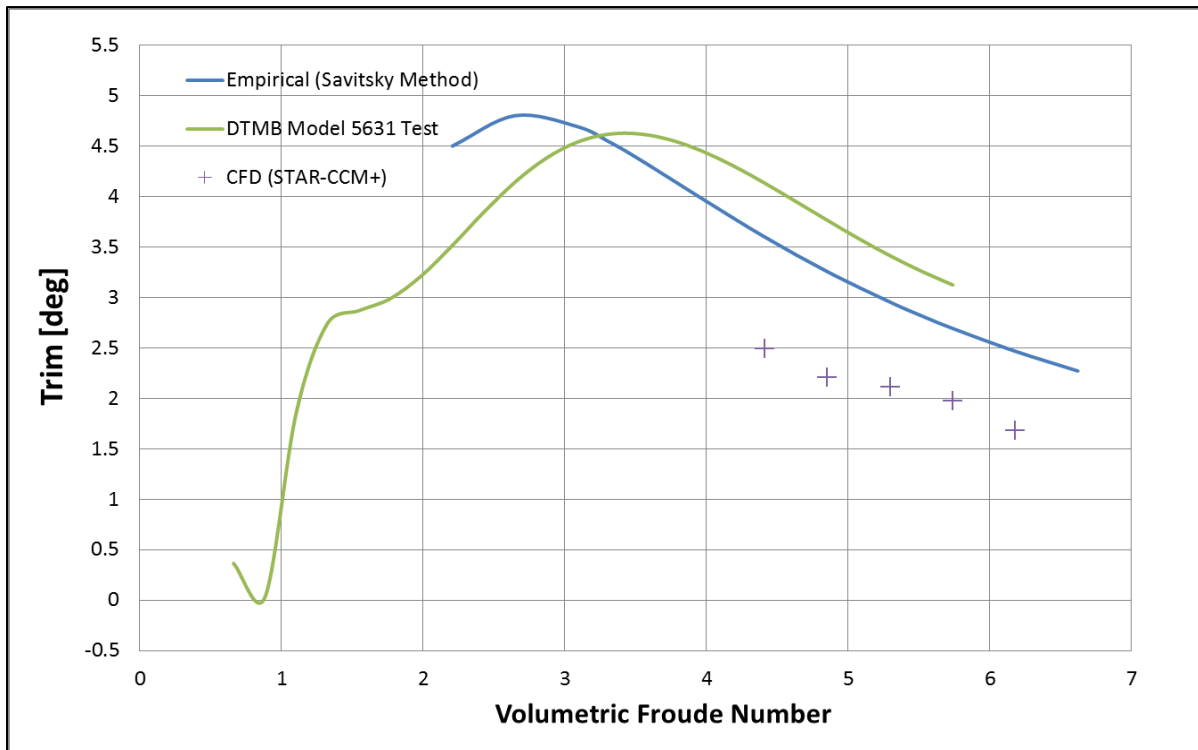


Figure 13: Trim Validation Results for 375 lb Model 5631

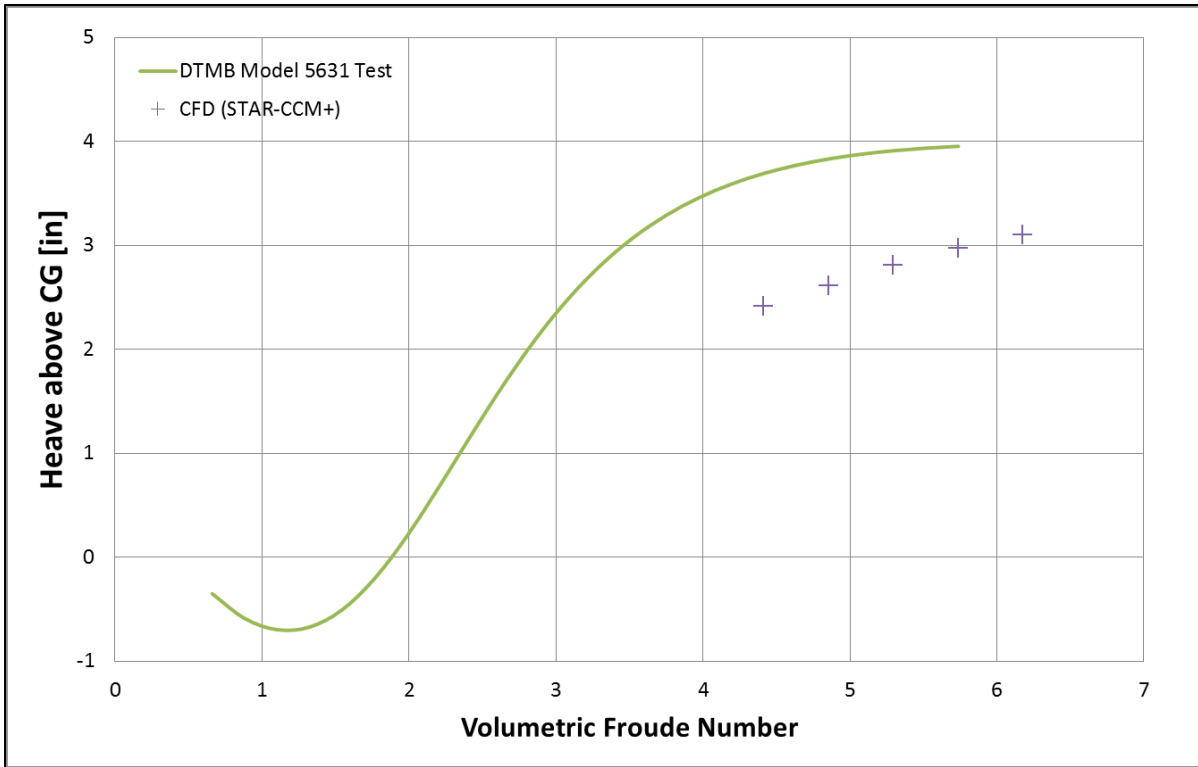


Figure 14: Heave (Vertical Translation) Validation Results for 375 lb Model 5631

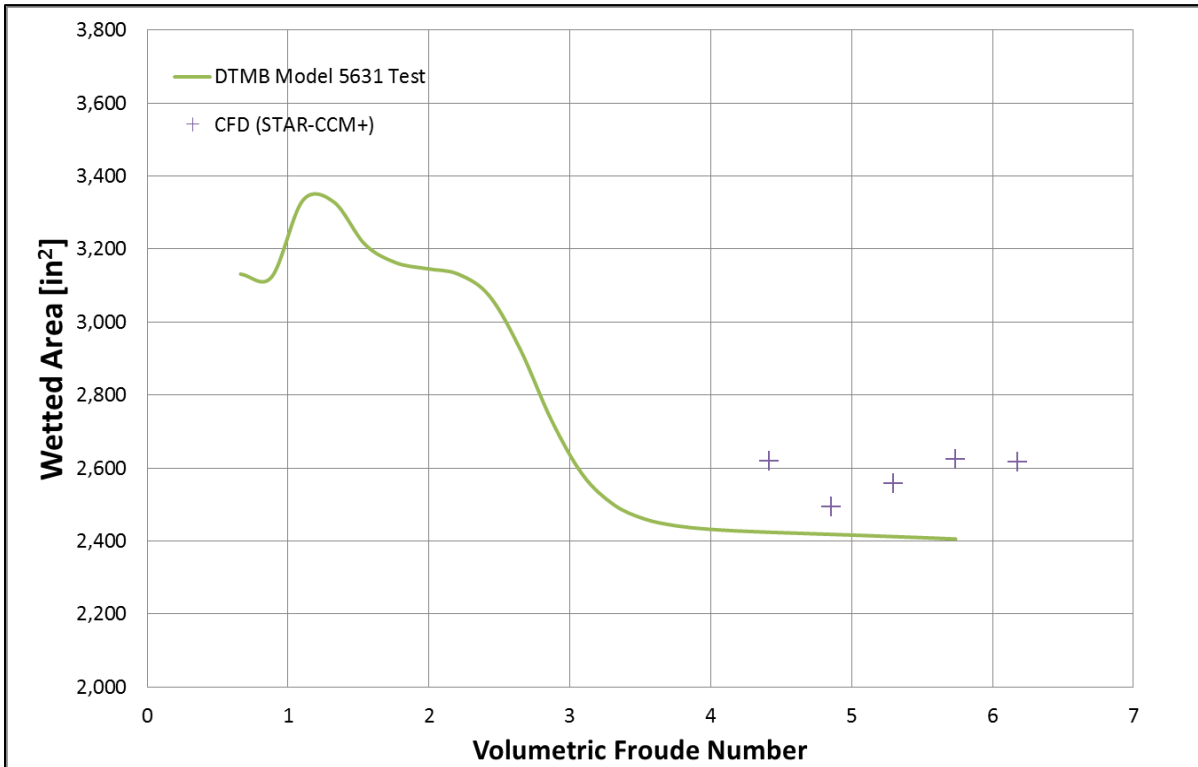


Figure 15: Wetted Area Validation Results for 375 lb Model 5631

### 483 lb Model 5631 STAR-CCM+ Validation

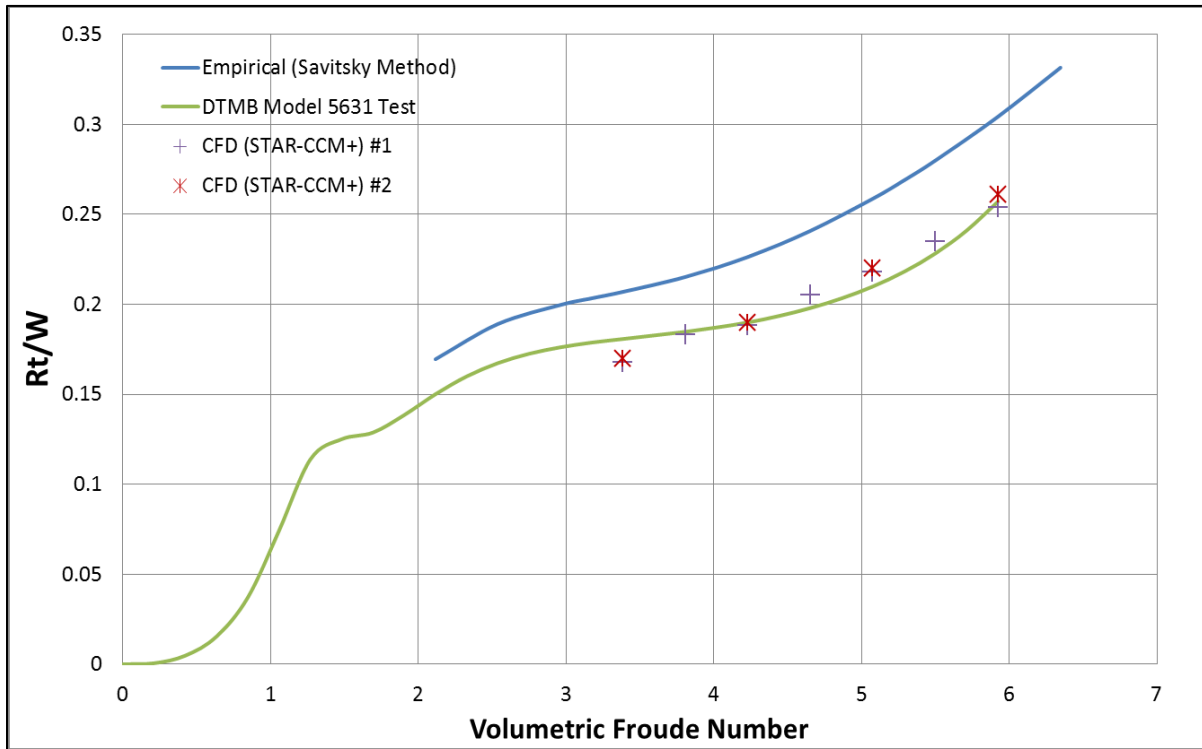


Figure 16: Resistance Validation Results for 483 lb Model 5631

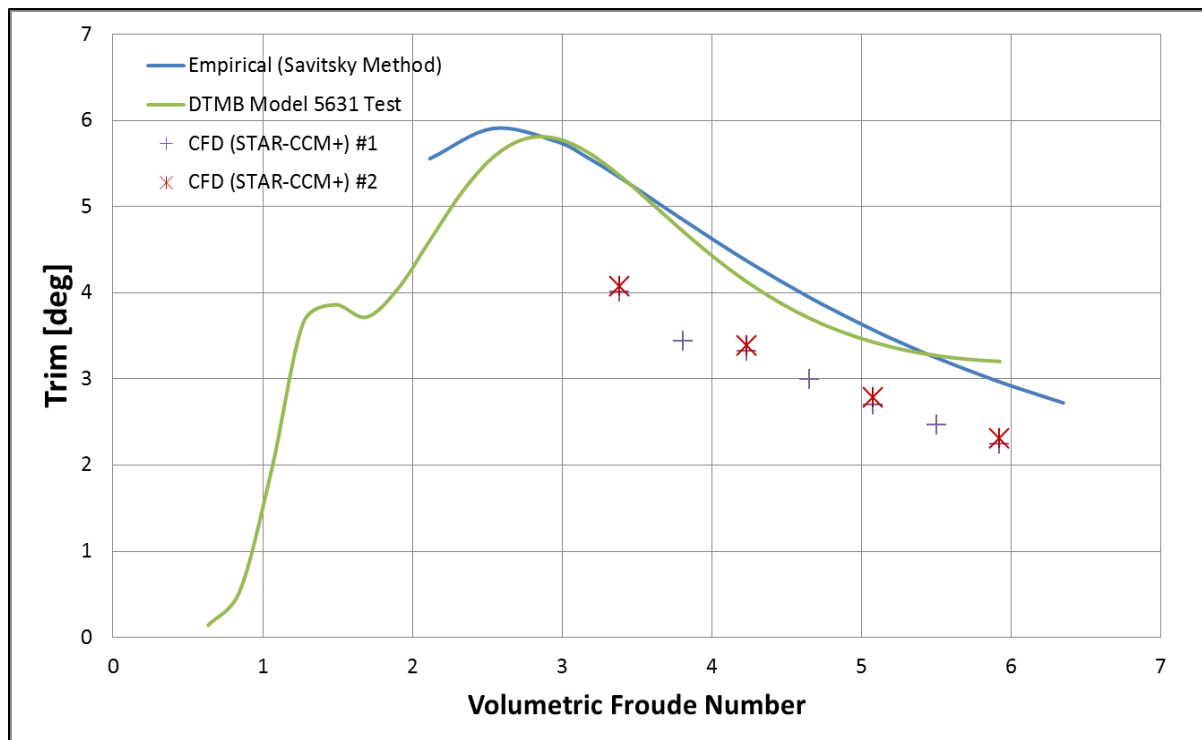


Figure 17: Trim Validation Results for 483 lb Model 5631

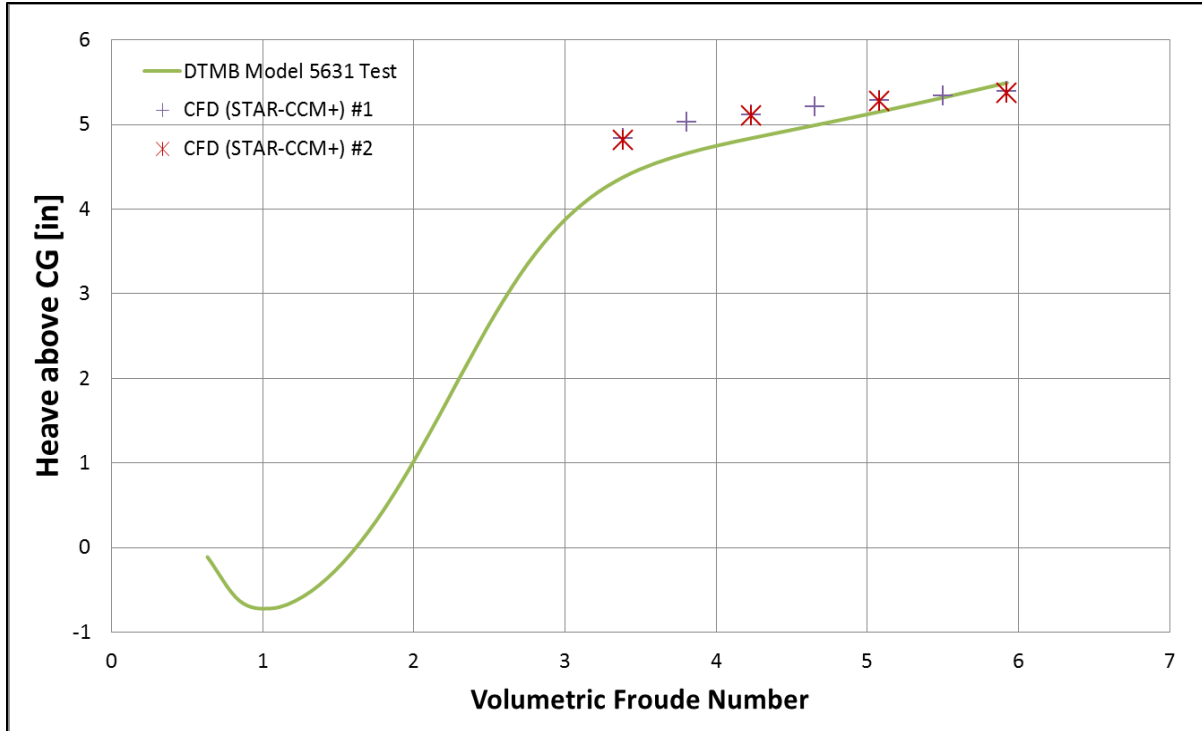


Figure 18: Heave (Vertical Translation) Validation Results for 483 lb Model 5631

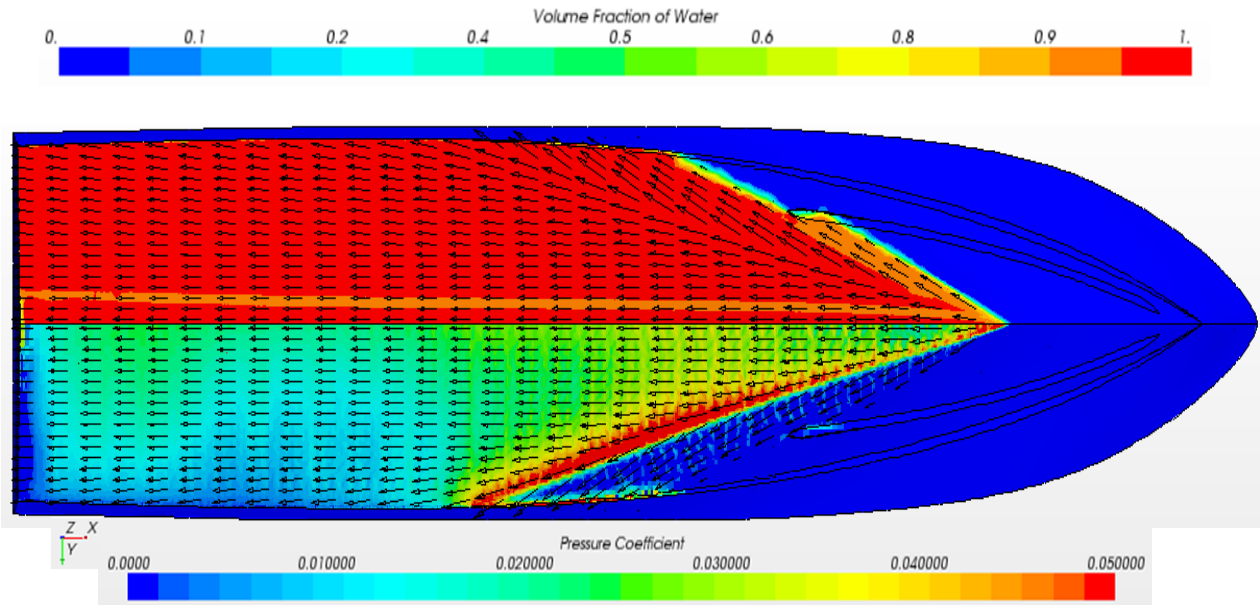


Figure 19: Pressure Coefficient and Volume Fraction of Water on 375lb Model 5631

Note the formation of the stagnation line depicted by the streamline vectors. Also, the bottom half hull illustrates the pressure distribution on the planing surface which accurately matches those predictions in Figure 2 (Savitsky, 1964).

## 2.4 Performance Enhancements

In the previous section, it can be concluded that the trim angle, heave equilibrium, and wetted surface area are all drivers for the resistance values. There are several options that designers can consider in enhancing the performance of their planing hull design. For example, spray rails can be implemented to reduce drag. A 7% drag reduction can be achieved at  $F_nV = 5.0$ ; and a further improvement of 15% drag reduction can be achieved at  $F_nV = 6.0$  (Clement, 1961).

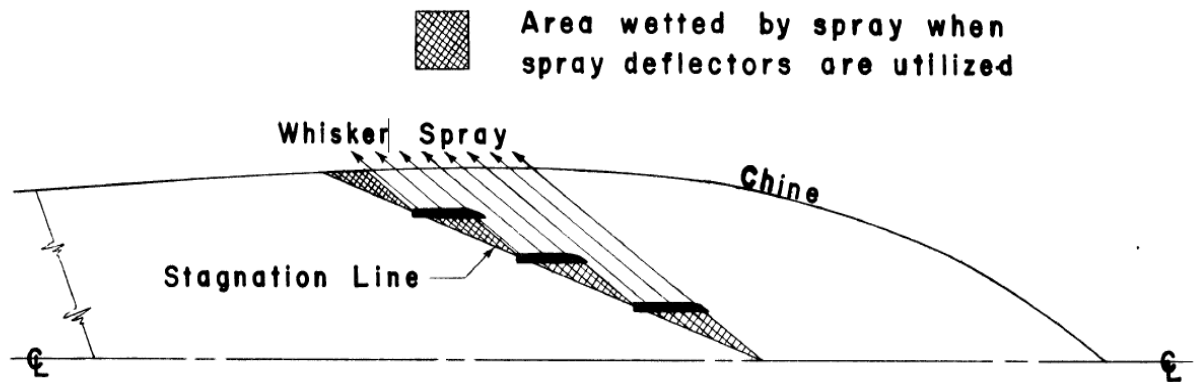


Figure 20: Reduced Wetted Surface Area Due to Spray Rails/Deflectors

As mentioned in Chapter 1 and through results in Model 5631 model tests, reducing the wetted surface area is the driver to improve drag reduction. For the Dynaplane design, the idea of a fully ventilated afterbody is used. As shown in Figure 22, a stepped hull creates a ventilated region just aft of the step which reduces the drag. In the Dynaplane design, the surface piercing hydrofoils are the only appendages accounting for the wetted area on the afterbody. Enhancing performance through ventilation of a stepped planing hull has been accomplished in recent research (Brizzolara and Federici, 2013). Their design incorporated a transverse step with a high aspect ratio and swept back angles called a V-step design, shown in Figure 21.

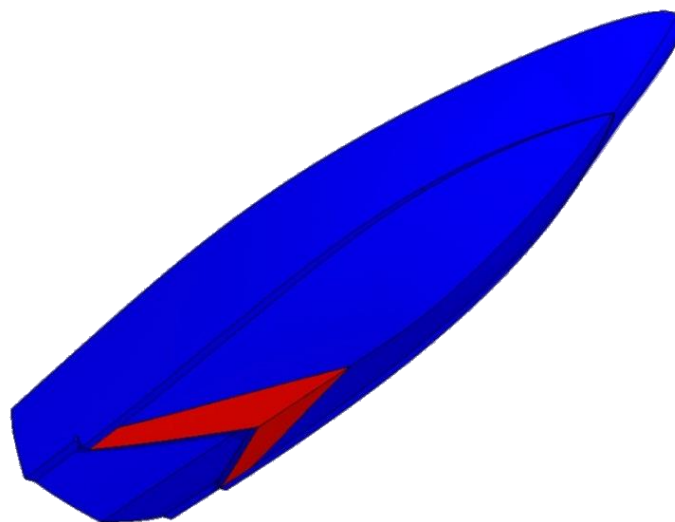
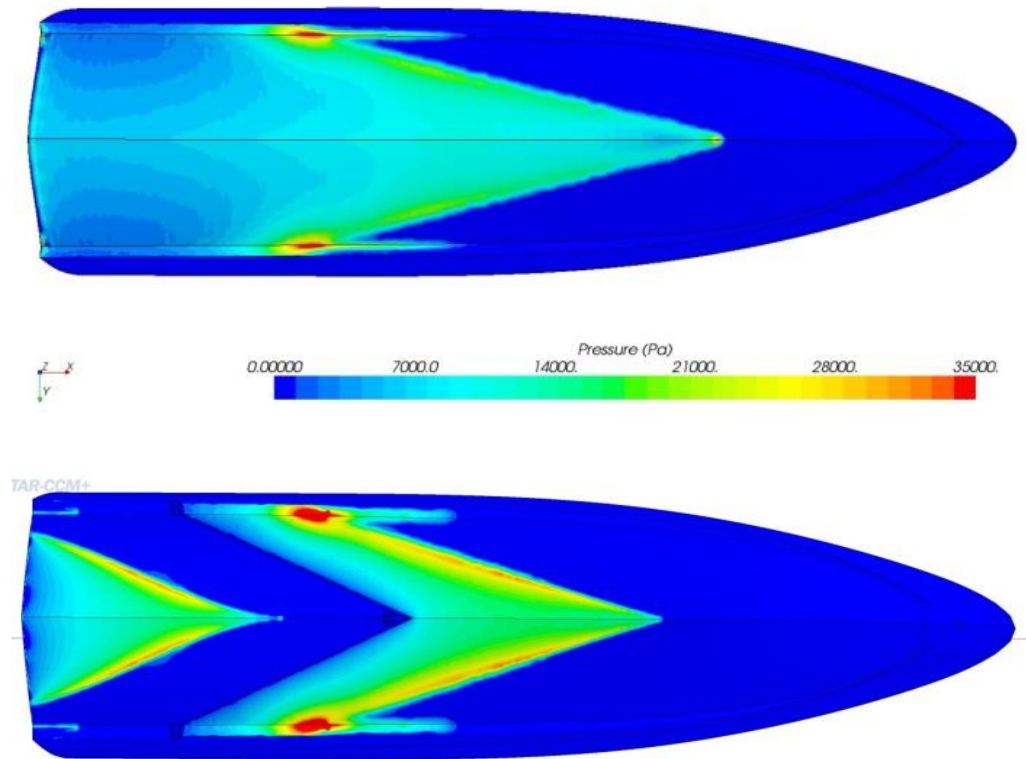


Figure 21: High Speed (50 kts) Patrol Craft with 20 degree Deadrise

In experimental results using CFD, a 19% drag reduction was achieved using the V-step. The comparison of the reduced wetted surface area and pressure distribution caused by the ventilation is shown in Figure 22. Clement's tow tank tests in the DTMB were able to achieve 10-15% drag reduction when comparing conventional and stepped planing hulls of various parametric variables (Clement, 1961).



**Figure 22: Wetted Area and Pressure Distribution Comparison for Stepless and Stepped Hulls**

	<b>Original Hull</b>	<b>V-Step Hull</b>
<b>Lift [N]</b>	115,797	115,797
<b>Drag [N]</b>	23,153	19,452
<b>L/D</b>	5	5.95
<b>Trim [deg]</b>	2.76	4.03
<b>Drag Reduction (% based on L/D)</b>	-	<b>19%</b>

**Table 2: Brizzolara and Federici's Drag Reduction Results**

The evidence that using a stepped hull and partially or fully ventilating the afterbody is substantial. The Model 5631 Dynaplane design combines the drag reduction of a swept back, cambered step with a fully ventilated afterbody. Trim control must be maintained by a stern stabilizer; which Clement discusses in his paper. In the next chapter, the conversion of Model 5631 to a new Dynaplane configuration is covered in detail.



## Chapter 3 – The Dynaplane Configuration

### 3.1 Clement's Dynaplane

The implementation of Eugene Clement's Dynaplane originates from its advantages of drag reduction (Clement, 1966). Furthermore, Clement discusses the performance predictions compared to a similar hull of lower deadrise, 12.5 degrees. The deep V hull has disadvantages dealing with its added resistance but it results in improved seakeeping. It also contributes to the reduction of vertical accelerations compared to a planing hull of shallower deadrise.

Stepped hulls begin to show their added benefit in Figure 4, which forms the basis for potential benefits of the Dynaplane design. There are several design options for a stepped hull including a traditional transverse step, multi-step, or a Dynaplane configuration. The traditional transverse step is a faired continuation of the bow shape yet it generally discontinues, or steps, aft of the center of gravity. The rest of the hull aft of the step is usually raised or angled to maintain proper ventilation. The Dynaplane configuration takes its name from its close relation to an airplane. It possesses a cambered step, resembling the bottom of an aircraft wing, which provides substantial lift at high speeds. It also creates a fully ventilated afterbody with maintaining trim control by using a stern stabilizer. Clement states, "A striking fact about the potential of the Dynaplane-type of stepped planing boat is that as the design speed increases, the hydrodynamic hull drag remains practically the same" (Clement, 2005). This thesis focuses on the improvement of the lift to drag ratio from the Dynaplane configuration and further improves on the options for an afterbody lifting surface.

In Clement's 2005 paper, design procedures are given based on a range of hull parameters. Specifically, he recommends choosing a hull with a deadrise no more than 15 degrees to achieve the best results. The Model 5631 Dynaplane design addresses the extension of Clement's design with respect to a 20 deadrise angle. The methodology of designing traditional airplanes closely resembles the design approach taken for the Dynaplane configuration because similar performance characteristics are desired such as producing sizeable lift with minimum drag, while remaining trim control and stability at high speeds. Clement's design procedures pay close attention to the lift and drag of the cambered surface. The longitudinal position of the cambered surface is dictated by the location of center of gravity. This becomes very important in the position of the afterbody lifting surface as well. Clement further recommends placing the center of gravity close to the mid-point of the planing hull length.

The Dynaplane design represents an improvement in powering requirements but it unfortunately introduces instabilities due to trim control deficiencies. This thesis addresses these instability issues at high speeds with the Dynaplane configuration, and attempts to provide a reasonable solution to not only predict but also solve instability at high speed. Clement discusses a limited range of applicability for this design. For example, the proposed afterbody lifting surface, or stern stabilizer has a limitation of 50mph or 43.4 knots. Later in this chapter, a newly designed surface piercing hydrofoil is introduced that can operate at cavitating speeds. This introduces unforeseen hydrodynamic considerations since the Model 5631 has a 20 degree deadrise and will operate at  $F_nV = 5$ .

### 3.2 Cambered Step Design

Using the Model 5631 reference hull, a cambered step will be designed (Clement, 2005). Results from model tests discussed in Clement's paper determine that the main planing surface supports majority of the planing hull's weight. The goal of the Dynaplane's design is for the main cambered step to support 90% of the hull's weight, with the remaining 10% being provided by surface piercing hydrofoils. The angle of attack of the cambered step depends on the hull's speed, weight and location of the center of gravity. Therefore, Clement recommends choosing a trim angle at a specific design speed and appropriate for the deadrise of the hull. Since Model 5631 has a 20 degree deadrise, it was decided to select a running trim angle at the given design speed of  $F_nV = 5$  (Metcalf et al, 2005). A resultant trim angle of 3.65 degrees was chosen from the Metcalf et al paper, which matched the design speed prediction.

Following Celano's critical trim angle equation (Celano, 1998); it was found that the recommended trim angle for avoiding porpoising was 3.5 degrees. This smaller trim angle was derived for high speed planing craft in order to avoid porpoising. For this reason, two versions or generations of the cambered step was designed for possibly testing both designs. With a given trim angle, deadrise, and speed, the cambered step design can proceed. The procedure below will guide you through the design process of Gen 2's construction. With Model 5631 being selected, the trim angle, deadrise, speed, beam, and weight have now been chosen.

	Trim Angle	Deadrise	$F_nV$
Gen 1	3.65 deg	20	5
Gen 2	3.5 deg	20	5

Table 3: Cambered Step Variant Generation

	Model 5631
Trim Angle [deg]	3.5
Deadrise at transom [deg]	20
Design Speed Coefficient [ $F_nV$ ]	5
W, Weight [lb]	375
b, Beam [ft]	2.24

Table 4: Chosen Design Parameters for Dynaplane Configuration

#### Design Procedure for a Cambered Planing Surface

1. Calculation of the lift coefficient for the cambered planing surface based on the beam and weight of Model 5631:

$$C_{Lb\beta} = \frac{0.9W}{0.5\rho v^2 b^2} = \underline{\underline{0.0474}}$$

2. Selection of camber curve method on the step:

It is recommended to use the Johnson 3-term equation, which is a function of the lift coefficient desired. Johnson's equation for the curvature of the cambered step promises a 50% increase in the lift to drag ratio compared to a flat plate, shown in Figure 23. These surfaces were tested with a zero deadrise and aspect ratio (AR) of 2. From the results of using a Johnson 3-term camber profile, the design proceeded.

$$\frac{Y}{C_L} = \left( -20X^{\frac{3}{2}} + 80X^2 - 64X^{\frac{5}{2}} \right) \frac{1}{7.5\pi}$$

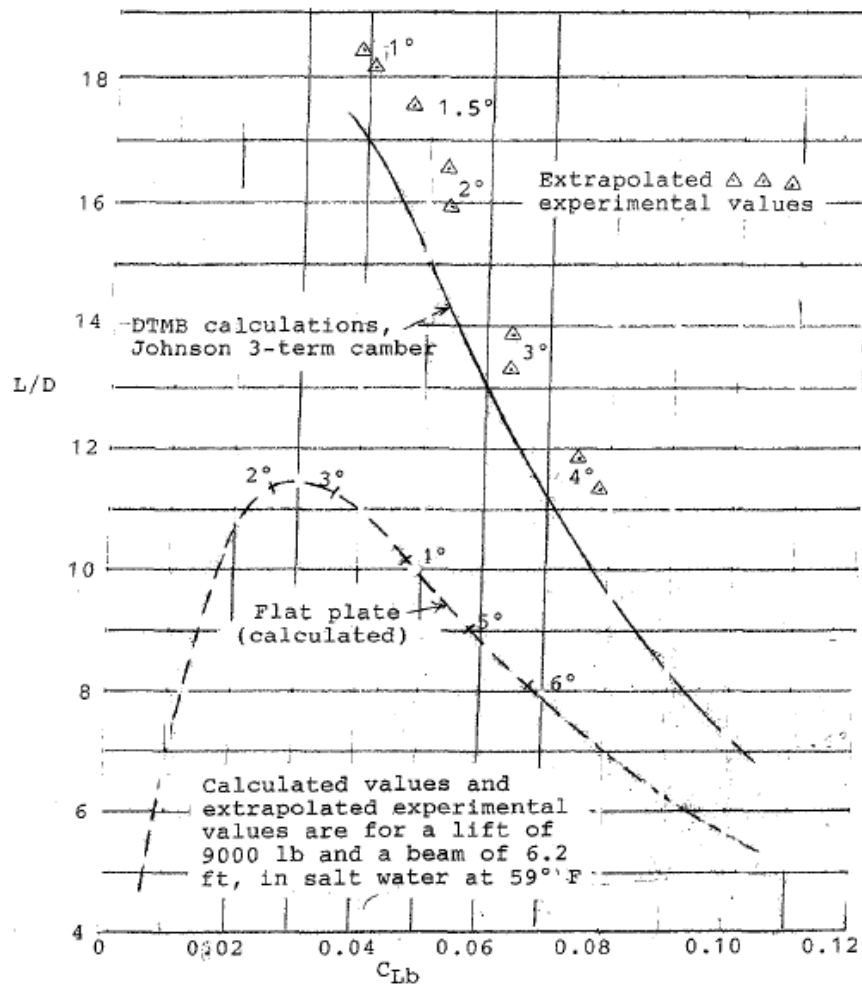


Figure 23: Comparison of Calculated and Experimental Results of L/D for Johnson 3-Term Cambered Surface and a Flat Plate, AR = 2.0

3. Select value for deadrise angle. This is based on the Model 5631 reference hull.

$$\beta = \underline{\underline{20 \text{ degrees}}}$$

4. Select ratios of tip chord to beam,  $l_t/b$ , and of root chord to beam,  $l_r/b$ :

$$l_t/b = \underline{\underline{0.2}} ; l_r/b = \underline{\underline{0.8}}$$

5. Calculate aspect ratio, AR:

$$AR = \frac{2}{\frac{l_r}{b} + \frac{l_t}{b}} = \underline{\underline{2}}$$

An AR of 2 was chosen due to the majority of the experimental and theoretical results using the same value of AR. Thus, the relationship of the tip chord and root chord was chosen.

6. Select appropriate value for trim angle,  $\tau$ :

$$\tau = \underline{\underline{3.5 \text{ degrees}}}$$

7. Determine value of angle between the spray root line and the centerline:

$$\gamma = \tan^{-1}\left(\frac{\pi \tan \tau}{2 \tan \beta}\right) = 14.79 \text{ degrees} + 5 \text{ degrees} = \underline{\underline{19.79 \text{ deg}}}$$

For cambered surfaces, a five degree correction factor is added to the original value.

8. Figure 24 shows the plan view illustration of the proposed cambered planing surface.

9. Determine sweep angle of 50% chord line:

$$\Phi = \tan^{-1}\left[\frac{1 - \tan \gamma \left(\frac{l_r}{b} + \frac{l_t}{b}\right)}{\tan \gamma}\right] = \underline{\underline{65.35 \text{ deg}}}$$

10. Determine sweep angle of the step:

$$\Theta = \tan^{-1}(2 \tan \phi - \tan \gamma) = \underline{\underline{57.66 \text{ deg}}}$$

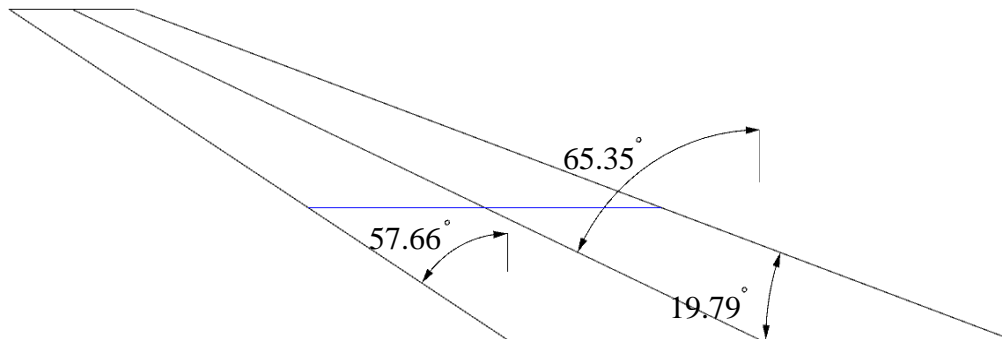


Figure 24: Swept Back Angles for Cambered Planing Surface, Plan View

11. Determine  $(C_{Lb\beta} / C_{Lb0})_{DL}$  from Figure 25, but first solve  $C_{Lb\beta}$ . The ratio of lift coefficient of a hull with deadrise and flat plate are considered. The experimental values are illustrated in Figure 25. Once the lift coefficient ratios are determined, then the actual design lift coefficient of the camber planing surface can be calculated through multiplying those found in the figures on the next two pages.

$$C_{Lb\beta} = C_{Lb\beta} - 0.0065\beta C_{Lb\beta}^{0.6} = \underline{0.075}$$

$$(C_{Lb\beta} / C_{Lb0})_{DL} = \underline{0.633}$$

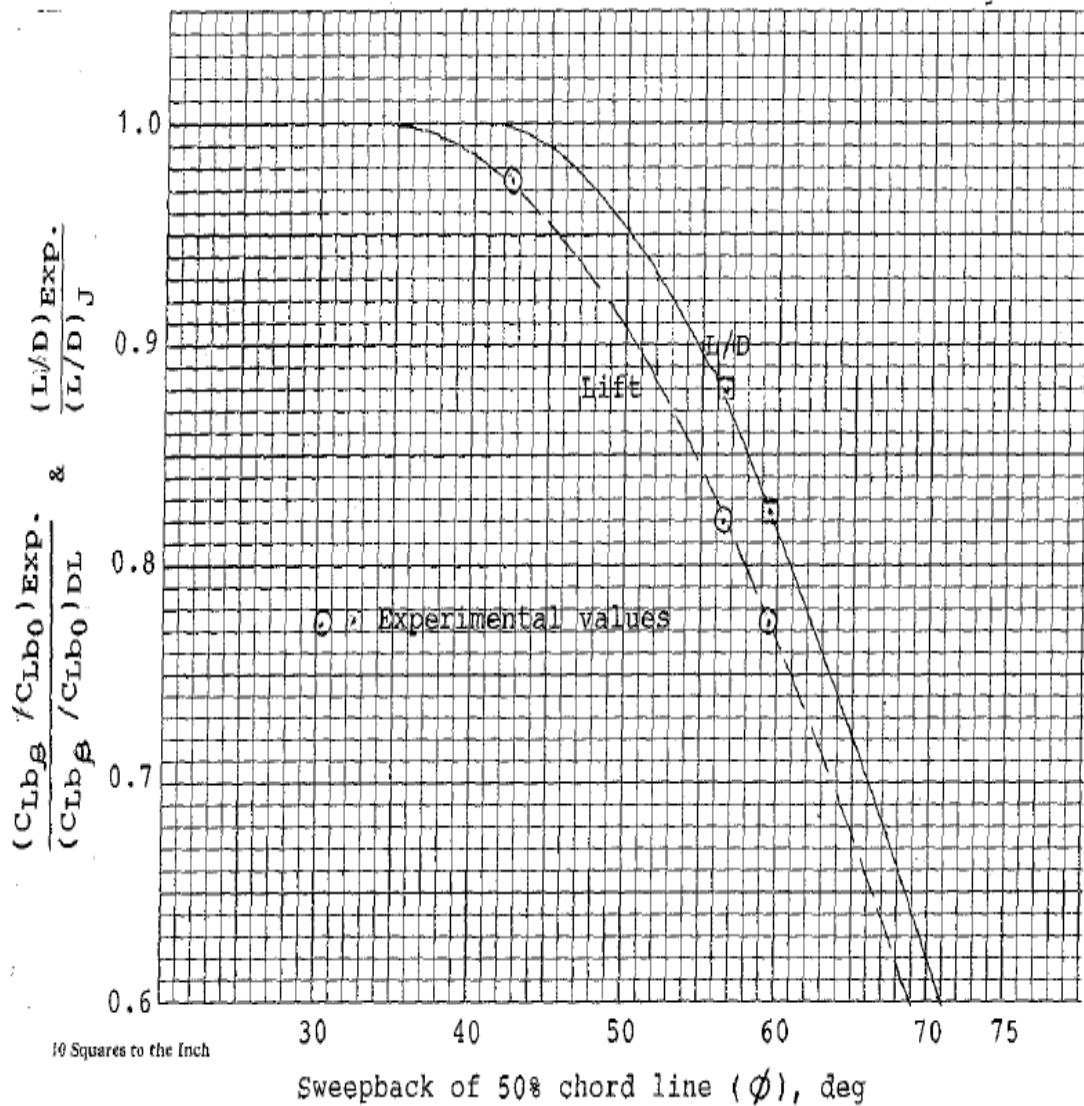


Figure 25: Correction Value for Swept Back Angle to Lift and L/D Ratio

12. Determine ratio of the experimental values potentially obtained with this design to the values determined at the Davidson Laboratory.

$$\frac{(C_{Lb\beta}/C_{Lb0})_{Exp}}{(C_{Lb\beta}/C_{Lb0})_{DL}} = \underline{\underline{0.67}}$$

13. Multiply value in Step 11 by the value in Step 12 to determine  $(C_{Lb\beta}/C_{Lb0})_{Exp} = \underline{\underline{0.424}}$

14. Divide  $C_{Lb\beta}$  by the value from Step 13 to obtain  $C_{Lb0} = \underline{\underline{0.112}}$

15. Now use the  $C_{Lb0}$  value in Figures 26-28 to determine the lift to drag ratio,  $(\frac{L}{D})_J$ , lift coefficient,  $C_{L,d}$ , and the ratio between the center of pressure and mean hydrodynamic chord length from the transom.

$$(\frac{L}{D})_J = \underline{\underline{10}} ; C_{L,d} = \underline{\underline{0.236}} ; \frac{l_{cp}}{l_m} = \underline{\underline{0.51}}$$

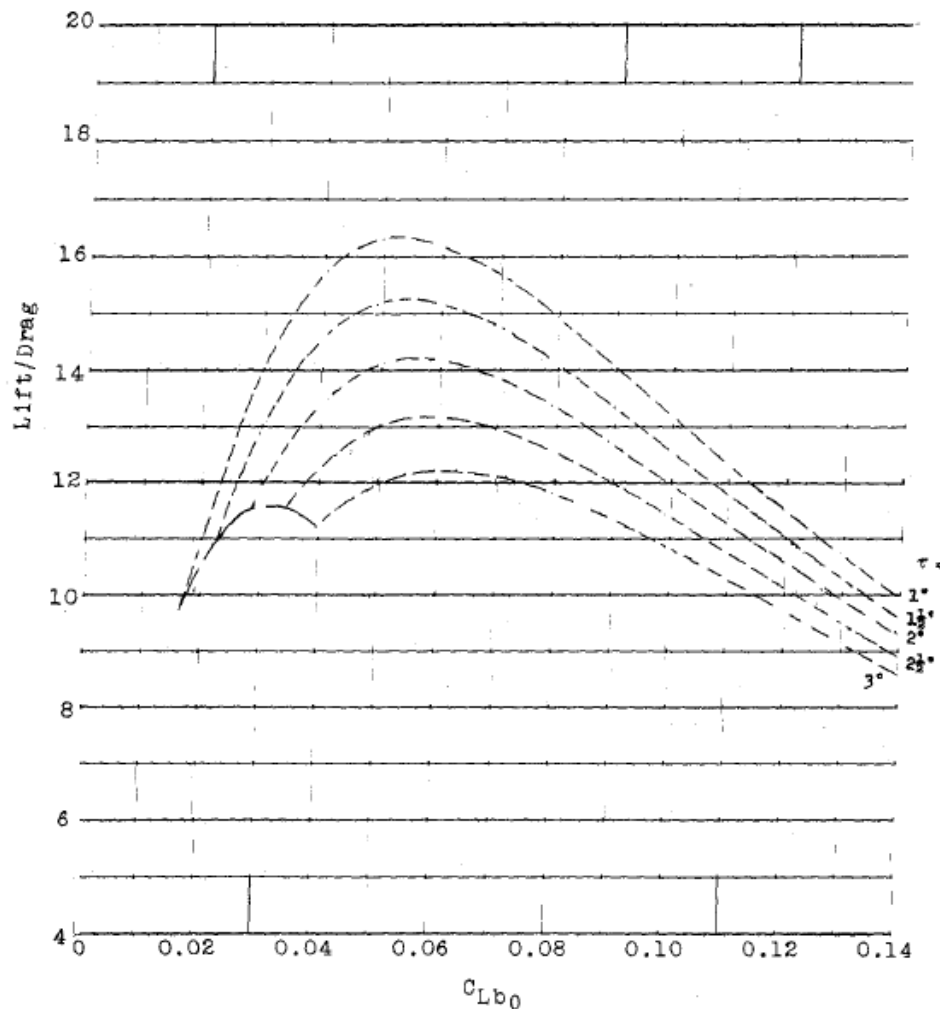


Figure 26: L/D Ratio Versus  $C_{Lb0}$  Results for a Johnson 3-Term Profile, AR = 2

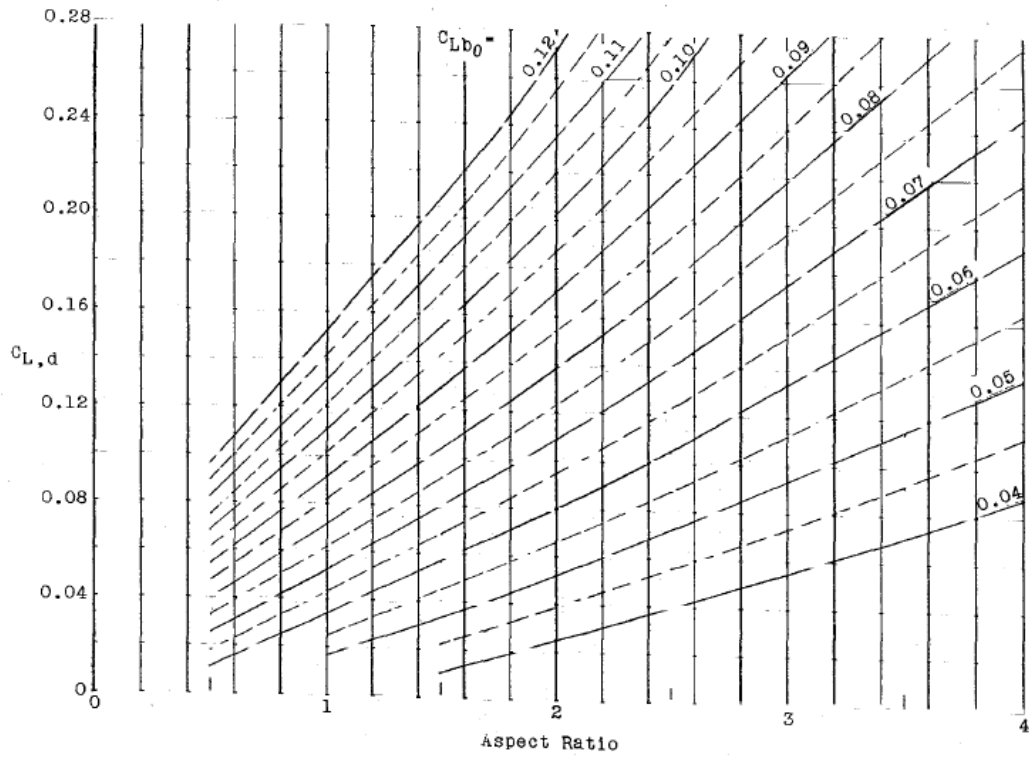


Figure 27:  $C_{L,d}$  Versus Aspect Ratio for a Johnson 3-Term Profile,  $\tau=2.5$  deg

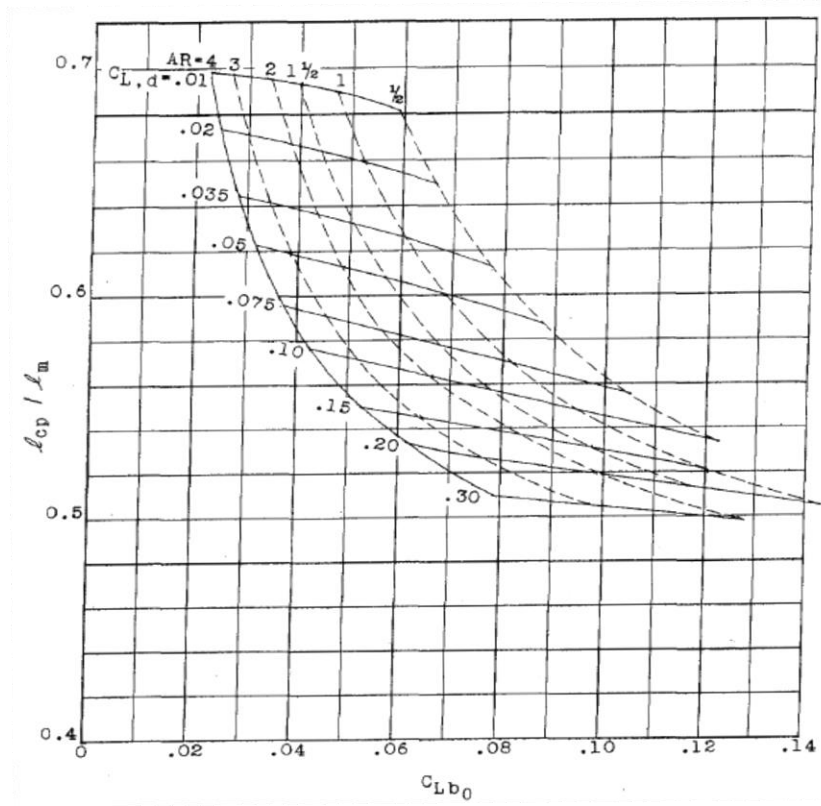


Figure 28: Center of Pressure Location Versus  $C_{Lb0}$  for a Johnson 3-Term Profile,  $\tau=2.5$  deg

16. Determine  $\frac{(\frac{L}{D})_{Exp}}{(\frac{L}{D})_J}$  from Figure 25

$$\frac{(\frac{L}{D})_{Exp}}{(\frac{L}{D})_J} = \underline{\underline{0.72}}$$

17. Multiply the value from Step 15 by the value in Step 16 to determine  $(\frac{L}{D})_{Exp} = \underline{\underline{7.18}}$

18. Multiply the value from Step 17 by 0.925 to get the final lift to drag ratio for a hull with a stern stabilizer. This calculation includes a correction factor for air drag,  $(\frac{L}{D}) = \underline{\underline{6.64}}$ .

19. Calculate the tip chord and root chord lengths.

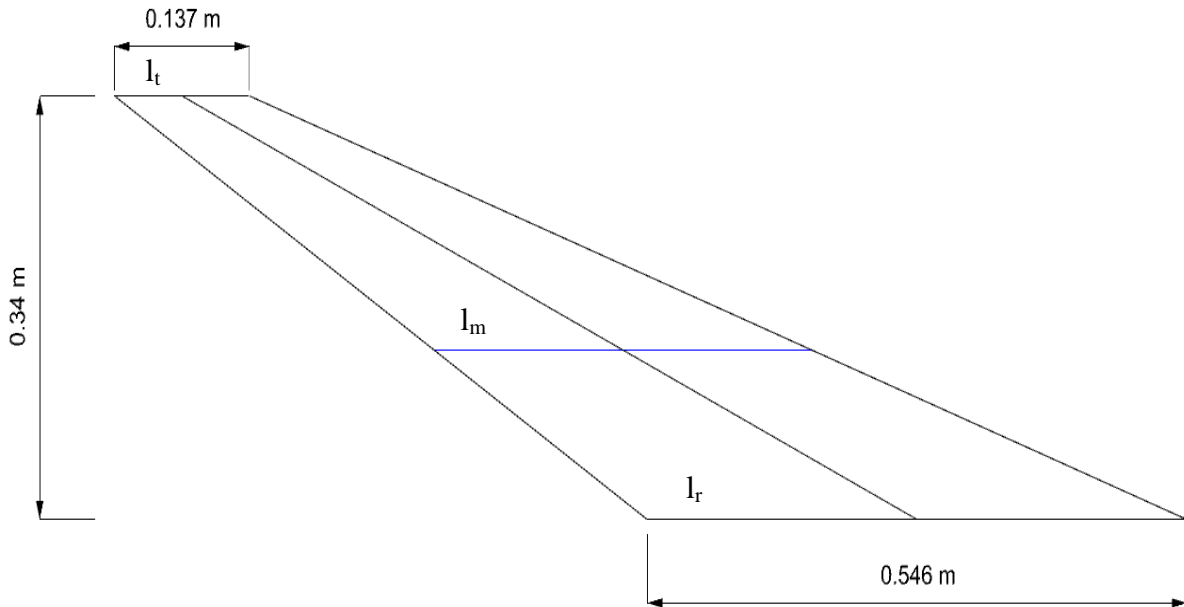


**Figure 29: Length Dimensions on Cambered Step**

Steps 20-23 outline the procedures for determining the center of pressure of the cambered step and the mean hydrodynamic chord. These values are important in the evaluation of the pressure distribution along the cambered surface. Later in this analysis, the pressure along the cambered step leads to the determination of the correct longitudinal placement compared to Clement's original predictions. Below is the calculation for the location of the center of pressure, cp, for a LCG located 42% forward of the transom.

$$0.9Wx = W(42\%LBP)$$

$$x = \underline{\underline{1.42 \text{ m}}}$$

The cambered planing surface was then constructed using  $C_{L,d} = 0.236$  in the Johnson 3-term equation.



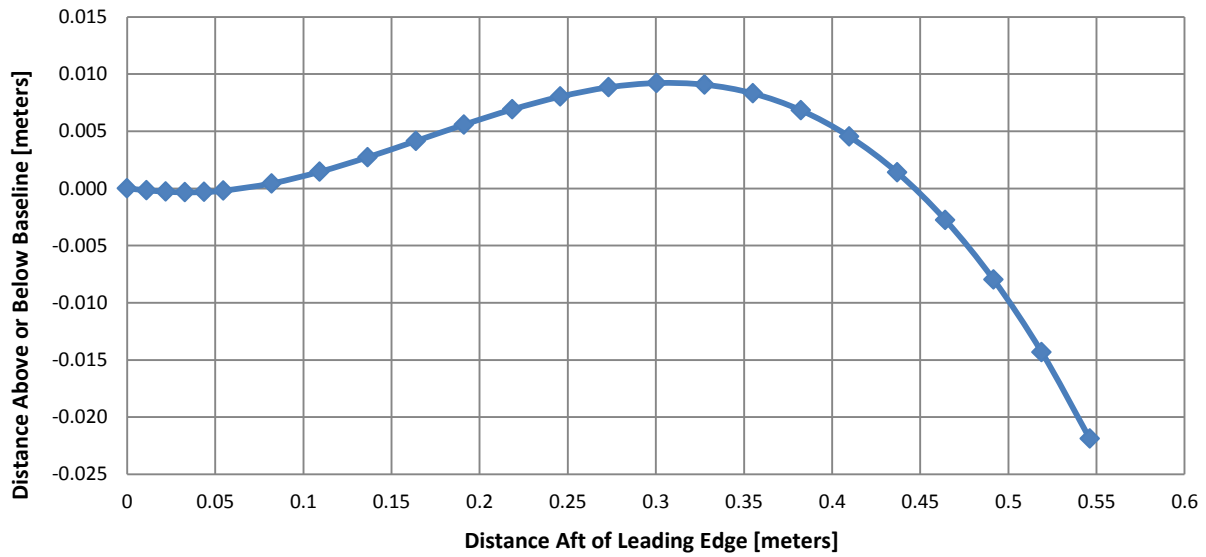


Figure 30: Camber Profile with Johnson 3-Term Equation,  $Cl,d=0.236$

The fully designed cambered step, Gen 2, was then constructed using Rhino 3D. The model can be developed iteratively for import into Star-CCM+. Below is a diagram of the completed cambered step mounted on the hull of Model 5631.

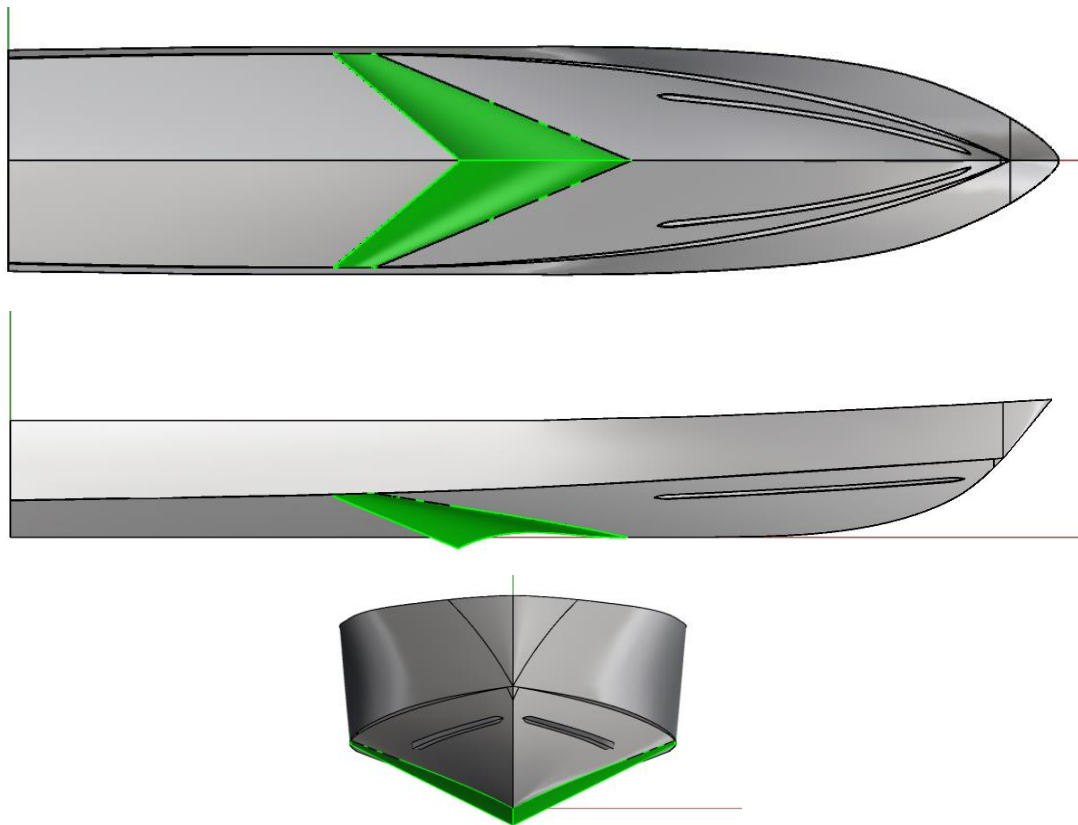
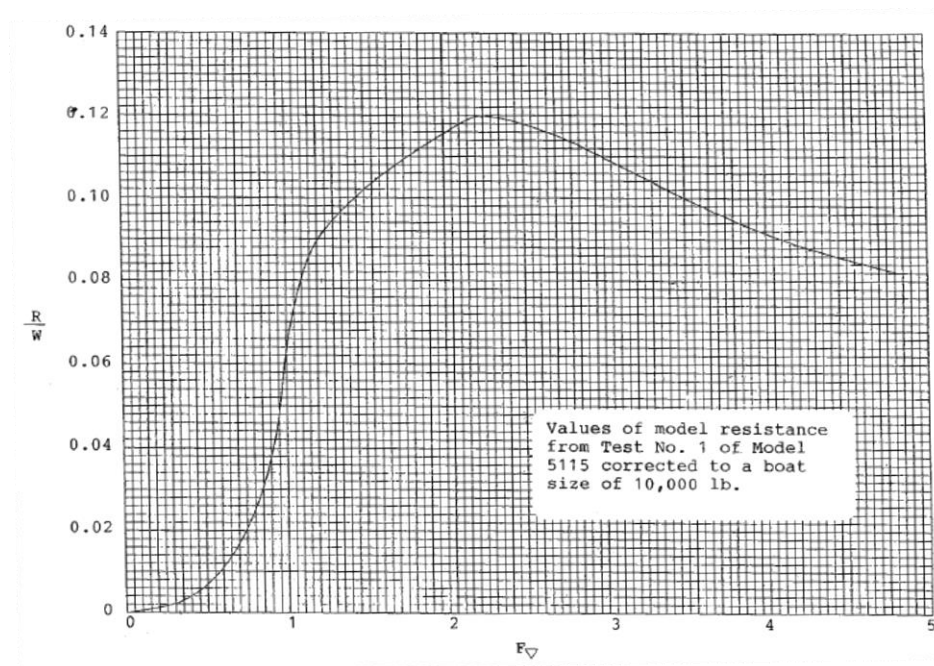


Figure 31: Plan, Profile and Body Plan Views of Preliminary Cambered Step on Model 5631

### 3.3 Afterbody and Stern Stabilizer Design

After completion of the cambered step, the next step in the design process is to design the afterbody and the stern stabilizer, or SPSC hydrofoils. It is recommended to raise the afterbody section of the hull a distance equal to 1% of the beam. The goal is to avoid getting any part of the afterbody wet by spray or free surface. Another suggestion to ensuring a fully ventilated afterbody is to rotate the afterbody 2 degrees so as to raise the transom with respect to the baseline. Clement mentioned that this design guidance was used to reduce the power to exceed hull speed. For a planing hull, the hull speed or “hump” speed must be achieved until the hydrodynamic forces take over. Reducing the afterbody profile too much causes an increase in low speed drag and the vessel will require more power to achieve “hump” speed. An illustration of these effects is shown in the figure below Figure 32.



**Figure 32: Dimensionless Resistance Versus Speed Curve for Dynaplane Configured Boat**

In the Model 5631 Dynaplane design, the height of the step is 10% of the beam. This value was chosen to absolutely ensure full ventilation on the afterbody. The emphasis of the afterbody design for the Model 5631 was not to determine the optimized height of step, angle afterbody, or efficiently achieving “hump” speed. Next, Clement intended to use a hydrofoil that carried 10% of the overall weight of the planing hull. The recommended hydrofoil design for Clement’s Dynaplane is a surface piercing V hydrofoil. A depiction of this design is shown in Figure 33. The surface piercing V hydrofoil uses a NACA 16-509 foil profile. From model testing, this particular foil profile possesses a constant pressure distribution, which is beneficial for maintaining 10% of the vessel’s weight. In keeping with NACA categorical system, the 16-509 profile has a 0.5 lift coefficient and a thickness which is 9% of the chord length. While this foil profile achieves high lift to drag ratios at speeds below 43 knots full scale, cavitation starts to occur at higher speeds. This effect will decrease the lift to drag ratio and suggest a need for an improved hydrofoil design.

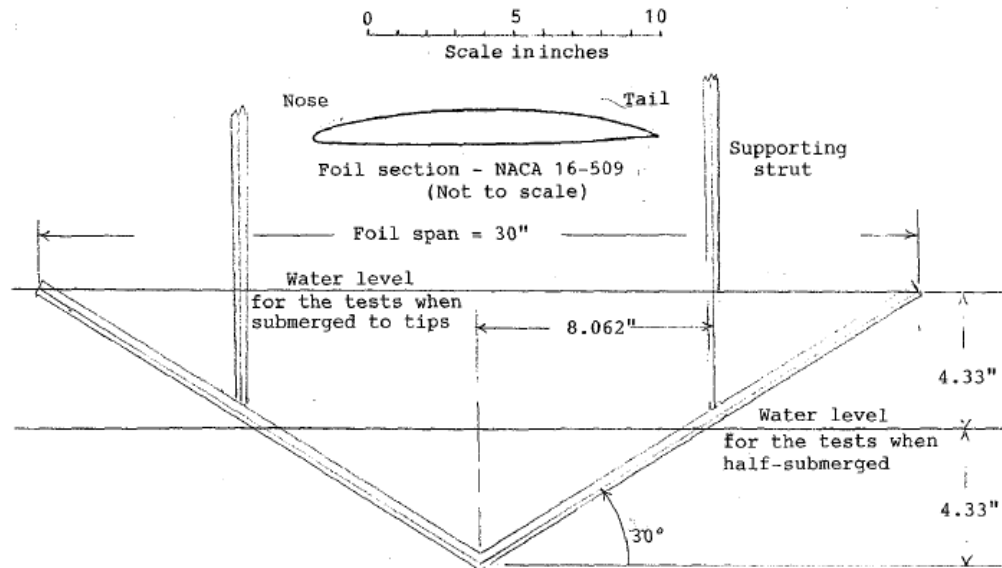


**Figure 33: Surface Piercing V Hydrofoil with a 30 degree Dihedral**

Since cavitation is nearly unavoidable at speeds greater than 43 knots (50+ mph), a new surface piercing hydrofoil designed by Dr. Stefano Brizzolara was analyzed using computational models and compared to existing super cavitating hydrofoil designs. The profiles of a sub-cavitating foil largely differ from super cavitating foils, shown in Figure 34.

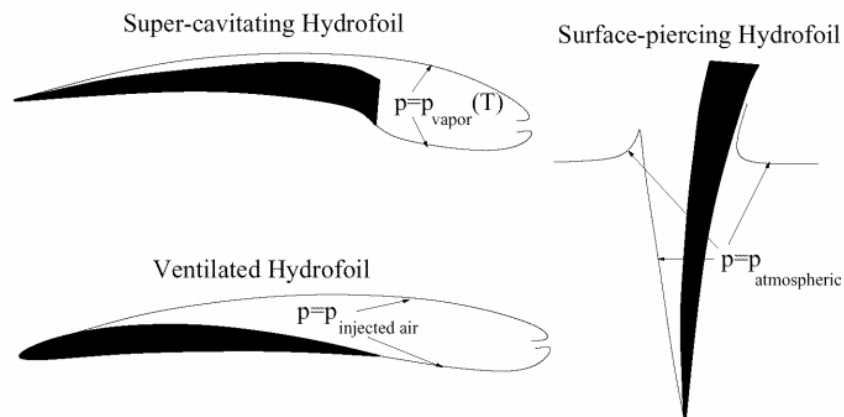


**Figure 34: 2D Profile Examples of Super Cavitating and Sub-Cavitating Hydrofoils**

Major studies and scientific advancements on super cavitating hydrofoils were completed from the 1960s to 1980s. These early design examples, TAP-1 and TAP-2 design by Boeing, were tested at speeds higher than 60 knots. The majority of design methods used today are based on linearized asymptotic theories (Brizzolara and Federici, 2011). The early theories by Tulin, Burkart, and Johnson are valid for cavitation numbers of zero and the shape of the back face was not given because it was assumed to lie in the fluid cavity. The introduction to efficient super cavitating hydrofoils began with Kinnas, who proposed optimizing the entire 2D profile based on the boundary element method (Kinnas, 2001). Specifically, the optimization of the Johnson series of profile designs which used a 3-term or 5-term equation to calculate the profile of the

foil. His super cavitating hydrofoils were designed for strictly high speeds, in the regime where pressure drops below the vapor pressure of water. However, the super cavitating, surface piercing hydrofoil that Dr. Brizzolara designed operates in low and high speeds. These recommended optimization techniques were used to develop an efficient surface piercing super cavitating hydrofoil (Brizzolara and Federici, 2011). The new hybrid profile design, show in Figure 35 and Figure 36, operates at a higher lift to drag ratio in both a wetted condition and a fully cavitating condition. It is an optimized design based on geometry from Johnson's series of tests. It can be shown in Figure 35 that the L/D value for Dr. Brizzolara's hydrofoil matches those from Johnson's test.

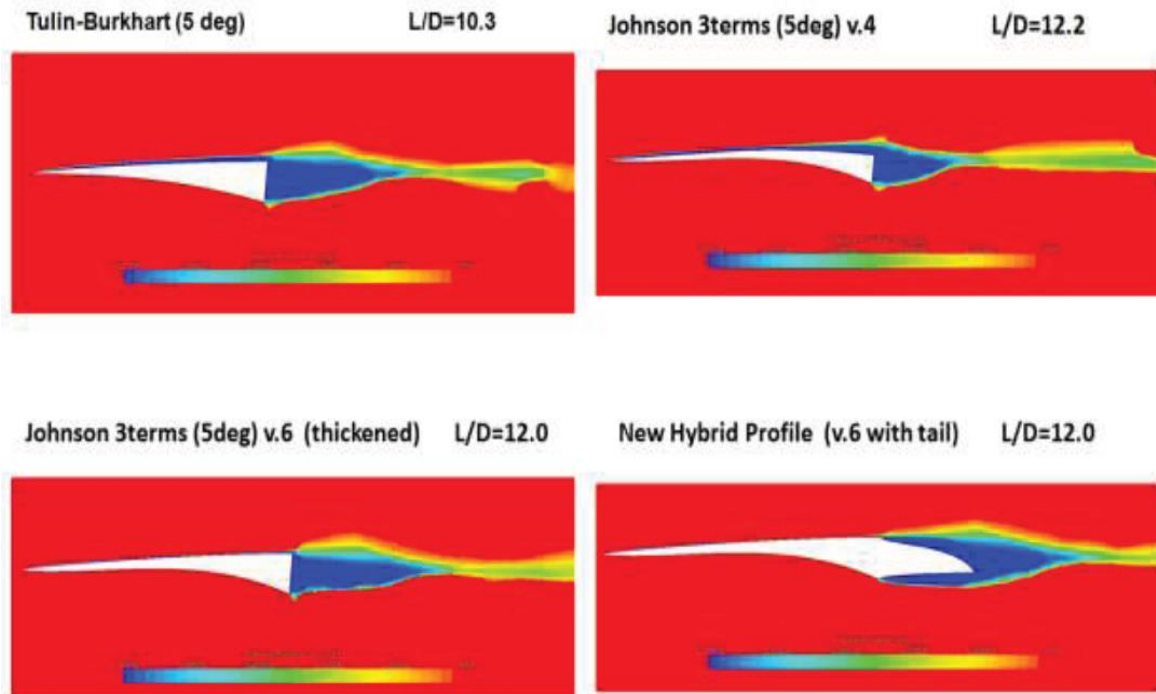


**Figure 35: 2D Profiles of Super Cavitating Hydrofoils at Sub-Cavitating Speeds**

In fully wetted or sub-cavitating speeds, Figure 36 shows a clear advantage to the new hybrid profile. Greater concentrations of high pressure, shaded in red, and low pressure, shaded in blue, provide evidence of the generation of large separation eddies in the wake of the conventional, truncated, SC hydrofoils. The new hybrid design is able to achieve good pressure recovery due to the attached streamlines at the trailing edge of the profile. The resultant lift to drag ratio of the new hybrid hydrofoil compared to traditional SC profiles gives an increase of over 150%. This realization reveals the importance of an optimized design for specific applications. In our very high speed Dynaplane configuration, the SPSC hydrofoils designed by Dr. Brizzolara proved to be the best option.

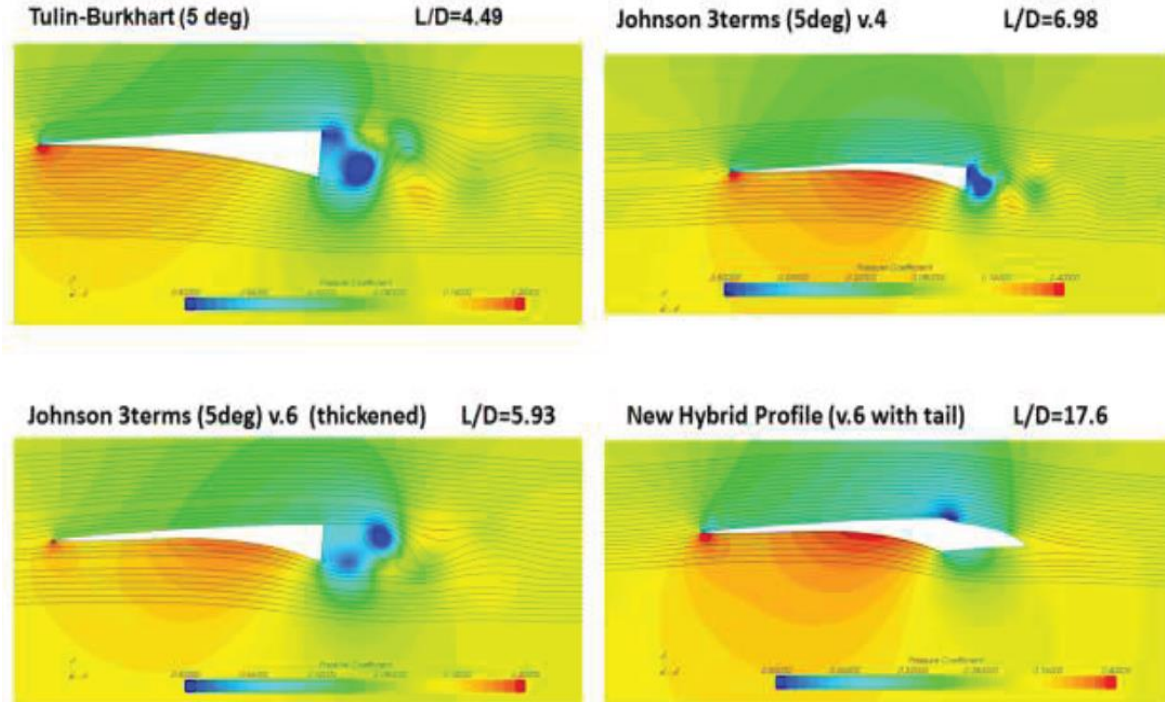


Figure 36: 2D Profiles of Super Cavitating Hydrofoils at Cavitating Speeds

The development of this SPSC hydrofoil continued with cavitation tunnel testing to further prove the legitimacy of the added L/D benefits from the new design. The tests were completed at the Technical University of Berlin (TUB) in 2012. The series of tests at TUB consisted of running experiments with different submerged lengths, ranging from 175 mm to 350 mm and different flow speeds, ranging from 6 m/s to 10.5 m/s. The report from the TUB test presented a set of empirical equations to determine the force coefficient in the z-direction and x-direction, lift and drag respectively. The third equation solves the wetted surface area based on a chosen submerged length. Using these equations as a design guide, the relative size of hydrofoil needed for the Model 5631 Dynaplane could be designed.

$$C_{F_z} = \frac{L}{0.5\rho_{water}v^2 A_{hydrofoil}}$$

$$C_{F_x} = \frac{L}{0.5\rho_{water}v^2 A_{hydrofoil}}$$

$$A_{hydrofoil} = 0.1768 \left( \frac{L_{Sub.Length}}{1000} \right)^2 + 0.0613 \left( \frac{L_{Sub.Length}}{1000} \right)$$

For an appropriately sized stern hydrofoil to provide 10% of the total weight, the required area of the hydrofoil's lifting surface,  $A_{hydrofoil}$ , was solved assuming the design lift coefficient of 0.3 and lift force,  $L = 0.1W$ , where  $W = 375$  lb.



$$A_{Req.hydrofoil} = \frac{L}{C_{Fz} 0.5 \rho_{water} v_A^2}$$

$$A_{Req.hydrofoil} = \underline{\underline{0.004 \text{ m}^2}} \text{ (area required for each foil)}$$

Once the required area for each foil was calculated, a scaling factor, SF, had to be calculated. The design draft for calculating the area of the original hydrofoil was 250 mm; therefore, we can say  $A_{Orig.hydrofoil} = 0.029 \text{ m}^2$

$$SF = \sqrt{\frac{A_{Req.hydrofoil}}{A_{Orig.hydrofoil}}} = \underline{\underline{0.376}}$$

The hydrofoil design was then imported into Rhino 3D for rendering. Applying the scaling factor, the geometry was exported as a .STL file for use in STAR-CCM+. Comparison of the flow and formation of the ventilation is compared in Figure 37 and Figure 38. A VOF comparison of the flow shows the distinction between the ventilated air along the wetted surface. The CFD model accurately captures the formation of ventilation and it is interesting to see the strakes that form on the top surface. The strakes are the localization of the reduced pressure areas to the point that it reaches below vapor pressure of water and allows for water vapor bubbles to form. CFD testing gave confidence that the model would accurately predict the lift forces of the SPSC hydrofoils used in the new Dynaplane design.

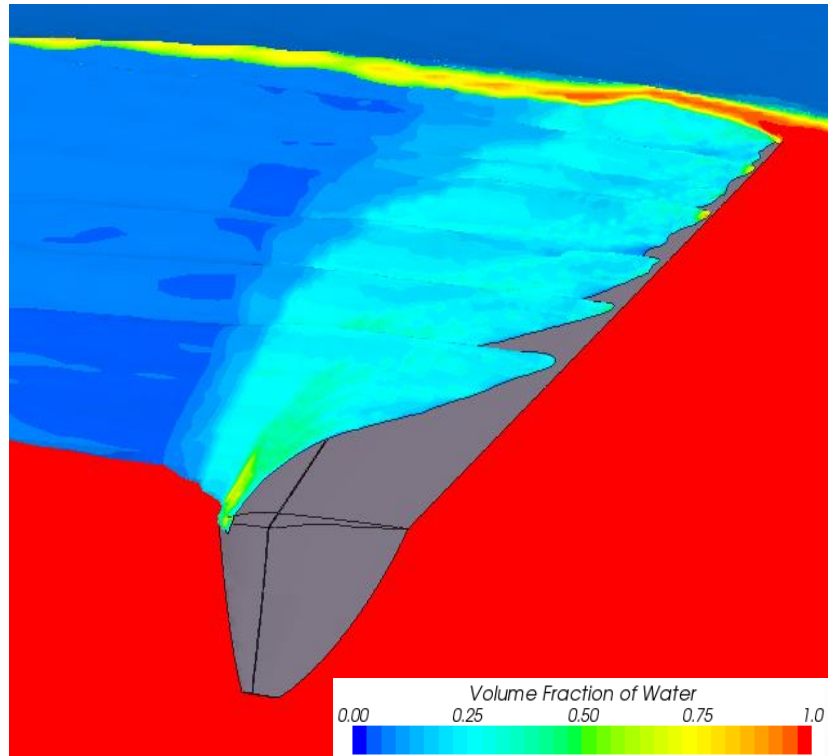
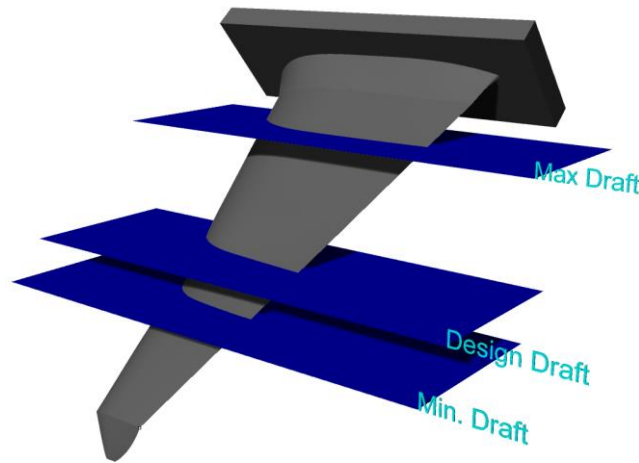


Figure 37: Ventilation Formation from CFD Simulation



**Figure 38: Ventilation Formation from Cavitation Tunnel Tests**



**Figure 39: Design Draft for Tested Submerged Lengths of Brizzolara's Hydrofoil**

Now that the proposed stern stabilizer has been designed, the exact placement on the afterbody became of particular importance. In Clement's Dynaplane design, the V hydrofoil is placed directly aft of the transom. However, for practical applications two SPSC hydrofoils must be placed on both sides of the afterbody and as close to the transom as possible. This is done due to ensure maximum trimming moment from the two aft hydrofoils. A more detailed explanation of these moment contributions from the aft two lifting surfaces is provided in the next chapter. With the longitudinal position decided upon, the next task was to determine how to ensure the right submerged length for each of the hydrofoils. The answer to this uncertainty consists of predicting

the wake geometry of the free surface created by the stepped hull. By understanding the wake geometry of the cambered step, the design draft can be achieved.

After a search of relevant literature on stepped hulls and predictions of their wake geometry, two potential papers were found, a 1948 report by Korvin-Kroukovsky, Savitsky, and Lehman called “Wave Contours in the Wake of a 20-degree Deadrise Planing Surface,” and a 2009 report by Savitsky and Morabito called “Surface Wave Contours Associated with the Forebody Wake of Stepped Planing Hulls.” The 1948 report is intended for use of planing surfaces used on seaplane hulls; and it lacks applicability with trim angles less than 6 degrees. Even though the deadrise angle was sufficient for our analysis, it did not provide the needed trim angle data for which our stepped hull operates. Therefore, the Savitsky and Morabito paper was chosen. Their analysis is a very recent study focusing particularly on stepped planing hulls at deadrise angles of 10, 20 and 30 degrees. Furthermore, it was beneficial to hear the need for more research in the prediction of wake geometry for stepped hulls using computational models, “The present report provides experimental data that can be used by researchers interested in developing a CFD solution for the planing hull wake geometry” (Savitsky and Morabito, 2009).

### 3.4 Wake Profile Comparison from Empirical and Computational Methods

In Savitsky and Morabito’s 2009 paper, an empirical approach led to the development of a set of equations where the designer can predict the height of the surface contour aft of a stepped hull. This becomes important in solving the dynamic lift pressures associated with the afterbody lifting surface. Knowing the exact location of the free surface generated by a stepped hull leads to the proper submerged length of the aft lifting surface. Savitsky and Morabito describe the benefits of this knowledge especially when using a stern, submerged hydrofoil in Figure 40.

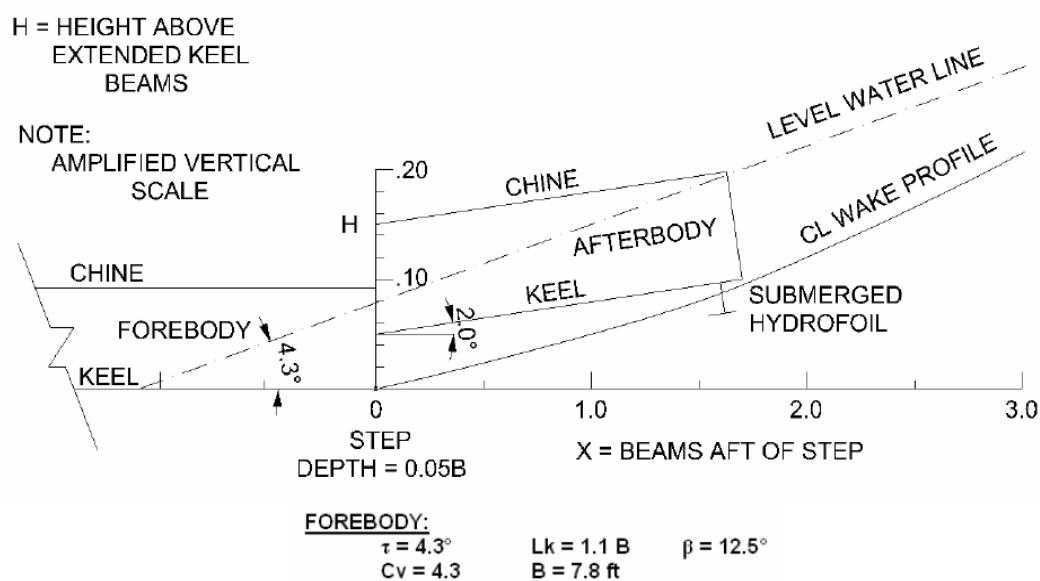


Figure 40: Stepped Hull Afterbody Orientation with a Stern, Submerged Hydrofoil



There exists a need to understand the wake geometry profile from a cambered step. No literature exists on predictions methods, similar to Savitsky and Morabito, for surface wave contours aft of a cambered step. For this reason, an analysis is conducted comparing the conventional transverse step from Savitsky and Morabito with two types of swept back steps, with camber and no camber. To ensure applicability for each specific hull type, Table 5 lists the limits of parameters of their study.

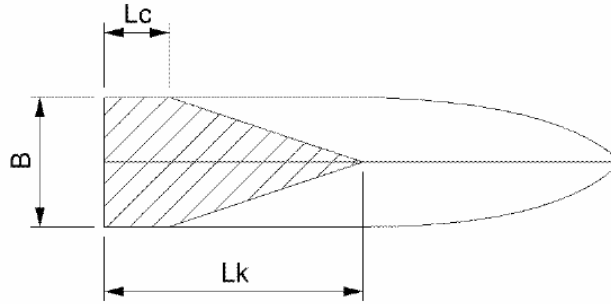


Figure 41: Wetted Area for Parameter Calculation

X: Distance aft of transom, [beams]      B: Beam  
 $L_k$ : Wetted keel length, [beams]       $L_c$ : wetted chine length  
 $C_v$ : Speed coefficient,  $v/\sqrt{gB}$   
H: Height of wake profile above extended keel,  $\frac{1}{4}$  buttock,  $\frac{1}{8}$  buttock, or full beam [beams]

$$\begin{aligned} 10 \text{ deg} &\leq \beta \leq 30 \text{ deg} \\ 3 \text{ deg} &\leq \tau \leq 5 \text{ deg} \\ L_k &\leq 0.10 \tan\beta/\pi\tan\tau \\ 0.017L_k\tau^{1.5} &\leq 0.18 \\ 4.0 &\leq C_v \leq 8.0 \\ X &\leq 3B \end{aligned}$$

Table 5: Application Limits for Savitsky and Morabito's Empirical Method

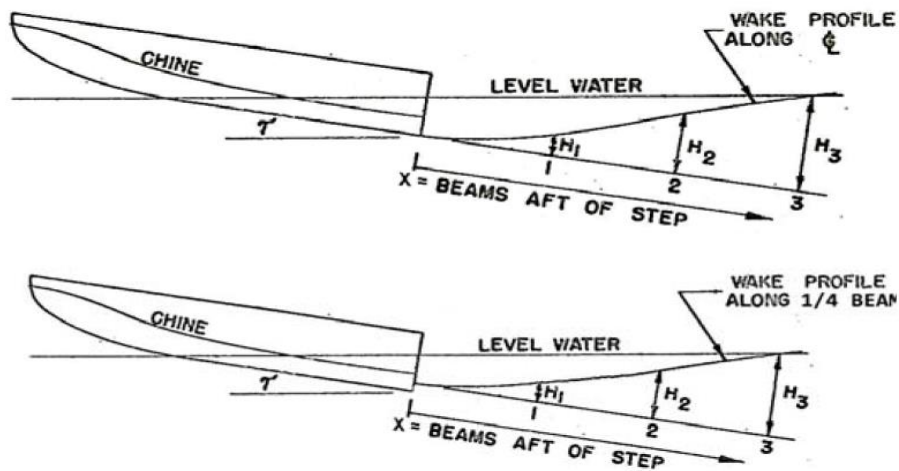
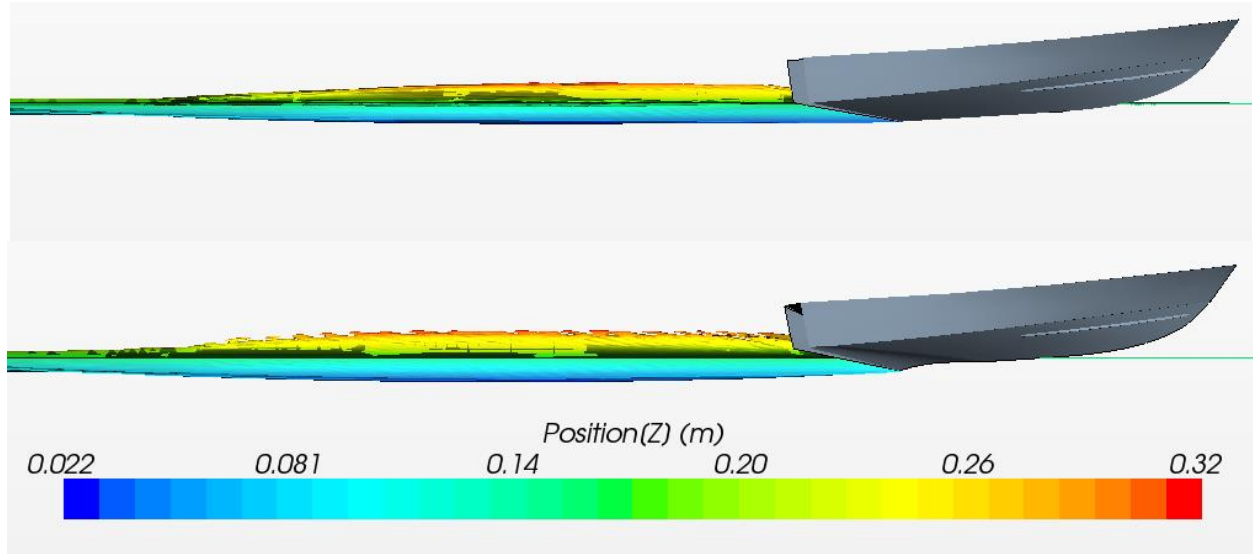


Figure 42: Reference Longitudinal Axis for Wake Profile



**Figure 43: Wake Profile Depictions, No Camber (top) vs Camber (bottom)**

With the Model 5631 hull parameters meeting all limits of application stated by Savitsky and Morabito, the comparison of wake geometry could continue. The two empirical equations for calculating longitudinal surface wake profiles are expressed below. The 1/8 buttock line and Full Beam buttock line are used in the computational formulation since the empirical method does not provide geometry at that distance from centerline; however, the empirical data is used for comparison of validity of the computational results. They are important because locating the correct position of the stern hydrofoils is necessary to achieve the designed waterline.

#### Centerline Profile

For  $\beta = 20$  deg

$$H = 0.17[2.0 + 0.03 L_k \tau^{1.5}] \sin \left[ \frac{\pi}{C_v} \left( \frac{X}{3} \right)^{1.5} \right]$$

#### 1/4 Beam Buttock

For  $\beta = 20$  deg

$$H = 0.17[0.75 + 0.03 L_k \tau^{1.5}] \sin \left[ \frac{\pi}{C_v} \left( \frac{X}{3} \right)^{1.5} \right]$$

To determine the surface wave contour of the stepped hull from CFD, six simulations were created. The first three tests consisted of running a traditional, swept back step, at three different trim angles, 3.5, 4.0, and 4.5 degrees and at  $F_n V = 5$ . The second set of tests consisted of running the cambered step, at the same trim angles and speed. The goal of these six tests is to determine the change in wake geometry caused by the cambered step and then compare the traditional swept back step with the transverse step tested by Savitsky and Morabito. Analysis of these different stepped hulls is intended to provide future researchers with data to make informative decisions based on the height of the wake profile at specific lengths aft of the step. Detailed plots on the following pages show the differences between these wake profiles at the three trim angles tested.

It was found that the swept back steps, whether camber or no camber, had a shallower profile compared to a conventional transverse step. The centerline wake profile of the swept back steps began at a steeper slope than the empirical method predicted; however, as you move athwartships, the free surface had a shallower slope, as shown in Figure 46. The benefit of this characteristic for the swept back design is decreased spray. As you start to incorporate the cambered step of the Dynaplane design, you begin to see more benefits of this design. When comparing Figure 44, the cambered planing surface forces the fluid flow down and aft from the trailing edge of the step, depicted in Figure 44. This allows for the fluid to be forced away from the afterbody, further preventing added wetted area and allowing the designer to create an afterbody with more volume.

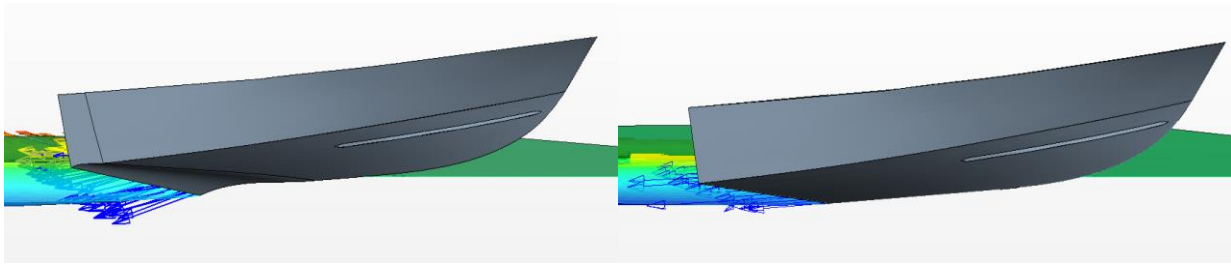


Figure 44: Flow Direction for Camber and No Camber

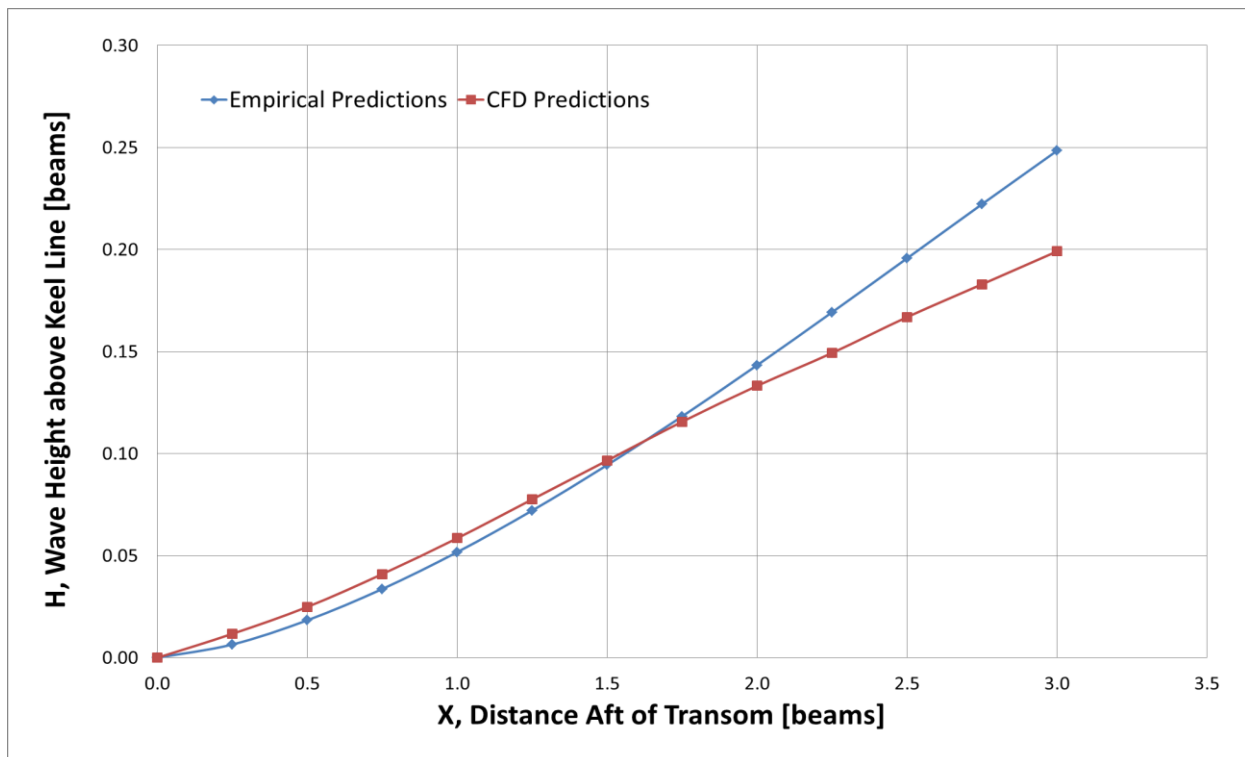


Figure 45: Wake Profile Comparison of Transverse Step vs Swept Back Step at Centerline, 3.5 deg Trim

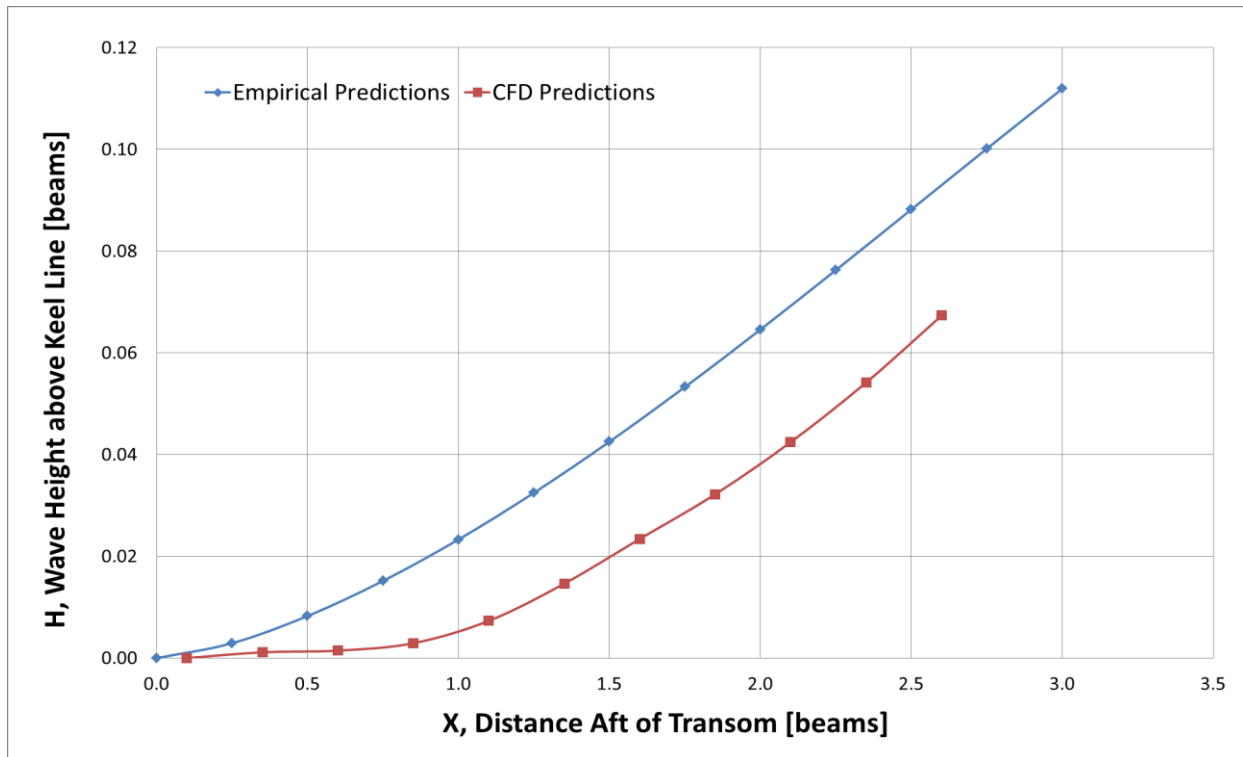


Figure 46: Wake Profile Comparison of Transverse Step vs Swept Back Step at 1/4 Buttock, 3.5 deg Trim

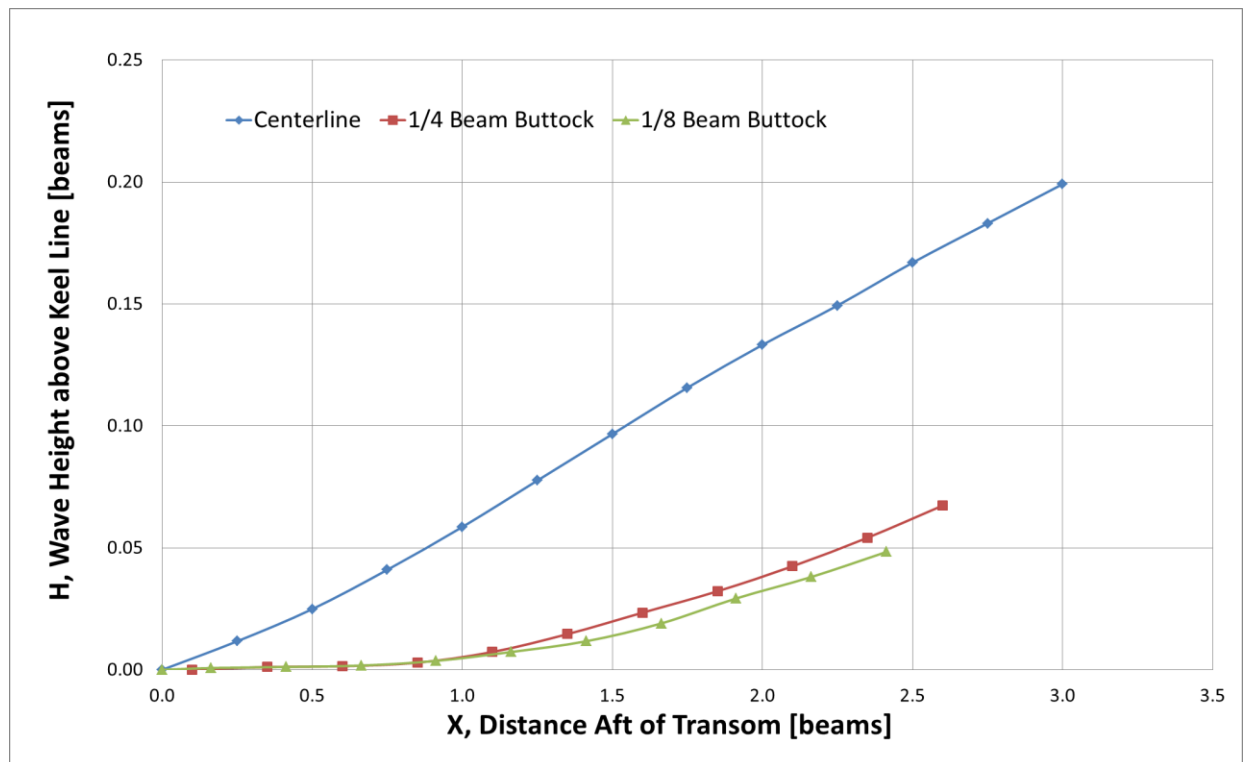


Figure 47: Wake Profile for Swept Back Step (No Camber) at 3.5 deg Trim

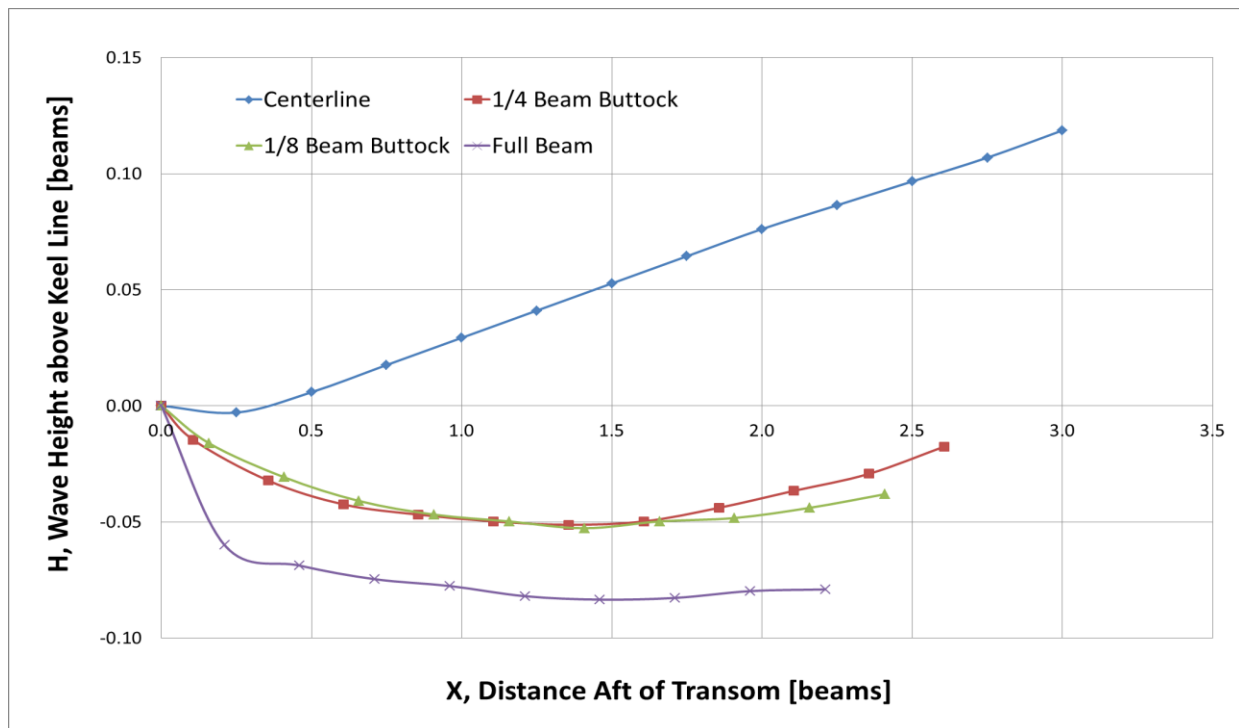


Figure 48: Wake Profile for Cambered Step at 3.5 deg Trim

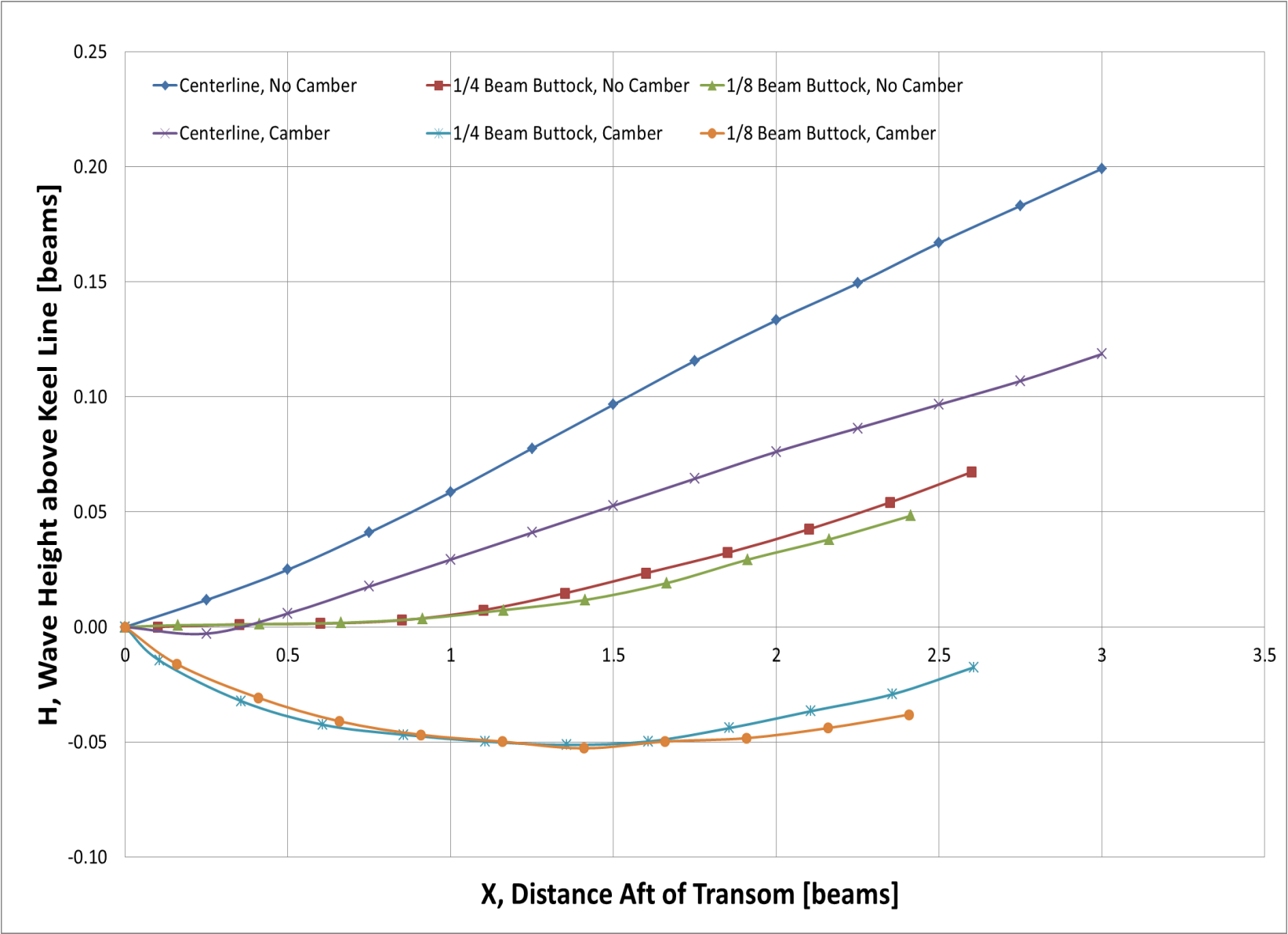


Figure 49: Wake Profile Comparison of Steps with Camber and No Camber at 3.5 deg Trim

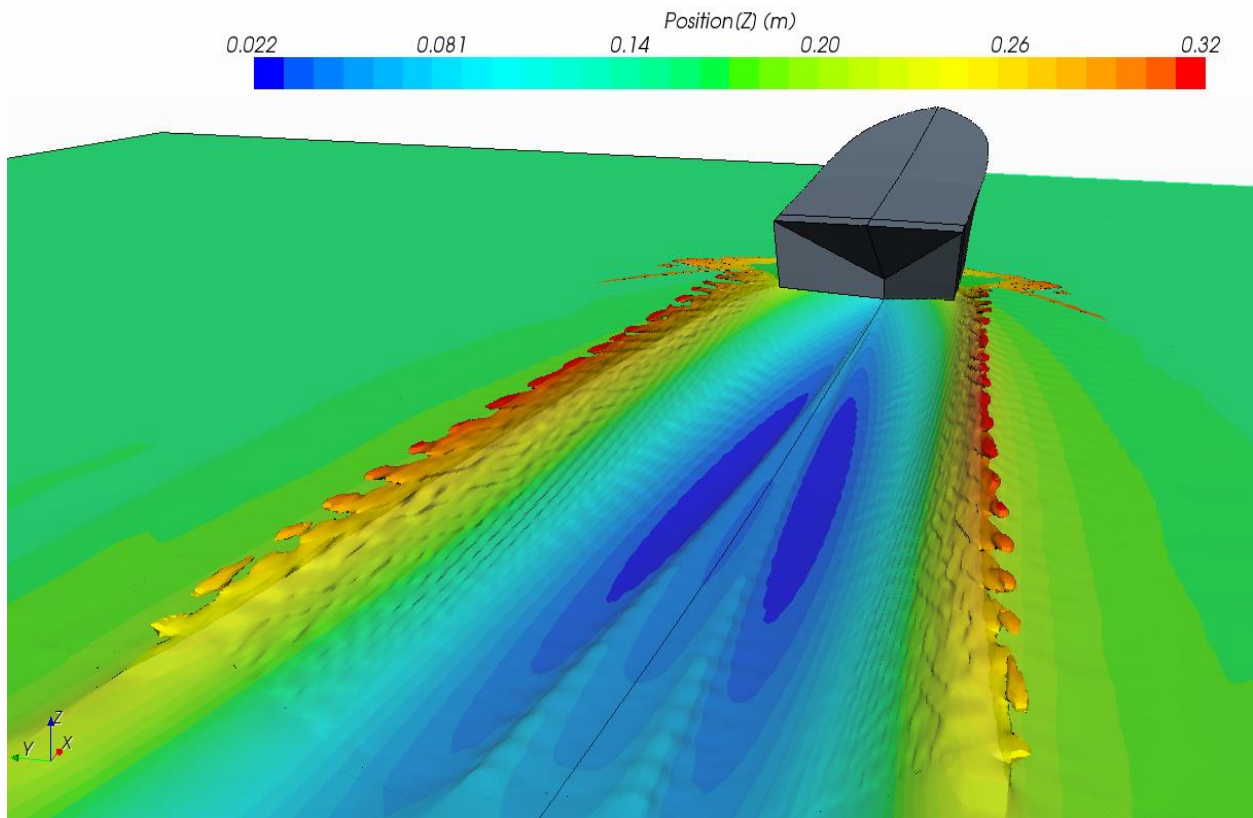


Figure 50: Perspective View of Wake Profile from Cambered Step at 3.5 deg Trim

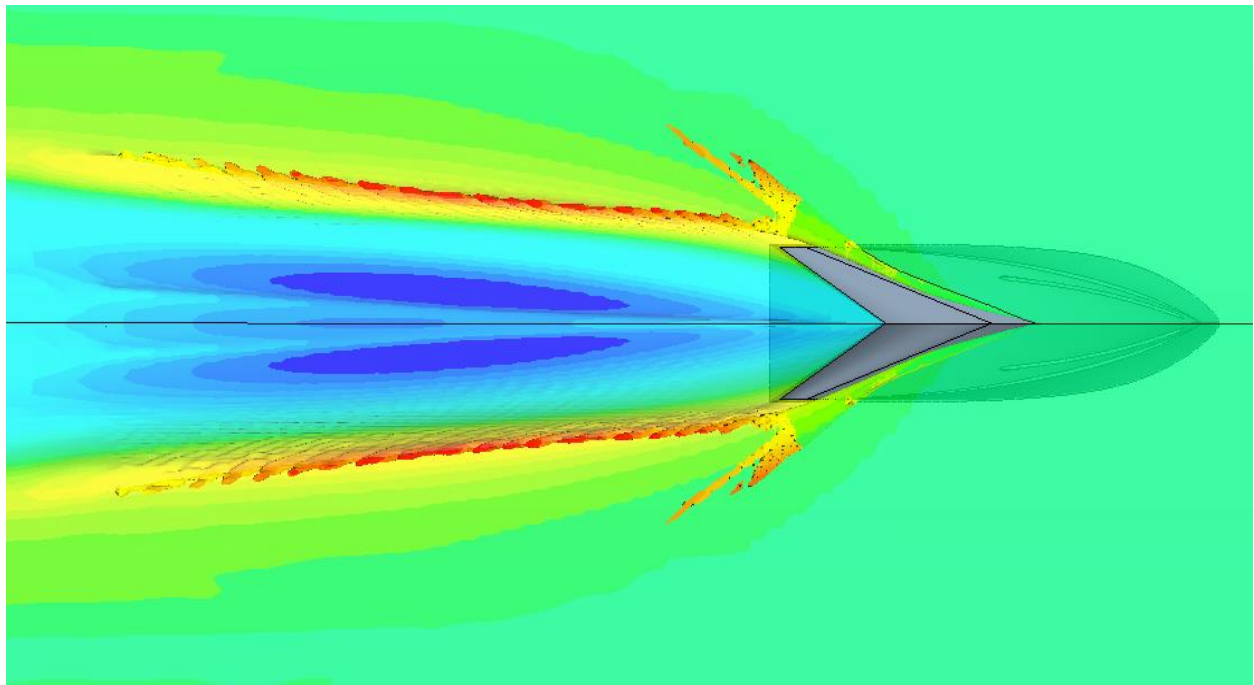
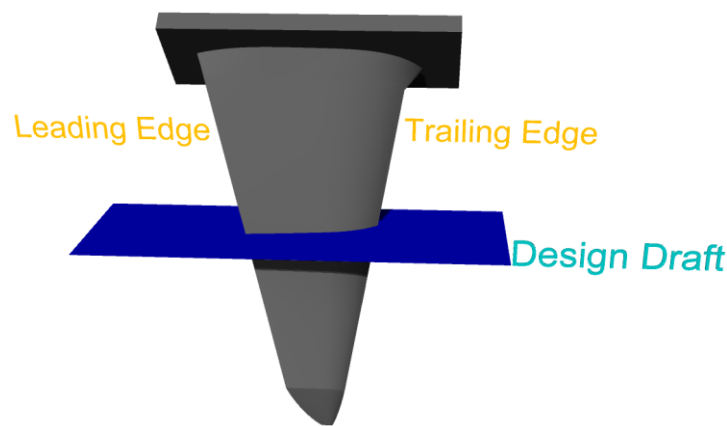


Figure 51: Bottom View of Wake Profile from Cambered Step at 3.5 deg Trim

The wake profile comparison gave great insight to the benefits of a swept back step. When the cambered planing surface is incorporated into the step, the advantages become even greater. With the comparison analysis complete, the wake profile is now accurately predicted using both empirical and computational methods. However, since the empirical method does not provide desired beam locations; the computational model was used for placement of the SPSC hydrofoil.

Keeping the same overall length of Model 5631, the hydrofoil was placed on the hull considering longitudinal, vertical, and transverse positions. The longitudinal position was limited by the transom; therefore the hydrofoil was placed 1.4 meters aft of the centerline trailing edge. With this in mind, the vertical and transverse positions were determined to be interdependent. Next, the hydrofoil was placed to capture the correct design waterline, , and to maximize the beam area for ensure transverse stability. The final hydrofoil position is shown in Figure 53.



**Figure 52: Rendering of SPSC Hydrofoil Used**

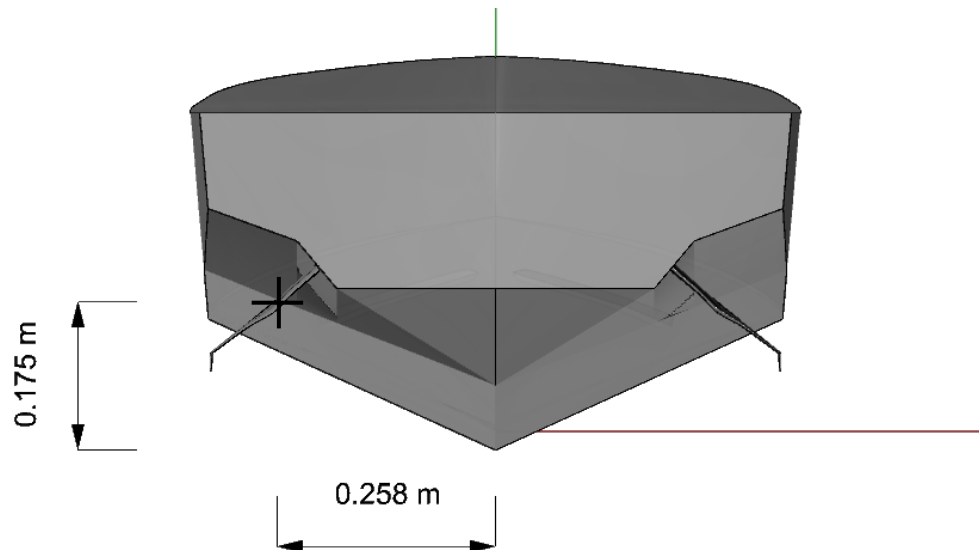


**Figure 53: Vertical and Transverse Positioning of SPSC Hydrofoil's Design Draft**



### 3.5 Final Design

After completion of Clement's Dynaplane design and implementation of the new hydrofoil design, the finished hull form was constructed in Rhino 3D for final rendering, Figure 54. The primary characteristics are listed in Table 6 below. It is important to note, the planing trim at  $F_nV = 5$  is designed to be 3.5 degrees. Resistance calculations for lower speeds, less than 20 knots, were not considered for this design. A recommendation for designing further is to investigate the power required to reach hump speed since the design of the afterbody did not take that into consideration.

Model 5631 Dynaplane Design	
<b>LOA</b>	3.3 m
<b>Lp</b>	3.2 m
<b>LWL</b>	3 m
<b>Bpx</b>	0.68 m
<b>Bf</b>	0.42 m
<b>T (with step)</b>	0.18 m
<b>T (without step)</b>	0.16 m
<b>Weight</b>	170 kg

Table 6: Primary Characteristics for the Model 5631 Dynaplane Design

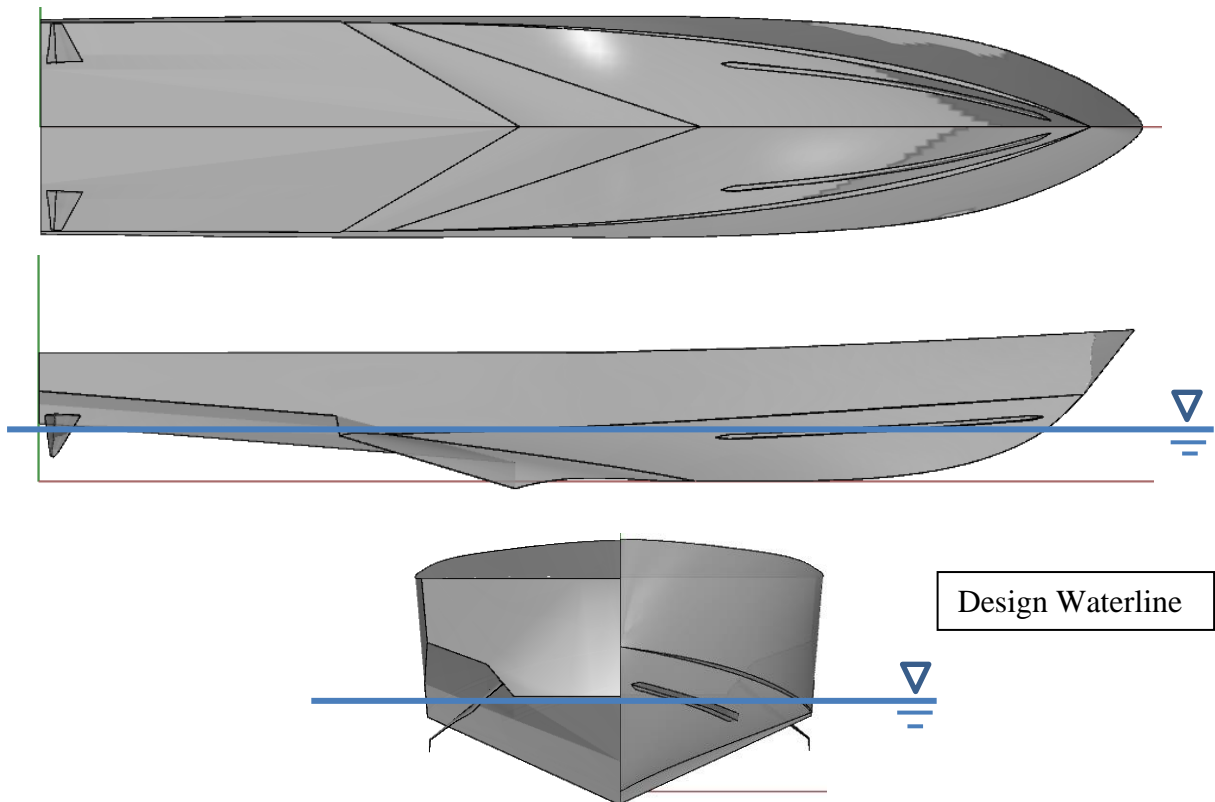


Figure 54: Plan, Profile, and Body Plan Views of Model 5631 Dynaplane Design

## Chapter 4 – Hydrodynamic Analysis

### 4.1 Stability Concerns

The transition from displacement to planing hulls introduces many uncertainties due to the high speed nature of the dynamic forces. The recommended approach to these issues is to solve the known problems by use of the hull's design and then provide operating instructions or active controls to mitigate the onset of any dynamic instability. Dynamic instabilities become more unknown and harder to predict at high speeds. The design of the Model 5631 Dynaplane configuration begins with calculating the planing hull's stability in equilibrium. Then predict the dynamic stability using results from computational modelling and existing literature from Clement, Blount, Codega, and Celano.

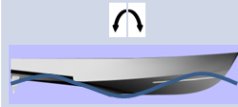
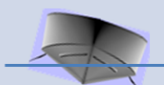
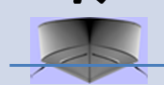
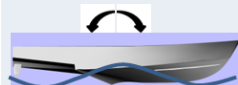


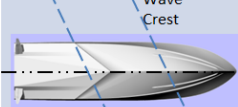


	Hydrostatic <span style="font-size: 1.2em;">→</span> Hydrodynamic			
	Displacement	Semi-Displacement	Planing	
	Increasing Froude Number <span style="font-size: 1.2em;">→</span>			
Transverse	Transverse Hydrostatics  $GM_T \leq 0$	Loss of $GM_T$ Due to Wave Effect 	Roll Instability Non-Zero Heel Non-Oscillatory 	"Chine Walking" Dynamic Roll Oscillation 
Longitudinal	Longitudinal Hydrostatics  $GM_L \leq 0$	Loss of $GM_L$ Due to Wave Effect 	Trim Instability Bow Drop Non-Oscillatory 	"Porpoising" Dynamic Pitch-Heave Oscillation 
Combined	Combined  $GM_T \leq 0$ $GM_L \leq 0$	Combined Wave Effect 	Broach Non-Oscillatory 	"Corkscrew" Pitch-Yaw-Roll Oscillation 

Figure 55: Planing Hull Dynamic Instabilities

In Figure 55, the different types of dynamic stability are listed and illustrated showing instability at high speeds with regards to transverse, longitudinal, and combined motions (Blount and Codega, 1992). Each motion category is just as important as the other; however, this thesis will analyze only two types of longitudinal instability, bow drop and porpoising. The Dynaplane design has inherent pitching moment issues as described by Clement. It cannot balance on the planing surface alone; it also requires a stern stabilizer to maintain trim angle. The design of the stern stabilizer, or aft hydrofoil in this design, becomes an important contributor to maintaining stability of the planing hull. The SPSC hydrofoil used in the Model 5631 Dynaplane has a tapered lifting surface, which provides a level of damping as the hull pitches back and forth. The size and scale of the hydrofoil along with its taper degree offer some insight into these damping

effects. This thesis does not cover those effects but it is recommended. In Figure 56, the two types of longitudinal instabilities are shown. Bow drop is a non-oscillatory phenomenon that occurs when the pitching moment becomes unstable at moderate speeds. This can either happen due to bow steering from a forward pitching moment or progressively high quantities of spray; all of which result in a sudden loss of running trim. Porpoising is the oscillation of dynamic pitch and heave. This phenomenon can be caused by the LCG being too close longitudinally to the main planing surface and thereby creating an exchange of pitching moments, whether positive or negative, usually occurring at moderate to higher speeds. Model 5631 Dynaplane will be analyzed for such effects using recommended prediction methods by Blount, Celano, and Codega.

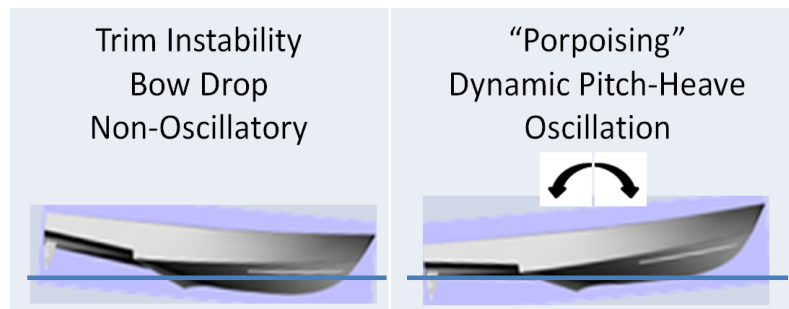


Figure 56: Dynamic Instabilities for Model 5631 Dynaplane Configuration

## 4.2 Previous Methods for Predicting Dynamic Stability

When analyzing high speed vessels, understanding the dynamic forces involved is needed for overall stability of the hull. From small to large displacement vessels, hydrostatic forces dominate and stability can be accomplished by analyzing intact conditions at a given sea state, wind conditions, and loading. However, as you increase in speed to  $F_nV > 3$  where dynamic forces begin to dominate, the unpredictability of the hull must be considered. For this reason, continued research has been devoted to understanding and predicting when dynamic instabilities occur. Preliminary research conducted by Savitsky, Clement, Blount, Cohen and Codega provided specific dynamic instability occurrences while model testing.

As you increase in speed, the prevalence of instability becomes apparent. For high speed vessels, this is an obvious concern. There are several literature papers on the onset of dynamic instability and the hull geometric considerations for avoiding occurrences. However, there exists a need to further model test data in the research area and more accurately predict dynamic instability not only from an empirical approach but also a theoretical approach as well. In 1998, Midshipman (1/C) Tullio Celano III analyzed a particular dynamic instability for his Trident Scholar report. He chose to study porpoising. His analysis studied planing hulls of high deadrise angles of 15 to 25 degrees. Furthermore, he developed a critical trim angle equation and design regimes to avoid porpoising. His methods were applied to the design of this thesis.

A designer can approach solving dynamic stability two ways, implement active controls or design a hull form which passively corrects for the onset of any dynamic instability. Examples of such active controls are trim tabs or interceptors. Passive measures are dictated by empirical methods and their predictions for when a planing hull may encounter dynamic instability.

## 1. Savitsky Porpoising Prediction

The data in this example is taken from model tests from Savitsky's 1964 report, and it considers porpoising limits for a range of deadrise angles. Based on a running trim angle, LCG, speed, and hull geometry, Figure 57 was created which determines a porpoising limit line based on a planing hull's trim angle and a lift coefficient parameter.

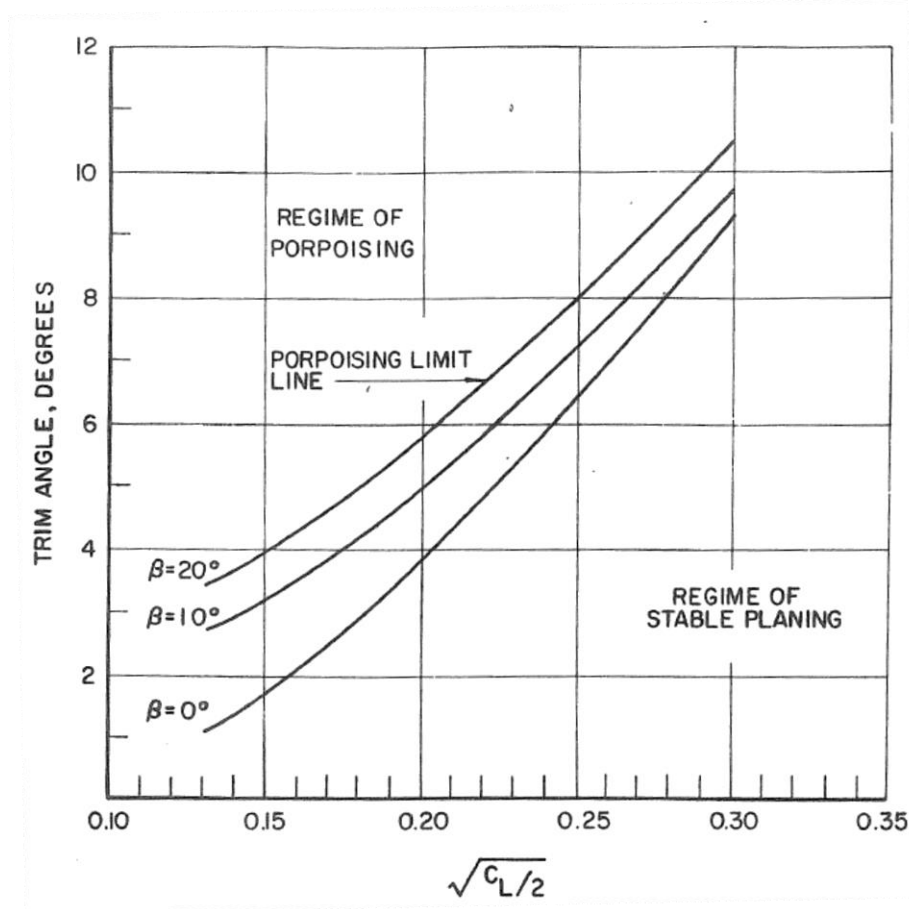


**Figure 57: Dynamic Transverse Instability (DTI) Regions**

The new Dynaplane design presented in this thesis takes advantage of the lift coefficient parameter. By incorporating a cambered step, a higher lift coefficient effectively gives the planing hull a larger regime of stable planing. This approach is different than designing to meet a running trim that keeps the planing hull stable. Figure 57 gives approximations for conventional planing hulls; however it provides insight for the Dynaplane design on how longitudinal stability can be achieved. Later in this chapter, the effects of the contributions from lift and drag on the Dynaplane's lifting surfaces reveal the nonlinearities in the overall dynamic stability.

## 2. Blount and Codega Dynamic Instability Prediction

This analysis can only be applied to hard chine planing hulls and not stepped hulls. There are several factors affecting dynamic stability, which include hull geometry, speed, and motion freedom. Blount and Codega state, "The technology and design criteria to assure that a craft will be dynamically stable are evolving, but data has yet to become widely available and design standards are not universally accepted."

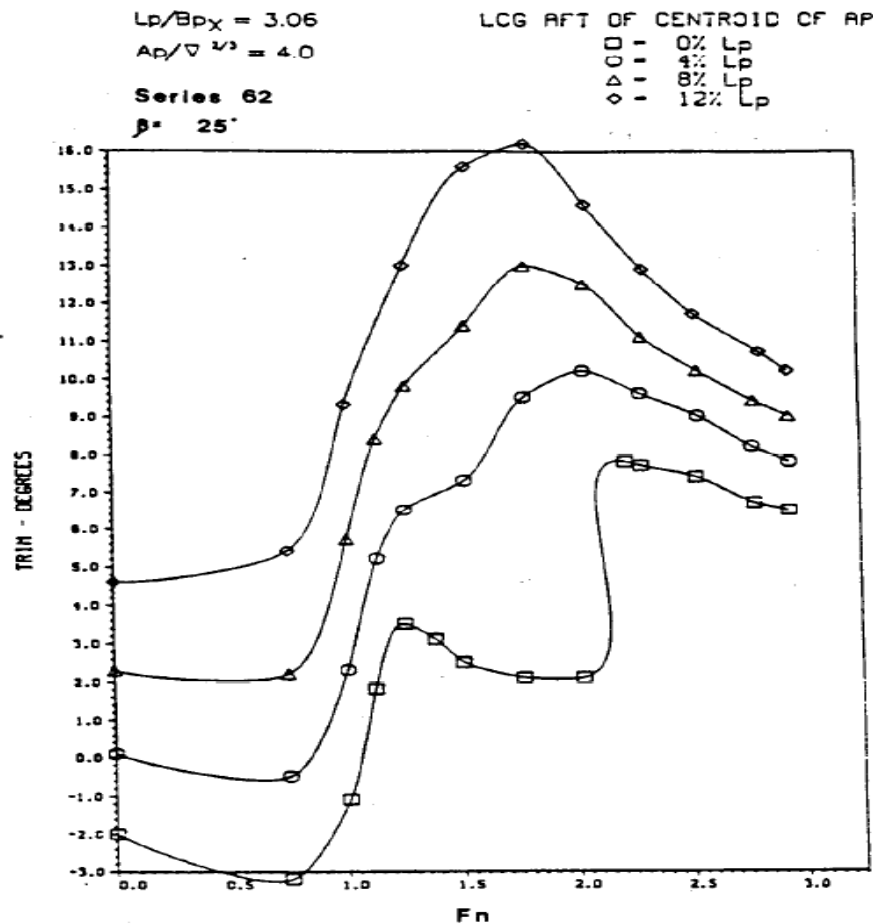


Figure 58: Trim versus Speed Curve for Predicting Bow Drop

Their paper presents Figure 58, which illustrates the change in trim with respect to increasing speed. This figure covers a range of 4 different LCG locations. They determined that the planing hulls that possess an inflection in their change in trim at low speeds exhibit dynamic instabilities. This inflection point becomes evident when the LCG is moved forward with a decreased running trim angle. However at higher speeds, this inflection in the running trim curve does not show itself (Blount and Codega, 1992). Their analysis gives great insight to predicting the stability of planing hulls. A researcher must not only look at speeds above  $F_n V=3$ , but also at lower speeds because they predict the possibility of dynamic instability.

### 3. Celano Critical Trim Angle Calculation

Using Celano's critical trim angle formula, it is shown that the deadrise and lift coefficient are contributors to the stability of the planing hull.

$$\tau_{crit} = 0.1197 \beta^{0.7651} \exp \left( 15.7132 \sqrt{\frac{C_{L\beta}}{2}} \beta^{-0.2629} \right)$$

Celano's critical trim equation is only valid for deadrise angles tested in his experiments, between 15 and 20 degrees. Therefore, it is appropriate to use his equation in the dynamic stability prediction of the Model 5631 reference hull, using the  $C_{L\beta}$  calculated in Chapter 3.

$$\tau_{crit} = \underline{\underline{3.8 \text{ degrees}}}$$

For higher deadrise angles, the regime for stable planing is increased. The calculated critical trim angle reveals that using the reference hull's parameters gives smaller angle than anticipated. However, by conducting model tests at the threshold region between stability and instability, the cause of porpoising and bow drop can possibly be determined in detail for the new Dynaplane design.

### 4.3 Model 5631 Dynaplane Pitch and Heave Moment Considerations

When analyzing the dynamic stability of a planing hull, several factors are considered including hull geometry, speed, and freedom of motion. The motivation behind this hydrodynamic analysis is to contribute to the data collected for determination and possible follow-on research of stability considerations for this new Dynaplane design. The hydrodynamic analysis began by calculating two states of equilibrium, static and quasi-static. First, theoretical calculations determined the required lift forces and the longitudinal positions of the center of pressure for both the cambered planing surface and the stern hydrofoils. These values were then compared to predictions made through the computational model simulations. In Figure 59, the lift forces are shown relative to the center of gravity or weight of the Model 5631; their relative distances from the LCG are also shown.

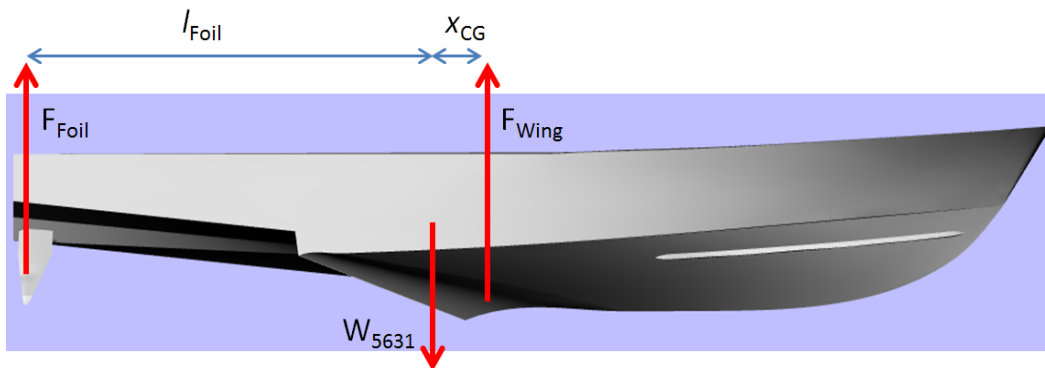


Figure 59: Free Body Diagram of Model 5631 Dynaplane

With the center of pressure location of the cambered planing surface being given by Clement and the hydrofoils being placed as far aft as possible, the value of  $x_{CG}$  could then be found for the sum of moments equal to zero. A trim by the bow, or bow down effect, is caused by a positive trimming moment; and a trim by the stern is caused by a negative trimming moment. This refers to a positive clockwise moment. A positive trimming moment is preferred because the damping effects or counter-trimming moment from the cambered planing surface, or wing, are larger.

$$\Sigma M = -F_{Wing}x_{CG} + F_{Foil}l_{Foil}$$

Given that  $W = 170$  kg,  $l_{Foil} = 1.2$  m,  $F_{Foil} = 83.4$  N,  $F_{Wing} = 750.6$  N, and ensuring  $\Sigma M = 0$ , it can be determined that the distance from the LCG to the center of pressure of the cambered planing surface,  $x_{CG} = 0.134$  m. A computational model at the designed trim angle of 3.5 degrees was ran allowing the model to freely heave, and simulate a speed of  $F_nV = 5$ . The half hulls were prepositioned 0.098 m [+z] to converge quicker (Metcalf et al, 2005). The results from this computational model simulation were then compared to the theoretical moment balance to ensure equilibrium. Further tests were conducted at 4.0 and 4.5 degree trim angles with freedom to heave.

Model 5631 Dynaplane, STAR-CCM+ Run 1: [Trim: 3.5 deg; Heave: Free,  $F_nV = 5$ ]

LCG (42%)	1.28 m
VCG	0.155 m
TCG	0 m
Displacement	375 lb

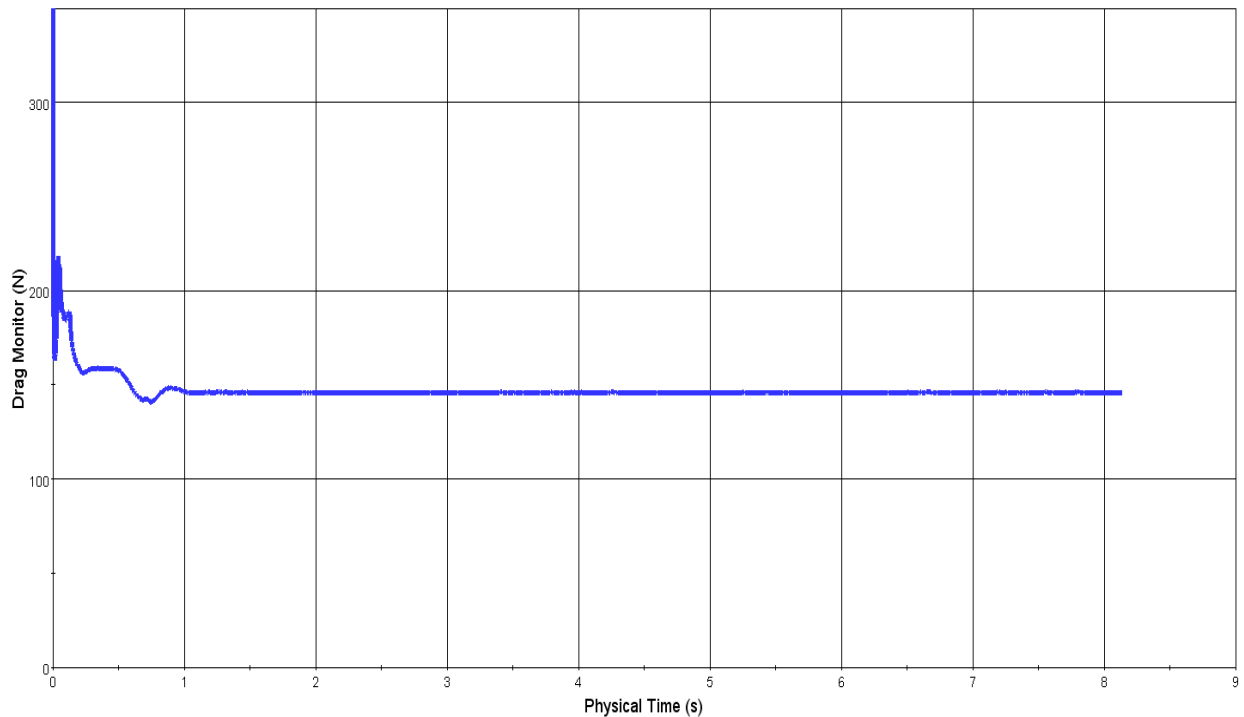
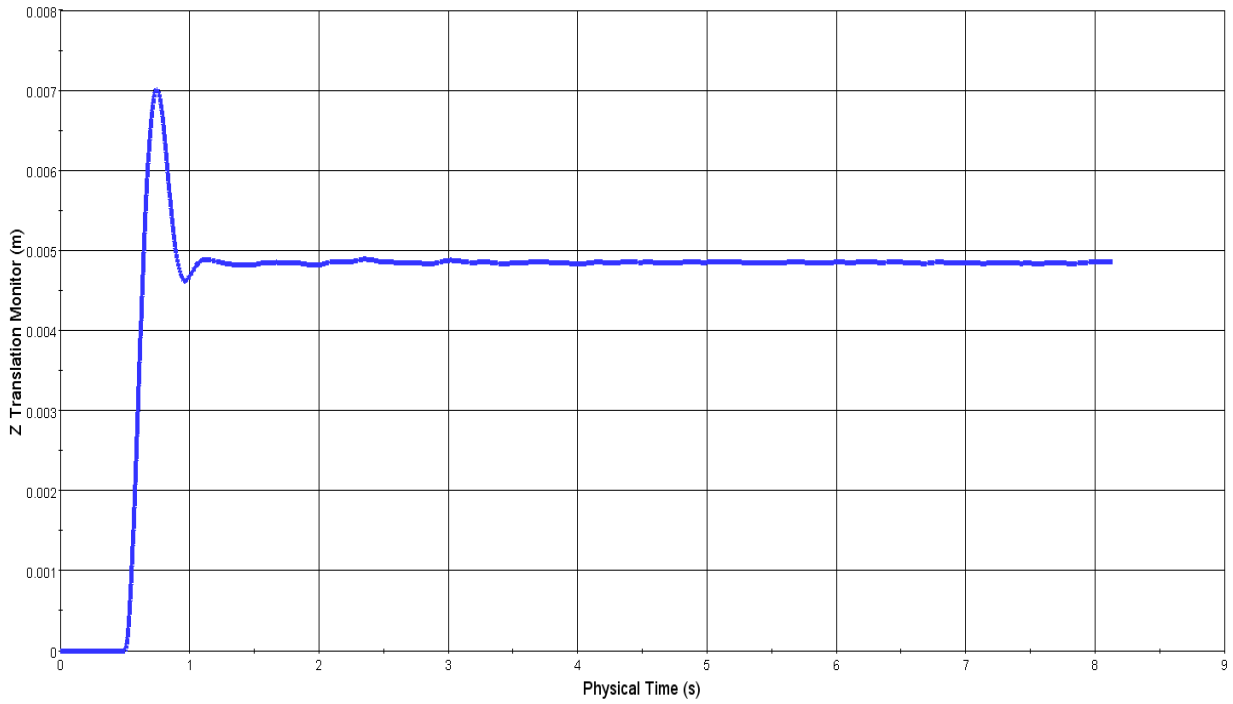
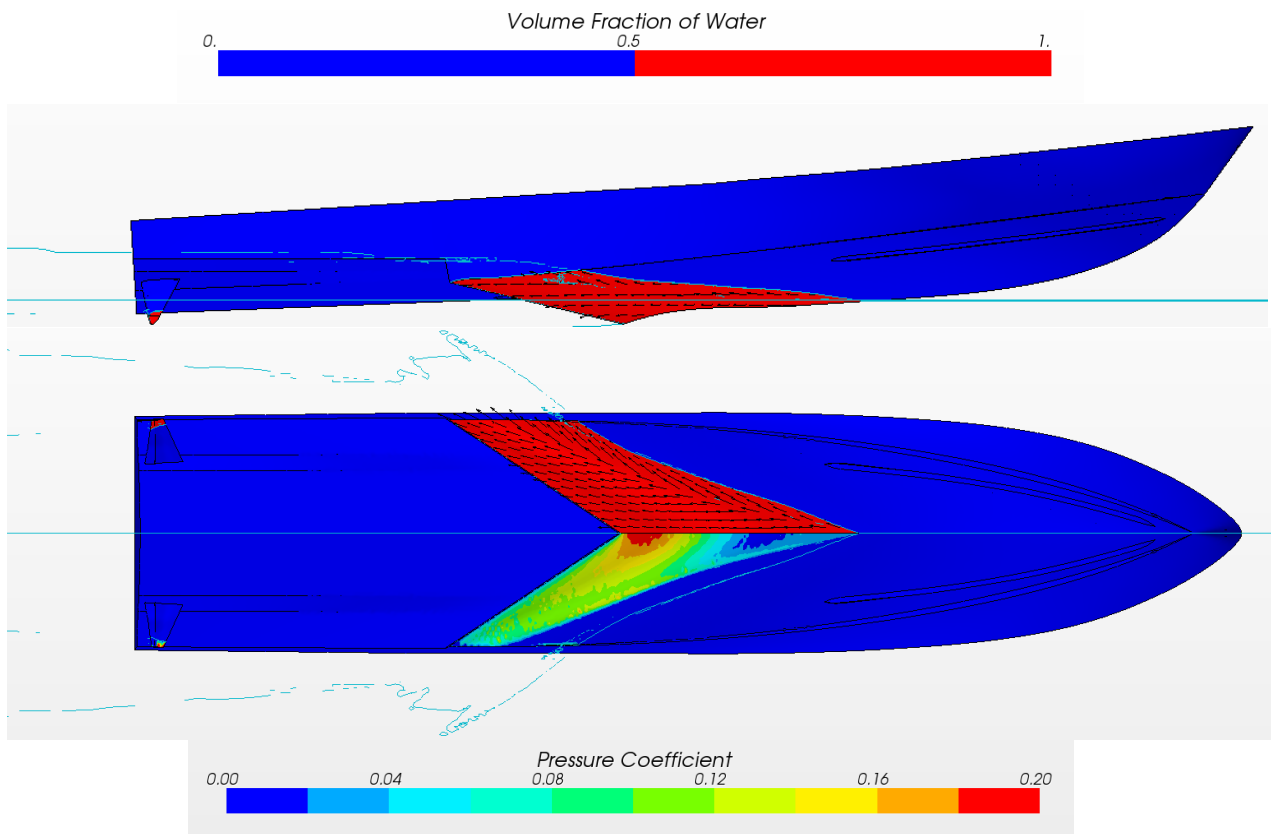


Figure 60: Drag Force Component of Model 5631 Dynaplane, Run 1



**Figure 61: Heave (Z Translation) Monitor for Model 5631 Dynaplane, Run 1**



**Figure 62: Pressure Coefficient and Volume Fraction of Water @ 3.5 deg Trim and  $FnV=5$**



Model 5631 Dynaplane, STAR-CCM+ Run 2: [Trim: 4.0 deg; Heave: Free, FnV = 5]

LCG (42%)	1.28 m
VCG	0.253 m
TCG	0 m
Displacement	375 lb

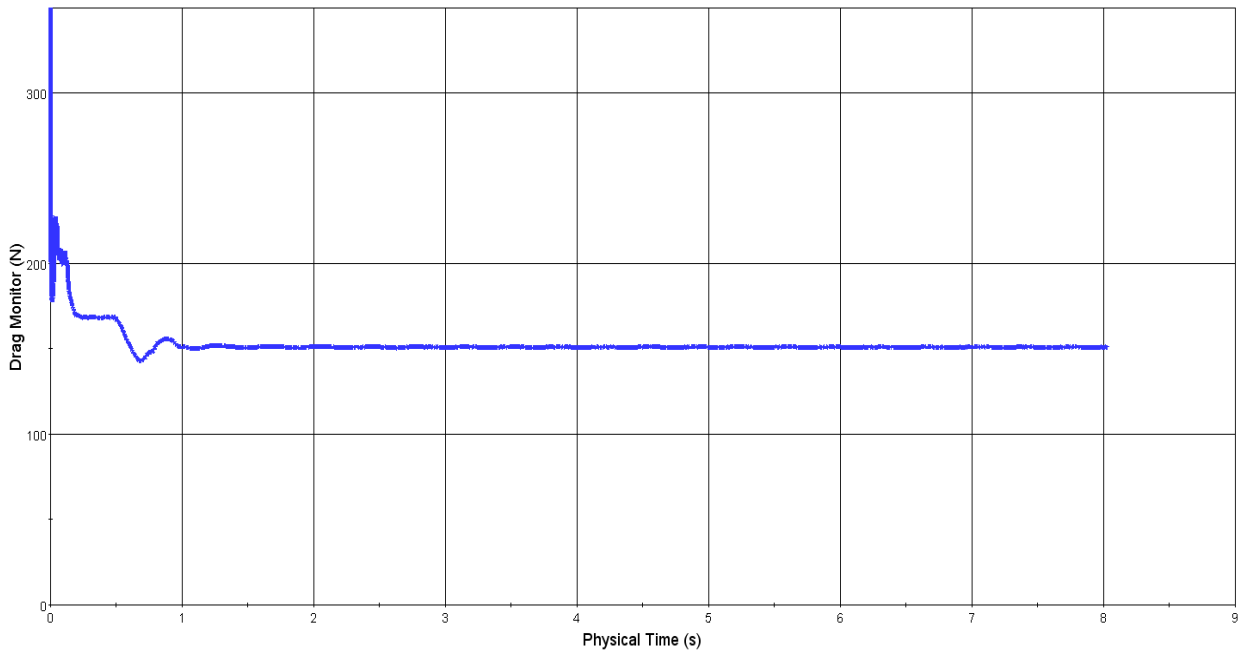


Figure 63: Drag Force Component of Model 5631 Dynaplane, Run 2

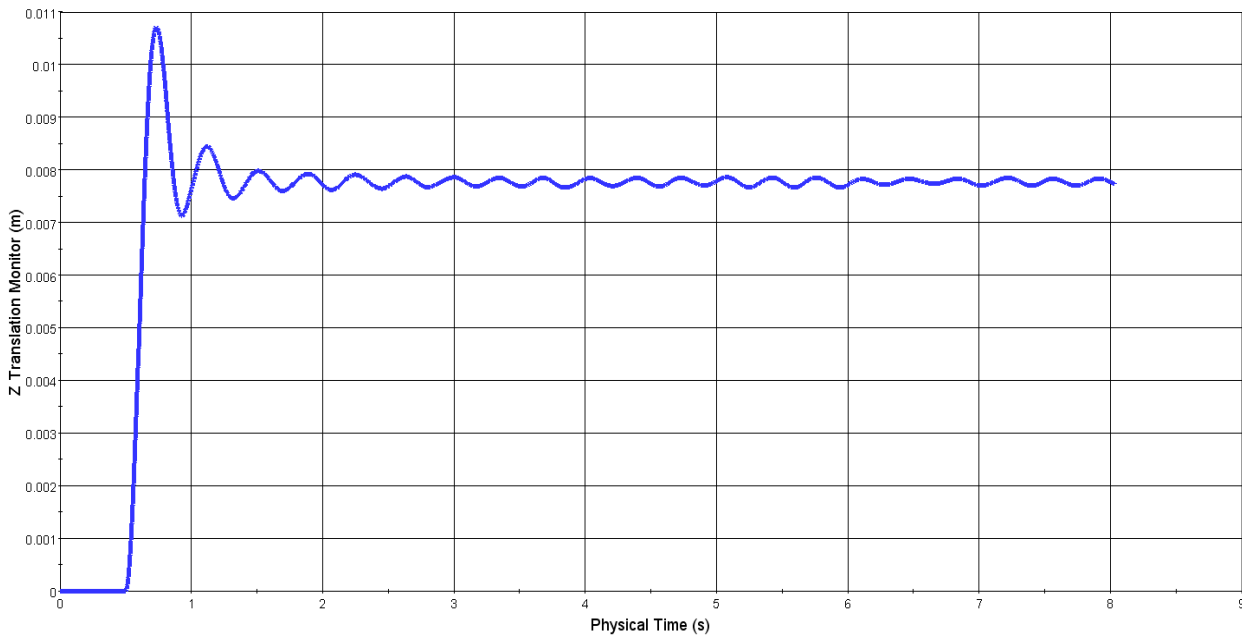


Figure 64: Heave (Z Translation) Monitor for Model 5631 Dynaplane, Run 2

Model 5631 Dynaplane, STAR-CCM+ Run 3: [Trim: 4.5 deg; Heave: Free, FnV = 5]

LCG (42%)	1.28 m
VCG	0.253 m
TCG	0 m
Displacement	375 lb

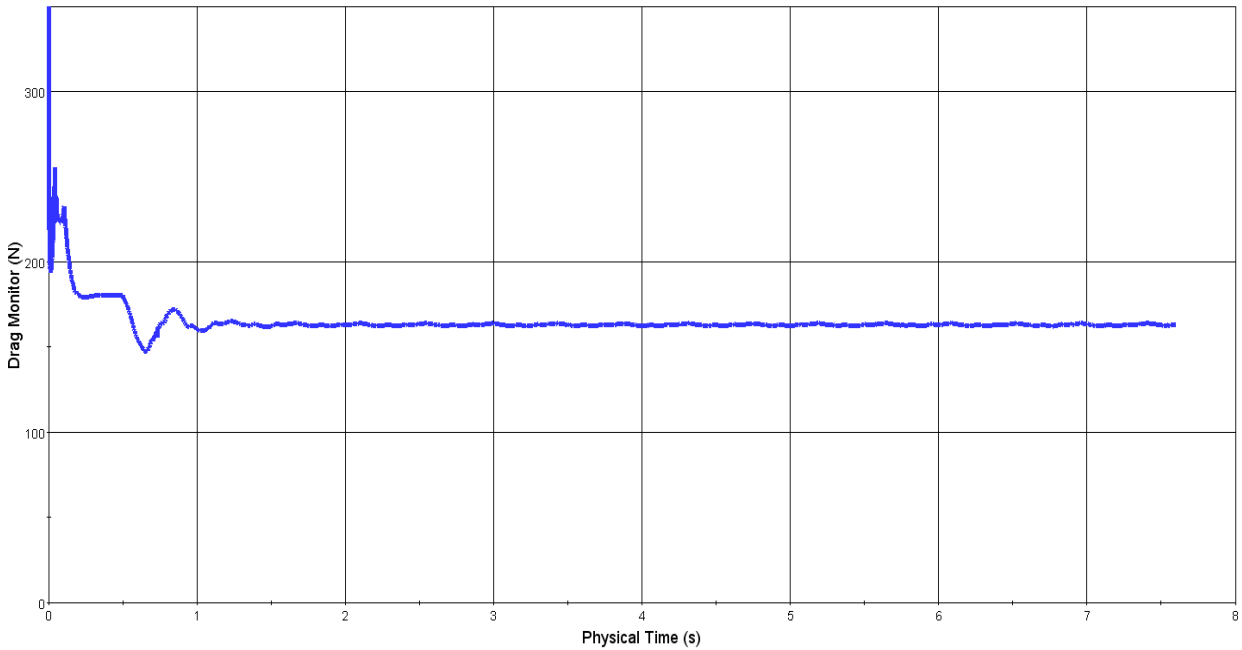


Figure 65: Drag Force Component of Model 5631 Dynaplane, Run 3

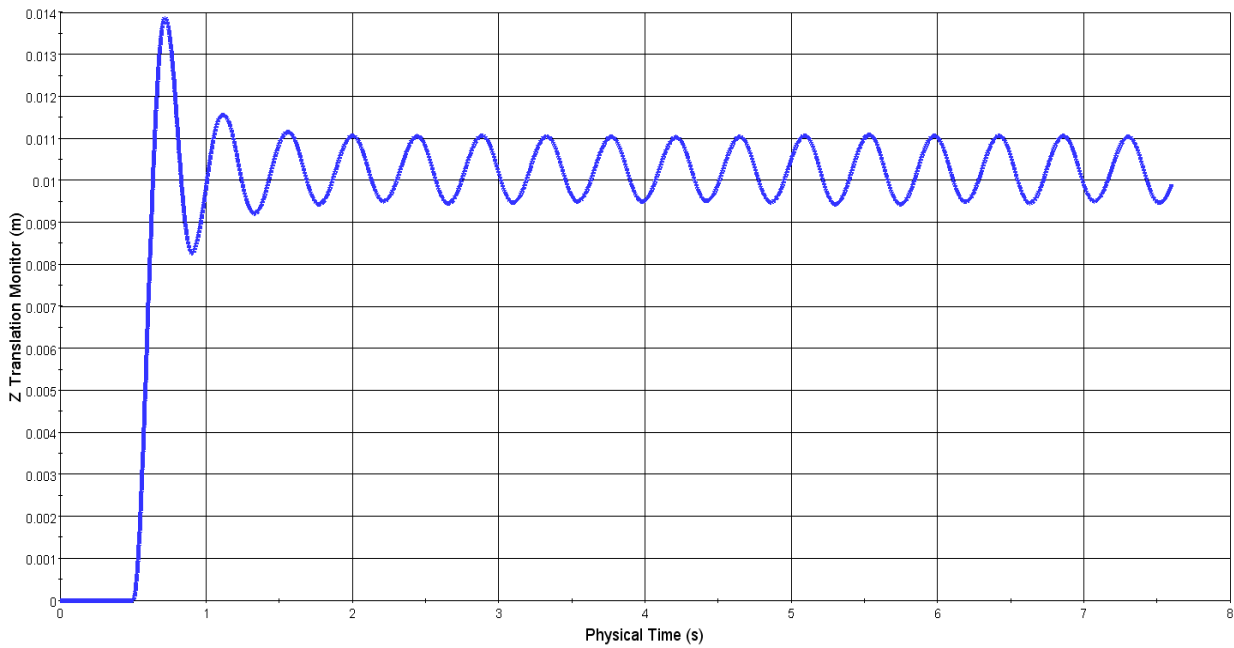


Figure 66: Heave (Z Translation) Monitor for Model 5631 Dynaplane, Run 3

Model 5631 Dynaplane, STAR-CCM+ Run 4: [Trim: 4.0 deg; Heave: Fixed, FnV = 5]

LCG (42%)	1.28 m
VCG	0.258 m
TCG	0 m
Displacement	375 lb

Model 5631 Dynaplane, STAR-CCM+ Run 5: [Trim: 4.5 deg; Heave: Fixed, FnV = 5]

LCG (42%)	1.28 m
VCG	0.258 m
TCG	0 m
Displacement	375 lb

The computational tests revealed that the stern hydrofoils and cambered step were not the only contributors to the pitching moment balance. The afterbody and forward section contributed a sizeable moment to the overall system. Therefore, the moment balance approach had to be revisited but with two additional moment contributors.

Total Moment Contributions [N-m]			
	Trim Angle		
	3.5 deg	4.0 deg	4.5 deg
<b>Forward Section</b>	-21.94	-14.99	-16.41
<b>Afterbody Section</b>	-16.32	-15.40	-13.64
<b>SPSC Hydrofoil</b>	119.10	151.23	190.64
<b>Cambered Step</b>	-84.29	-77.45	-63.95
<b>Total</b>	<b>-3.45</b>	<b>43.39</b>	<b>96.64</b>

Table 7: Moment Contributions of Model 5631 Dynaplane

Recall the sum of the moment prediction of the static equilibrium for the Dynaplane design. We must now include the contributions from the afterbody and forward section. An interesting point is the afterbody produced a negative moment which can be caused from the force of air pressure. The derivative of that equation yields  $\delta M / \delta \tau$ , which represents the change in moment with respect to the change in trim angle.

$$\Sigma M = -F_{Wing} x_{CG} - F_{Fwd} l_{Fwd} + F_{Foil} l_{Foil} - F_{Aft} l_{Aft}$$

$$\frac{\delta M}{\delta \tau} = -\frac{\delta F_{Wing}}{\delta \tau} x_{CG} - \frac{\delta F_{Fwd}}{\delta \tau} l_{Fwd} + \frac{\delta F_{Foil}}{\delta \tau} l_{Foil} - \frac{\delta F_{Aft}}{\delta \tau} l_{Aft}$$

From the computation results, it was determined that the 4.0 and 4.5 degree trim angle runs needed to have fixed heave. Run 1 converged at a vertical translation, or heave, of 0.0048 m. Runs 2 and 3 seemed to be oscillating and not converging in heave. Therefore, Runs 4 and 5 were conducted with fixed trim and heave positions. Their results are shown on the next page in Figure 67.

Using a quasi-static approach to assess the dynamic stability of the hull around the equilibrium condition, stable pitching moment can be achieved through a small trim angle range, 3.4 to 4.3 degrees, shown in Figure 67. The dynamic change in pitching moment with respect to the change in trim was analyzed but only from a quasi-static approach. A complete dynamic approach would require more tests.

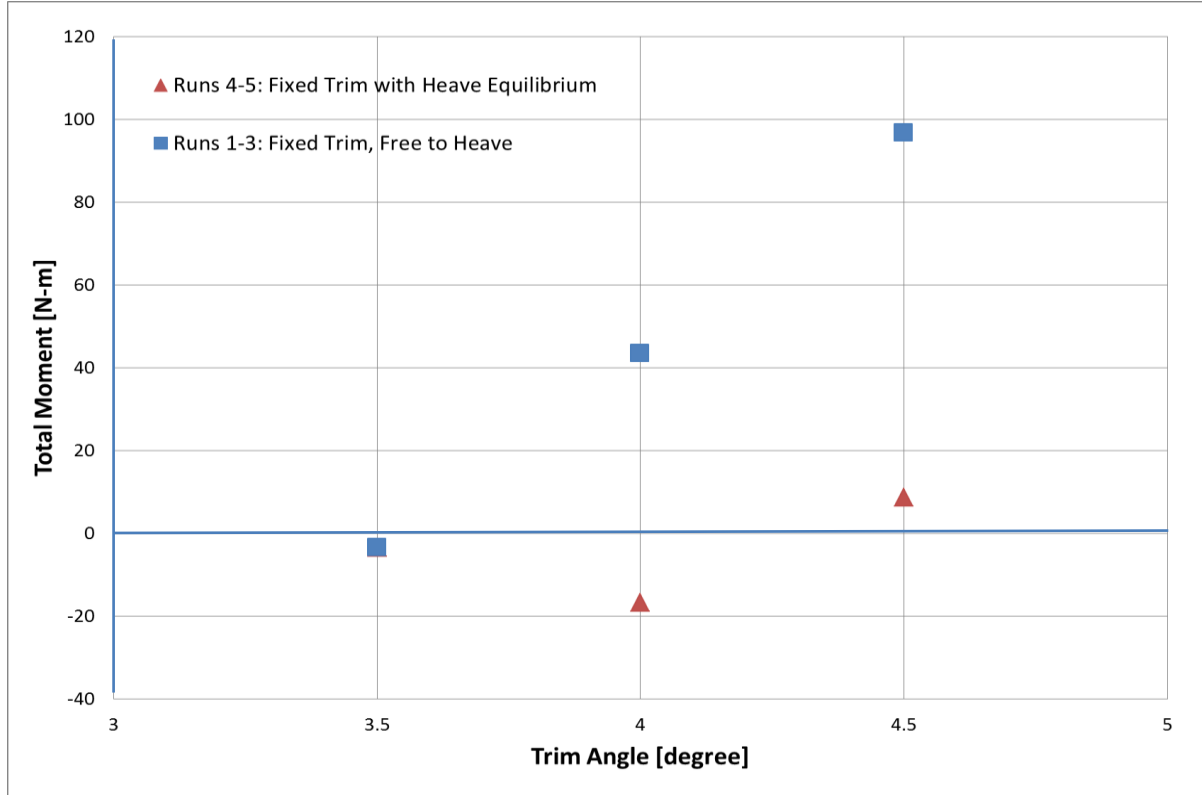


**Figure 67: Total Pitching Moment for CFD Runs 1-5**

If we treat the sum of all forces as one force and then account for the distance that that force is acting upon, then we can devise a distance term,  $h$ , which represents the longitudinal stability margin (LSM). This margin term is often used in aeronautical engineering and has been used at MIT's iShip Lab. A positive  $h$  value is desired.

$$M = h (F_{Wing} + F_{Fwd} + F_{Foil} + F_{Aft})$$

After taking the derivative of the sum of moments with respect to the change in trim, we can solve for  $h$ , shown below.

$$h = \frac{\frac{\delta M}{\delta \tau}}{\frac{\delta F_{Wing}}{\delta \tau} + \frac{\delta F_{Fwd}}{\delta \tau} + \frac{\delta F_{Foil}}{\delta \tau} + \frac{\delta F_{Aft}}{\delta \tau}}$$

In order to calculate the LSM, or  $h$ , we must calculate the derivatives for each of the contributing moments. Figure 69 shows the comparison of all contributing forces applied to the Model 5631 Dynaplane during Runs 1, 4, and 5. Figure 68 illustrates the particular sections for reference.

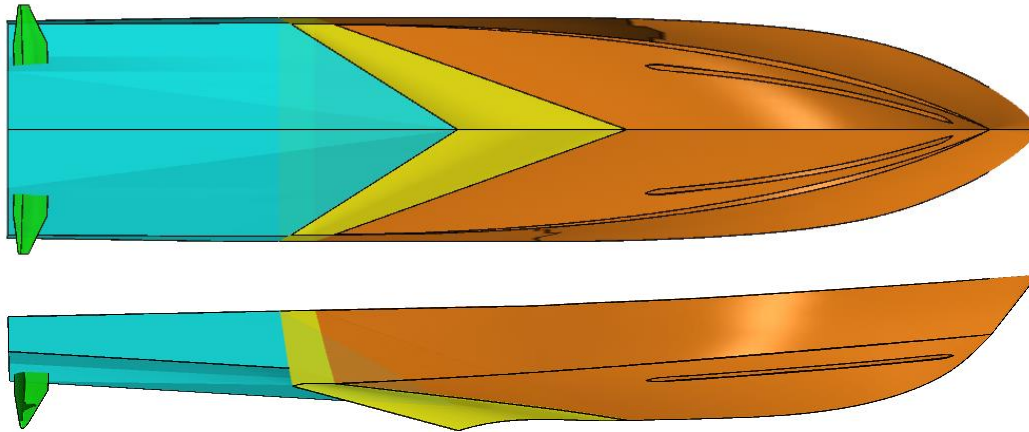


Figure 68: Depiction of the Four Sections Analyzed

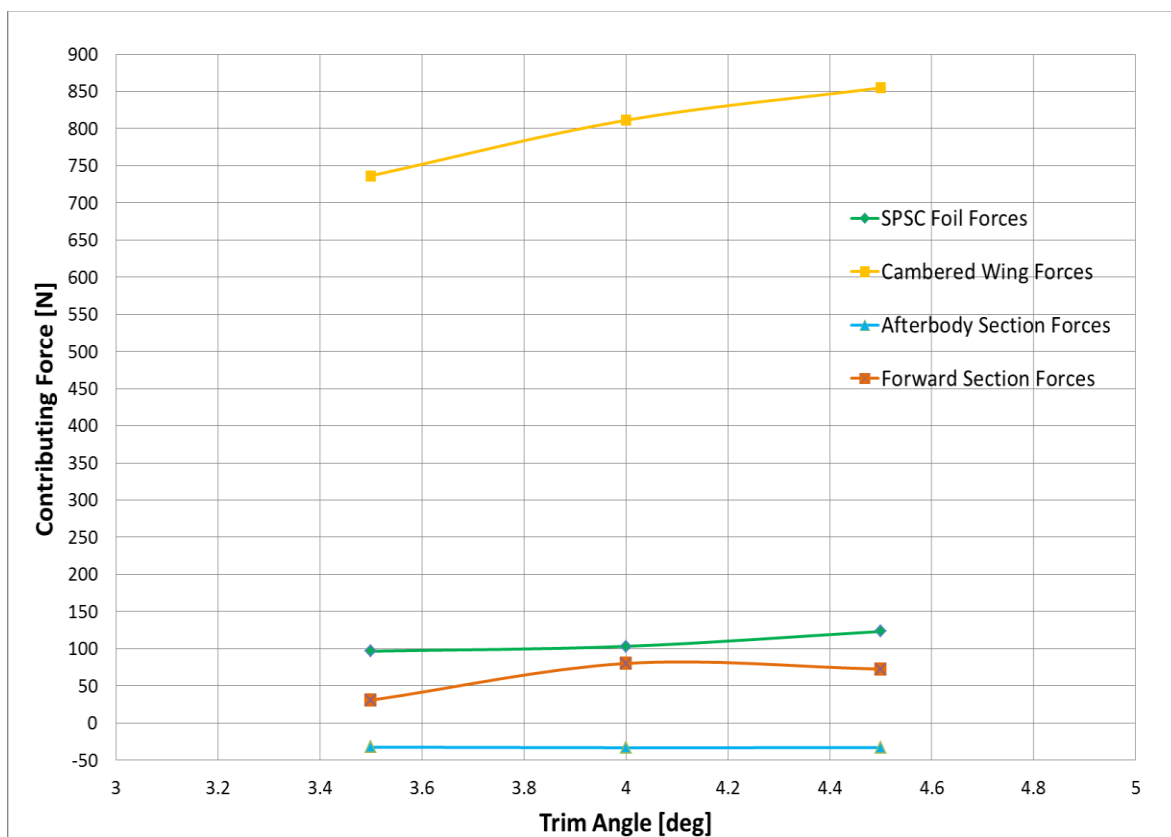


Figure 69: All Contributing Forces to Pitching Moment for Model 5631 Dynaplane

Once all forces were calculated, the LSM could now be determined. Figure 70 shows the change in stability margin with the change in trim angle for the Model 5631 Dynaplane configuration. The model begins with a small amount of negative dynamic stability from 3 to 4 degrees. It does

not begin to diverge, or decrease, until 4 degrees of trim, which matches the computational results at that same trim angle. The recovery time from the sudden perturbation took greater than one degree of trim. This reveals an indifferent dynamic stability where the system does not recover promptly.

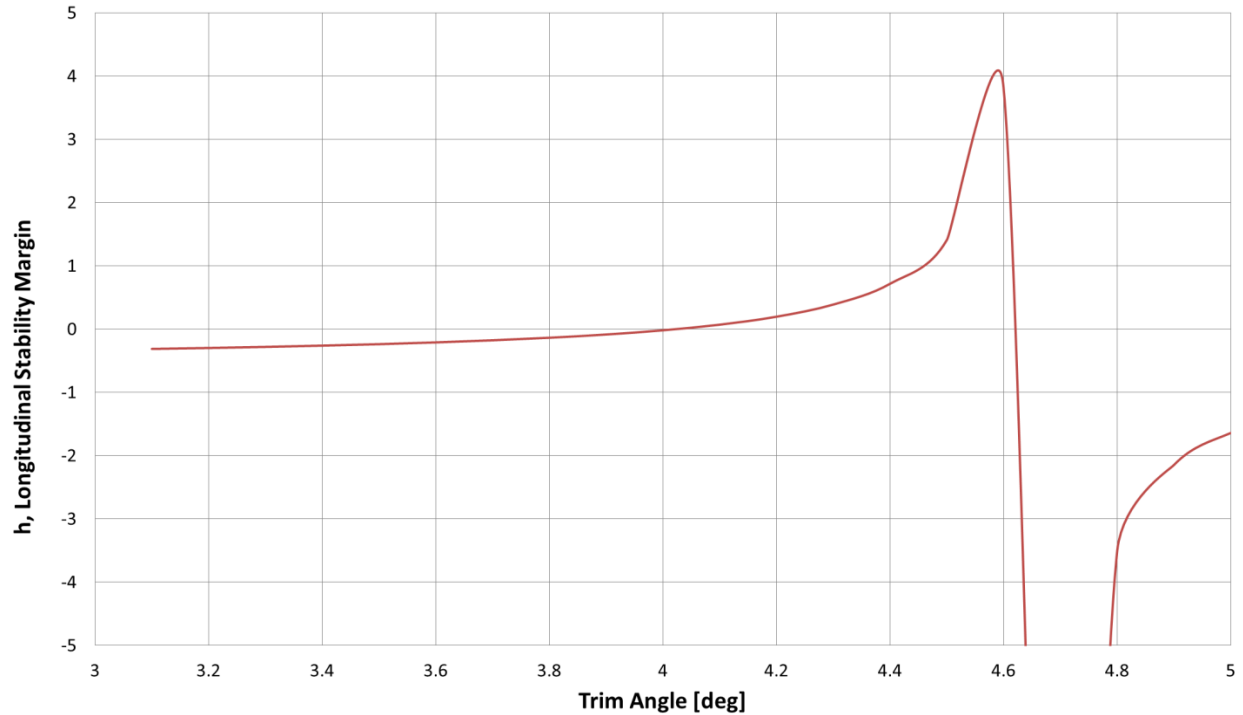


Figure 70: Longitudinal Stability Margin, h, versus Trim Angle

#### 4.4 Model 5631 Dynaplane Longitudinal Center of Gravity Analysis

From the previous studies of Blount, Codega and Savitsky, a planing hull's running trim angle and associated lift coefficient has a large impact on dynamic stability and performance. A simulation was ran with Model 5631 Dynaplane to freely trim and heave at speed of  $F_n V = 5$  to determine the trim and heave equilibrium.

Model 5631 Dynaplane, STAR-CCM+ Run 6: [Trim: Free; Heave: Free,  $F_n V = 5$ ]

LCG (42%)	1.28 m
VCG	0.155 m
TCG	0 m
Displacement	375 lb

After running the simulation, it was determined that there is an instability problem with the LCG location; results are shown below. The placement of the LCG largely dictates the moment balance between the two main lifting surfaces and the allowance for the LSM to become stable.

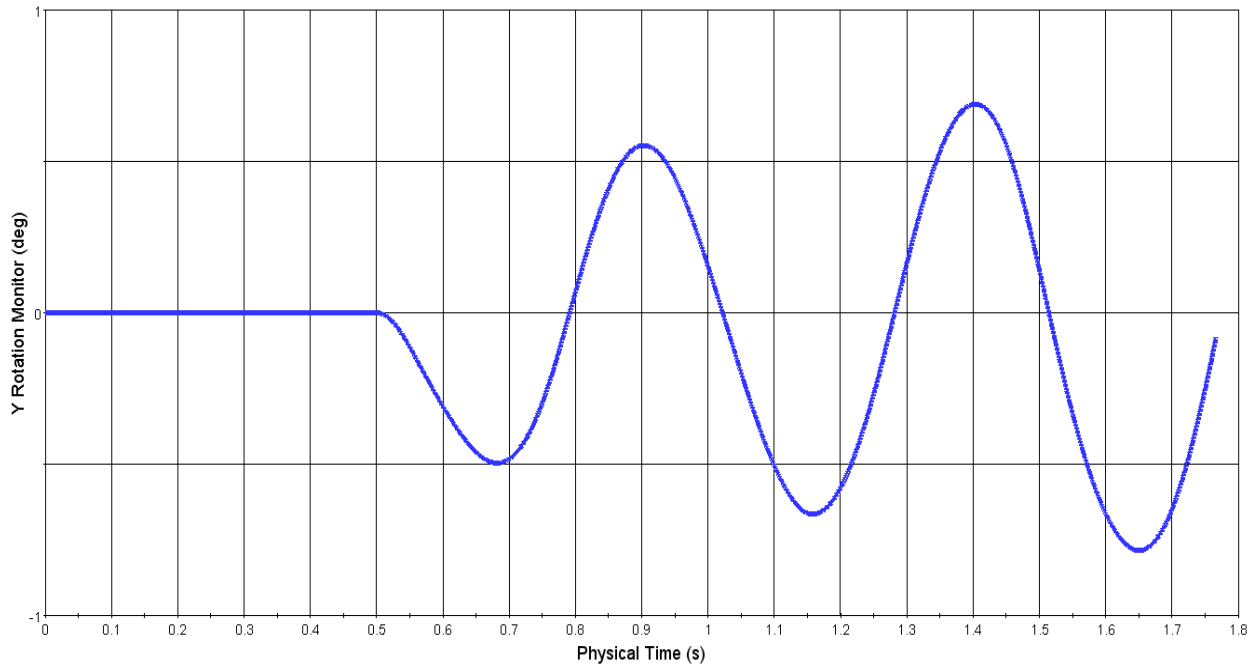


**Figure 71: Trim Monitor for Model 5631 Dynaplane, Run 6**

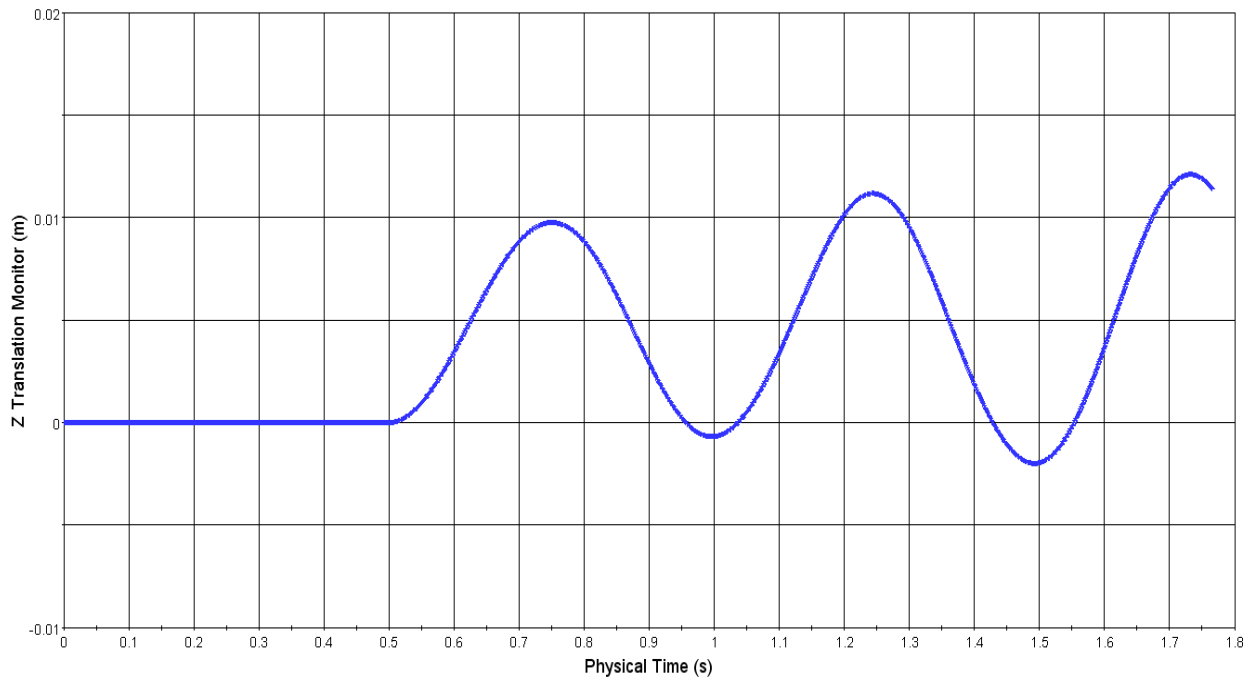


**Figure 72: Heave (Z Translation) Monitor for Model 5631 Dynaplane, Run 6**

The results from Run 6 did not converge, revealing the dynamic instability of the coupled heave and pitches motions. The optimal LCG location largely depends on the shape of the hullform and the design speed. For the first series of CFD simulation runs, the LCG was placed at 1.28 meters forward of the transom, or 42% of the LBP. The trend of changing the LCG location was

considered (Blount and Codega, 1992). Therefore, the Model 5631 Dynaplane was tested with LCG locations of 40%, 42%, 44%, and 46%. All simulations from this series of tests were run at the same design speed of  $F_nV=5$  and were free to heave and pitch.

The 40%, 42%, 44%, and 46% locations failed to converge. The 40% LCG run tended to cause an increase in trim and without proper lift stability from the hydrofoils, it diverged. The 44% and 46% runs both diverged at the release of the model and caused an overall decrease in trim creating a bow down occurrence. Since the 44% run's divergence was not as steep as the 46% run, it was concluded that an additional run at 43% could provide interesting data on the stability predictions for the design.

Model 5631 Dynaplane, STAR-CCM+ Run 11: [Trim: Free; Heave: Free,  $F_nV = 5$ ]

LCG (43%)	1.31 m
VCG	0.155 m
TCG	0 m
Displacement	375 lb
Moments of Inertia, $I_{ii}$	[3.57,40,40] $\text{kg}\cdot\text{m}^2$

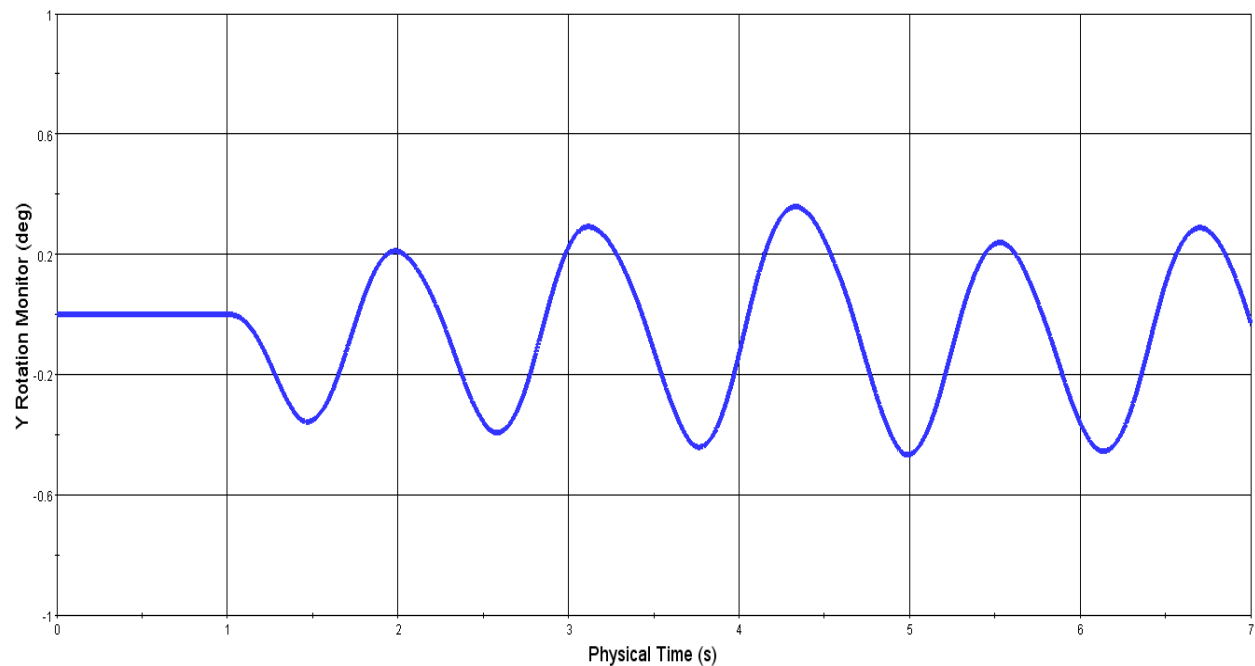


**Figure 73: Trim Monitor for Model 5631 Dynaplane, Run 11**



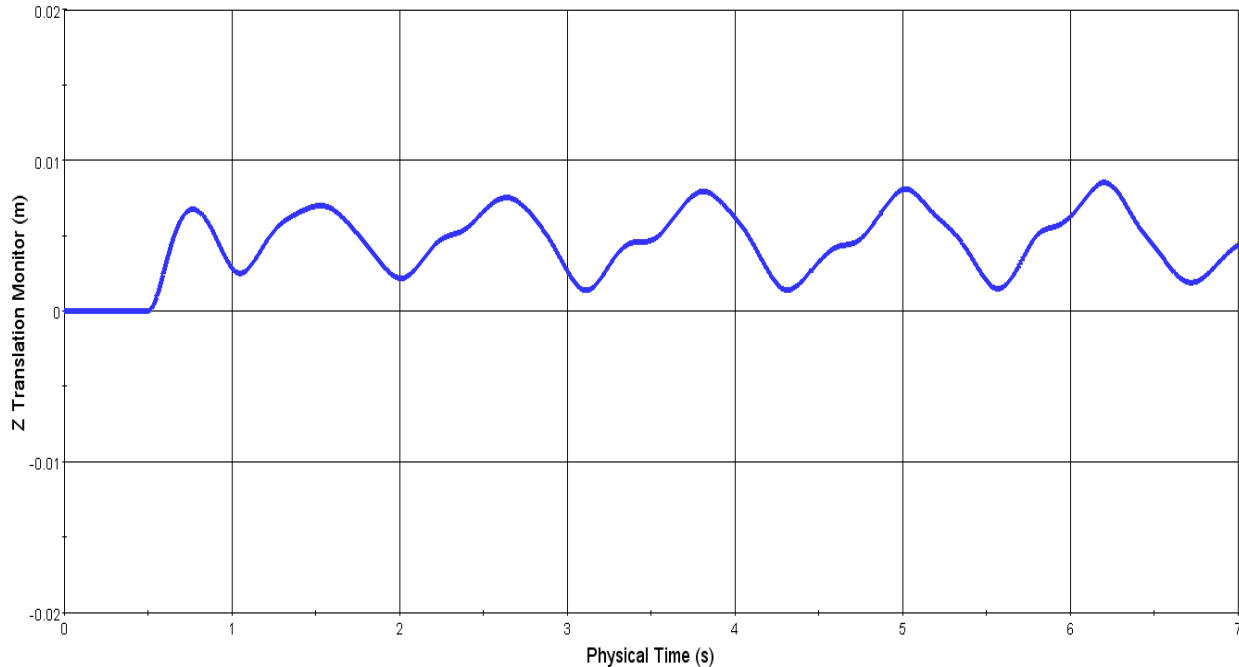


**Figure 74: Heave (Z Translation) Monitor for Model 5631 Dynaplane, Run 11**

The results from Run 11 proved to be reassuring because they provided an indication of positive static stability. After analyzing the 43% simulation, it was determined that the stern SPSC hydrofoils were not providing the necessary restoring moment. As the model pitches, the hydrofoils were not able to restore the system back to equilibrium. The lift force required to meet the 10% weight requirement was met, however the change in lift force with respect to the change in trim did give positive dynamic stability. A possible reason for this is that the scaling could be wrong. A larger scaled hydrofoil above the design submerged length would provide a greater lifting surface area as the model increased in trim. Lastly, the wake geometry of the cambered step could be a contributing factor as to why the hydrofoils were not able to provide the proper restoring moment. In Figure 75, the surface contour of the wake is steep where the hydrofoils enter the water; therefore, as the trim changes the hydrofoils are not being submerged enough to provide that extra lift force. An indicator of this is shown in Figure 69, where the increase in 1 degree of trim produces less than 8% of the total force applied.

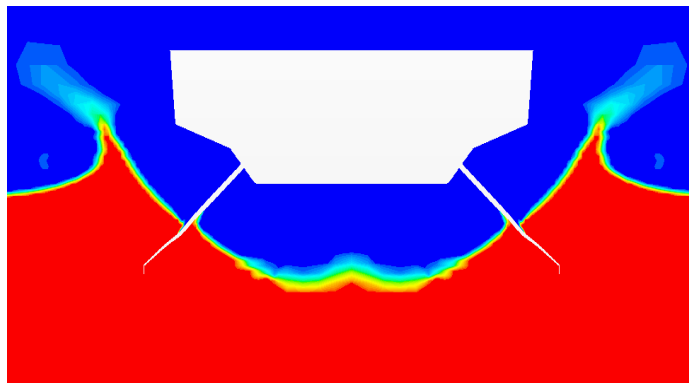


**Figure 75: Surface Contour Aft of the Cambered Step where SPSC Hydrofoils Enter Water**

## 4.5 Final Results Comparison to Reference Hull

After completion of the hydrodynamic analysis, the following table was developed to show the percent difference between the Reference Hull of Model 5631 and the new Dynaplane configuration. There is a clear indication to the advantages of the Dynaplane design.

	Reference Hull	Dynaplane	% Diff.
<b>Total Drag [N]</b>	388.02	292.08	<b>-25%</b>
<b>Wetted Area, [m<sup>2</sup>]</b>	1.621	0.396	<b>-75%</b>
<b>Lift to Drag Ratio</b>	4.28	5.72	<b>+34%</b>

**Table 8: Final Comparison of Reference Hull and new Dynaplane design**

## Chapter 5 – Conclusions

### 5.1 Summary

The Dynaplane configuration has proved to become a viable option for a designer of high speed vessels. The U.S. Coast Guard 47 ft MLB initially was designed for operating in the offshore environment with breaking surf up to 6 meters in height. Its design was critical to the missions it would encounter. This thesis took an existing planing hull and converted it into a new Dynaplane configuration. The goal of the conversion was to address the benefits of improving the lift to drag properties of such a design and make recommendations based on the results of a hydrodynamic analysis. The Model 5631 Dynaplane design produced 34% higher L/D ratios than the reference hull in the tests conducted at the DTMB, (Metcalf et al, 2005). Further improvement was the 25% drag reduction in calm water, given by the validation of the computational model. The results from this design also provide future designers test data for the validity of Clement's Dynaplane design for hulls with a deadrise greater than 15 degrees. It was also proven that CFD models give the designer an advantage over physical model testing. CFD modeling provides quicker results when conducting parametric analyses. A change to the model or inertial frame of reference takes hours as opposed to weeks or even months with constructing another physical model. It is the hope of this thesis to provide the reader with potential design considerations to improve the performance of planing hulls.

### 5.2 Future Work

As discussed in Chapter 1 and in the previous section of this chapter, the planing craft industry will benefit from further research based on the results of this analysis. Below are suggested research opportunities that would contribute in such a way.

- Clement's Dynaplane configuration is restricted to a range of geometric and performance parameters. Further development of Clement's method using a wider range of geometrical properties, such as trim and deadrise, would enable the use of the Dynaplane configuration on a larger design group of hulls. This design extended that range to hulls with 20 degree deadrise.

- As Dr. Brizzolara approached the SPSC hydrofoil problem with an optimization analysis, it is suggested to prepare and create a parametric optimization program based on empirical results and experimental studies. This would enhance the performance of the Dynaplane design and addressing these issues within the optimization program would provide insight to the trim and LCG restrictions of traveling at such high speeds.

- The next step after conducting a hydrodynamic analysis using computational modeling is validating such tests with physical model tests. The CFD model was validated with USCG model data, but physical model testing of the Model 5631 Dynaplane design would give further validation and confirmation of results found.

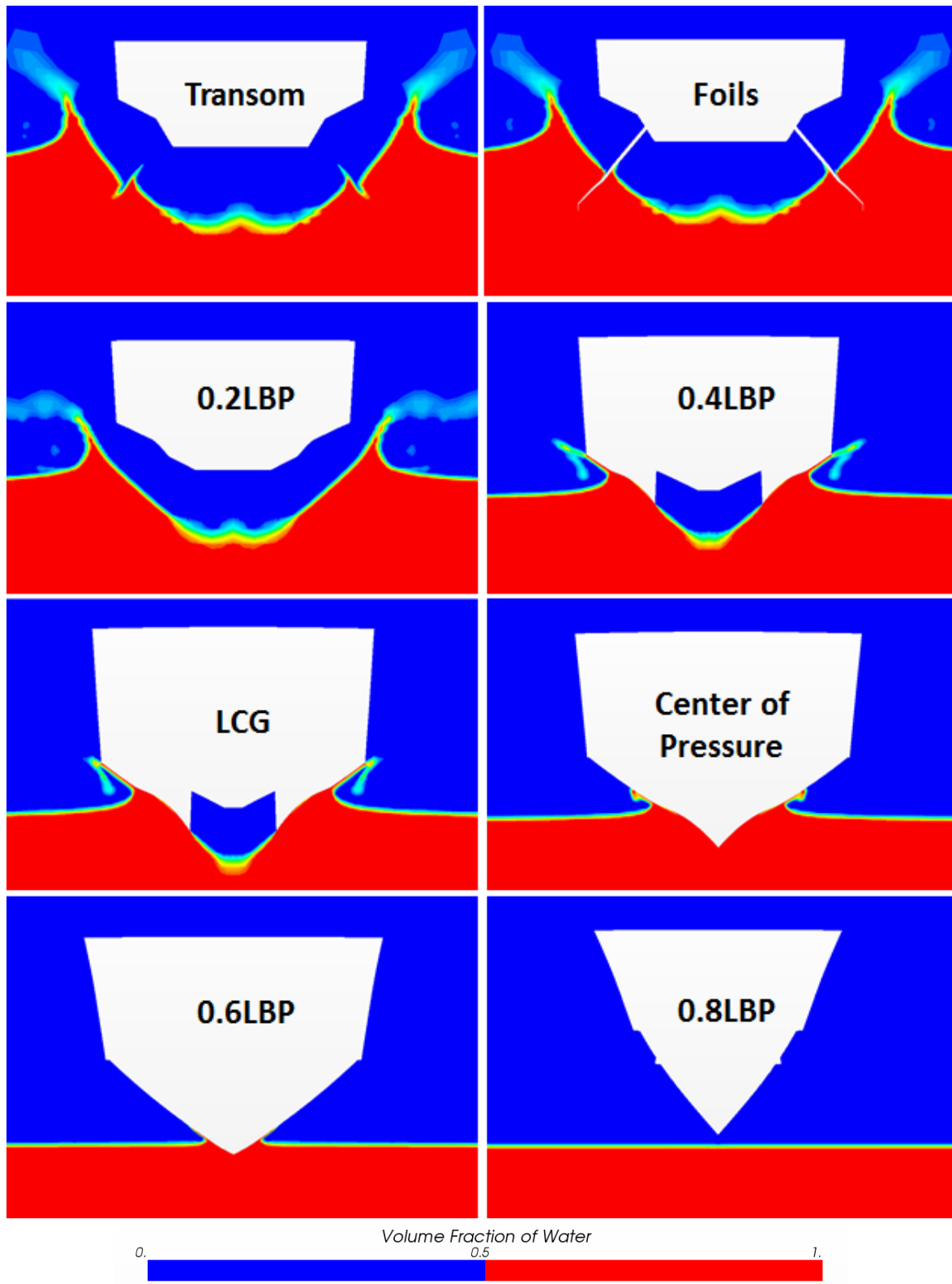
- This thesis took Savitsky and Morabito's surface wake contour results and validated similar computational modeled hullforms using their empirical equations. However, prediction of the wake profile for a cambered step and swept back step were compared to a conventional

transverse step by a set of three runs at different trim angles. The author suggests conducting tests on the same conventional transverse step in the Savitsky and Morabito paper to further validate the use of computational modelling.

- Since the dihedral arrangement of the SPSC hydrofoils did not provide enough restoring force with respect to the change in trim due to the surface contour of the wake, it is recommended to design a stern stabilizer with the same SPSC hydrofoil profile but in a V-foil fashion on the afterbody.

- Lastly, the pitching moment contributions from the super cavitating surface piercing hydrofoil were estimated using a scaled down version of the lifting surface. Also, a cavitation model was added to the existing computational model in STAR-CCM+ in an effort to match the results from the physical tests conducted in a cavitation tunnel. More accurate prediction of the lifting force and pitching moment can be accomplished by conducting a more extensive series of tests with a computational model according to the model's cavitation tunnel test data.

## Appendix A: Spray Formation for Model 5631 Dynaplane



## Appendix B: Empirical Resistance MATLAB Code

The MATLAB Script below calculates a planing hull's resistance, effective horsepower, trim, and vertical accelerations at a specified speed range, all based on the following empirical methods.

- Savitsky Method with Blount and Fox Multiplier – Resistance, EHP, and trim
- Hoggard and Jones Method– Vertical Accelerations

This code is adapted from the Resistance Module from the Planing Hull Analysis and Selection Tool created by a student design team in 2007 at MIT for their 2.705 design project (Lawler et al, 2007).

```
%%%%%%%%%%%%%%%%%%%%%%%%%%%%%%%%%%%%%%%%%%%%%%%%%%%%%%%%%%%%%%%%%%%%%%%%%%%%%%
% Model 5631 Empirical Resistance Calculations
% Written by: Leon Faison
% Date: 04FEB2014
% Adapted from original code written by Greg Mitchell and Clint Lawler
% for use in the Resistance Module for the Planing Hull Analysis and
% Selection Tool (PHAST), 08 NOV 2007
% Description: For Calculating Resistance Using Savitsky Method with
% Blount & Fox Multiplier. This Code Can Calculate Resistances for All
% Applicable % Ranges of the Savitsky Method with Blount & Fox Multiplier,
% also includes Hoggard and Jones vertical accelerations calculations.
% Derivation Outlined in "Small-Craft Power Prediction" (Blount & Fox, 1976)
% and "Examining Pitch, Heave and Accelerations of Planing Craft Operating
% in a Seaway" (Hoggard & Jones, 1980)
%%%%%%%%%%%%%%%%%%%%%%%%%%%%%%%%%%%%%%%%%%%%%%%%%%%%%%%%%%%%%%%%%%%%%%%%%%%%%%
clc
clear all
close all
% Constants
rho = 62.4;
rho_a = 0.0765;
Cx = 0.6;
dCa = 0.0004;
g = 32.17;
nu = 0.0000121;
kts_fps = 1.6878;
a_rad = 0.017453293;
% User Boat Input Variables
WT = 375; % Weight of high speed craft
LCG = 4.2; % 42 percent
Bpx = 2.24;
DR = 20;
Lp = 10;
Speeds = [5 10 12 14 15 16 18 20 22 24 25 26 28 30] % in knots
H13 = 4;
A = Bpx*(1.5)+0.5*(0.75*Bpx)*3; % An arbitrary deckhouse and hull profile
% Multipliers and Simplification
rhom = rho/g; % [lb-s2/ft4] Mass Density of Fresh Water at 59F
K=0.5; % Blount and Bartree Modifier
ns = length(Speeds);
```

```

for a = 1:ns
    V=Speeds(a)
    vel = V*kts_fps; % Converts knots to ft/s
    vol13=(WT/rho)^(1/3); % Converts weight to volume
    FNV=vel/sqrt(g*vol13); % Volumetric Froude Number
    % Algorithm Below is only for FNV greater than 1.0. If V is such
    % that FNV is less than one then linear interpolation between
    % 1.1*FNV and 0.
    if FNV<1
        pre_planing=1.1*FNV;
        FNV=1;
        vel=FNV*sqrt(g*vol13);
    else
        pre_planing=1;
    end
    %%
    %%%%%%%%%%%%%%%%%%%%%%%%%%%%%%%%%%%%%%%%%%%%%%%%%%%%%%%%%%%%%
    % Savitsky Method for Resistance Prediction with Blount Fox Multiplier,
    % the R_BH value is using only Savitsky's prediction depending on the
    % user's requirements or needs.
    %%%%%%%%%%%%%%%%%%%%%%%%%%%%%%%%%%%%%%%%%%%%%%%%%%%%%%%%%%%%%
    Cv=vel/sqrt(g*Bpx); % (20)
    CLB=WT/(0.5*rhom*vel^2*Bpx^2); % (21)
    Lam=fzero(@(Lam)((0.75-(1/((5.21*Cv^2)/Lam^2)+2.39)))...
        -LCG/(Bpx*Lam)),10); % (22)
    CL0=fzero(@(CL0)(CL0-0.0065*DR*CL0^0.6-CLB),0.5); % (23)
    Tau=(CL0/(0.012*sqrt(Lam)+(0.0055*Lam^(5/2))/Cv^2))^(1/1.1); % (23)
    Vm=vel*(1-0.012*sqrt(Lam)*Tau^1.1 -...
        (0.0065*DR*(0.012*sqrt(Lam)*Tau^1.1)^0.6)/(Lam*cos(a_rad*Tau)))^0.5; %
(25)
    Re=Vm*Lam*Bpx/nu; % (26)
    Cf=fzero(@(Cf)(log10(Re*Cf)-0.242/sqrt(Cf)),5); % (27) ATTC Line
    Cf=0.472/(log10(Re))^2.58; % Modified by Norwood in Savitsky paper
    R_BH=WT*tan(a_rad*Tau)+(rhom*Vm^2*Lam*Bpx^2*(Cf+dCa))/...
        (2*cos(a_rad*DR)*cos(a_rad*Tau)); % (28)
    % Blount-Fox Multiplier - for "hump" speed prediction
    M=0.98 + 2*(LCG/Bpx)^1.45*exp(-2*(FNV-0.85)) - 3*(LCG/Bpx)*exp...
        (-3*(FNV-0.85)); % (1)
    % Modified Blount-Fox prediction recommended in "High Speed Propulsion
    % Design"
    MP=K*(M-1)+1; % from (Blount & Bartee 1996)
    % Modified resistance of bare hull
    R_BHM=pre_planing*MP*R_BH;
    %%
    %%%%%%%%%%%%%%%%%%%%%%%%%%%%%%%%%%%%%%%%%%%%%%%%%%%%%%%%%%%%%
    % Hoggard Method of Added Drag Prediction - "Examining Added Drag of
    % Planing Craft Operating in a Seaway," Mark Hoggard, Presented to
    % Hampton
    % Road Section of SNAME, 1979.
    %%%%%%%%%%%%%%%%%%%%%%%%%%%%%%%%%%%%%%%%%%%%%%%%%%%%%%%%%%%%%
    %
    Raw=WT*1.3*FNV*(H13/Bpx)^0.5*(Lp/vol13)^-2.5;
    %%
    %%%%%%%%%%%%%%%%%%%%%%%%%%%%%%%%%%%%%%%%%%%%%%%%%%%%%%%%%%%%%
    % Added Aerodynamic Resistance - Taken from example in "Design of
    % Propulsion
    % Systems for High Speed Craft," Donald Blount and Robert Bartee,

```

```

% Presented
% to Hampton Road Section of SNAME, 1996. - Not Calculated at this point.
%%%%%%%%%%%%%%%%%%%%%%%%%%%%%%%%%%%%%%%%%%%%%%%%%%%%%%%%%%%%%%%%%%%%%%%%
Raa=0.5*rho_a*Cx*A*vel^2;
Raa = 0;
%%
%%%%%%%%%%%%%%%%%%%%%%%%%%%%%%%%%%%%%%%%%%%%%%%%%%%%%%%%%%%%%%%%%%%%%%%%
% OPC Calculation - Numbers come from NSWCCD Spreadsheet. The graph
% looks identical to the one published in "Prospects for Hard Chine,
% Monohull Vessels" by Donald Blount, 1993
%%%%%%%%%%%%%%%%%%%%%%%%%%%%%%%%%%%%%%%%%%%%%%%%%%%%%%%%%%%%%%%%%%%%%%%%
% These are the numbers for a minimum performing waterjet.
a1=3.19e-1; %max = 3.81e-1
b=-2.25e-2; %max= -2.09e-2
c=-1.04e-3; %max = -3.84e-4
d=2.01e-4; %max = 2.05e-4
%
OPC=(a1+c*V)/(1+b*V+d*V^2);
%%
%%%%%%%%%%%%%%%%%%%%%%%%%%%%%%%%%%%%%%%%%%%%%%%%%%%%%%%%%%%%%%%%%%%%%%%%
% Effective Horsepower Calculations
%%%%%%%%%%%%%%%%%%%%%%%%%%%%%%%%%%%%%%%%%%%%%%%%%%%%%%%%%%%%%%%%%%%%%%%%
EHP_BHM=R_BHM*V/325.9;
R_t=R_BHM+Raw;
EHP_t=R_t*V/325.9;
SHP=EHP_t/OPC;
R_t_sa = R_BHM+Raw+Raa; % Added sea and air resistance to bare hull
EHP_sa = R_t_sa*V/325.9;
Trim(a) = Tau;
R_BH(a) = R_BHM;
R_T(a) = R_t;
EHP_BH(a) = EHP_BHM;
EHP_T(a) = EHP_t;
OPC(a) = OPC;
SHP_T(a) = SHP;
Volumetric_Froude_Number = FNV % Show FNV to determine > 1
Trim = Tau % Trim angle at speed
Total_Resistance = R_t % Total resistance in seaway with 4 ft H13
Total_Effective_HP = EHP_t % EHP at the seaway resistance
Total_Resistance_Savitsky = R_BH % Savitsky only
Total_Resistance_calmwater = R_BHM % Total resistance in calm water
Total_Effective_HP_calmwater = EHP_BHM % EHP in calm water
Total_Resistance_sea_and_air = R_t_sa % Total resistance in seas and air
Total_Effective_HP_sea_and_air = EHP_sa % EHP in seas and air
%%
%%%%%%%%%%%%%%%%%%%%%%%%%%%%%%%%%%%%%%%%%%%%%%%%%%%%%%%%%%%%%%%%%%%%%%%%
% Calculate Vertical Accelerations - Hoggard and Jones Equations
%%%%%%%%%%%%%%%%%%%%%%%%%%%%%%%%%%%%%%%%%%%%%%%%%%%%%%%%%%%%%%%%%%%%%%%%
% Impact Acceleration (Hoggard and Jones) - 1/10 highest
eta_110_CG = 7.0*(H13/Bpx)*(1+Tau/2)^0.25.*((FNV)./(Lp/Bpx)^1.25); % [g]
eta_110_Bow = 10.5*(H13/Bpx)*(1+Tau/2)^0.5.*(((FNV)^0.75)./(Lp/Bpx)^0.75);
Vert_Accel_CG = eta_110_CG % Vertical acceleration at CG
Vert_Accel_Bow = eta_110_Bow % Vertical acceleration at Bow
%%
%%%%%%%%%%%%%%%%%%%%%%%%%%%%%%%%%%%%%%%%%%%%%%%%%%%%%%%%%%%%%%%%%%%%%%%%
% Exporting data into an Excel spreadsheet
%%%%%%%%%%%%%%%%%%%%%%%%%%%%%%%%%%%%%%%%%%%%%%%%%%%%%%%%%%%%%%%%%%%%%%%%

```



```

if a == 1 % Setting column number
    b = 'A2';
elseif a == 2
    b = 'A3';
elseif a == 3
    b = 'A4';
elseif a == 4
    b = 'A5';
elseif a == 5
    b = 'A6';
elseif a == 6
    b = 'A7';
elseif a == 7
    b = 'A8';
elseif a == 8
    b = 'A9';
elseif a == 9
    b = 'A10';
elseif a == 10
    b = 'A11';
elseif a == 11
    b = 'A12';
elseif a == 12
    b = 'A13';
elseif a == 13
    b = 'A14';
elseif a == 14
    b = 'A15';
elseif a == 15
    b = 'A16';
elseif a == 16
    b = 'A17';
end
%
%   speed_data = {'Speed','Volumetric Froude Number','Trim','Total
%   Resistance',...
%   'Total EHP','Total Resistance Calm Seas','Total EHP Calm Seas',...
%   'Total Resistance Seas and Air',' Total EHP Seas and Air',...
%   'Vert Accel'; V FNV Tau R_t EHP_t R_BHM EHP_BHM R_t_sa EHP_sa ...
%   eta_110_CG};
%
speed_data = {V FNV Tau R_t EHP_t R_BHM EHP_BHM R_t_sa EHP_sa eta_110_CG};
xlswrite('Model5631_BH_Results.xls',speed_data,'Hull 5631 BH 3751b',b);
end

```

## Bibliography

- [1] Ayob, Ahmad F. Mohamad, and Warren Smith. "A Hydrodynamic Preliminary Design Optimization Framework for High Speed Planing Craft." *Journal of Ship Research* 56, no. 1, March, 2012: pp 35-47.
- [2] Benen, L. *General Resistance Test of a Stepless Planing Hull with Application to a Hydrofoil Configuration*. Research and Development Report, David Taylor Model Basin, USN, 1965.
- [3] Benson, James M., and Norman S. Land. *An Investigation of Hydrofoils in the NACA Tank I - Effect of Dihedral and Depth of Submersion*. Wartime Report, National Advisory Committee for Aeronautics, Langley Field, VA: Langley Memorial Aeronautical Laboratory, 1942.
- [4] Blount, Donald L. "Achievements with Advanced Craft." *Naval Engineers Journal*, September 1994: pp 49-59.
- [5] Blount, Donald L. "Beyond Displacement Speeds: The Evolution of Performance Boats and Craft." *Marine Technology*, 2013: pp 20-27.
- [6] Blount, Donald L. *Dynamic Instability at Speed*. Donald L. Blount and Associates, Inc., n.d.
- [7] Blount, Donald L., and David L. Fox. "Small-Craft Power Prediction." *Marine Technology* 13, no. 1, January 1976: pp 14-45.
- [8] Blount, Donald L., and Louis T. Codega. "Dynamic Stability of Planing Boats." *Marine Technology* 29, no. 1, January 1992: pp 4-12.
- [9] Brizzolara, S. "Forces on a Super-Cavitating Hydrofoil." Final Report, Department of Dynamics of Maritime Systems, Technical University of Berlin, 2012.
- [10] Brizzolara, S., and A. Federici. "CFD Modeling of Planing Hulls with Partially Ventilated Bottom." *The William Froude Conference: Advances in Theoretical and Applied Hydrodynamics - Past and Future*. Portsmouth, England: Royal Institution of Naval Architects, Nov. 2010.
- [11] Brizzolara, S., and A. Federici. "Designing of V-Stepped Planing Hulls: CFD in Support of Traditional Semi-Empirical Methods." May 2013.
- [12] Brizzolara, S., and A. Federici. "Super-Cavitating Profiles for Ultra High Speed Hydrofoils: a Hybrid CFD Design Approach." *9th Symposium on High Speed Marine Vehicles*. Naples, Italy, 2011: pp 1-13.
- [13] Brizzolara, S., and D. Villa. "CFD Simulations of Planing Hulls." *Seventh International Conference on High-Performance Marine Vehicles*. Melbourne, FL, 2010.
- [14] Brizzolara, S., S. Gaggero, D. Grassi, D. Villa. "CFD Modelling for Powering and Propulsion of Motor Yachts, Recent Developments and Applications of the Marine CFD Group (Genoa)." *Design, Construction and Operation of Super and Mega Yachts*. Genoa, IT, April 1-2, 2009.

- [15] Brizzolara, S., and F. Serra. "Accuracy of CFD Codes in the Prediction of Planing Surfaces Hydrodynamic Characteristics." *2nd International Conference on Marine Research and Transportation*. 2007.
- [16] Brizzolara, S., and Y. Young. "Physical and Theoretical Modeling of Surface-Piercing Hydrofoils for a High-Speed Unmanned Surface Vessel." *ASME 2012 31<sup>st</sup> International Conference on Ocean, Offshore and Arctic Engineering*. 2012.
- [17] Celano, Tullio III. *The Prediction of Porpoising Inception for Modern Planing Craft*. Trident Scholor Project Report, Annapolis, MD: U.S. Naval Academy, 1998.
- [18] Clement, Eugene P. *The Planing Characteristics of a 15-Degree Deadrise Surface with Circular-Arc Camber*. Research and Development Report, David Taylor Model Basin, USN, 1966.
- [19] Clement, Eugene P. "A Configuration for a Stepped Planing Boat Having Minimum Drag (Dynaplane Boat)." Second Edition, 2005.
- [20] Clement, Eugene P. *Merit Comparisons of the Series 64 High-Speed Displacement Hull Forms*. Research and Development Report, David Taylor Model Basin, USN, 1965.
- [21] Clement, Eugene P. *The Design of Cambered Planing Surfaces For Small Motorboats*. Research and Development Report, Washington, D.C.: Naval Ship Research and Development Center, 1969.
- [22] Clement, Eugene P., and Donald L. Blount. "Resistance Tests of a Systematic Series of Planing Hull Forms." *SNAME Transactions*. New York, 1963: pp 491-579.
- [23] Clement, Eugene P., and James D. Pope. *Stepless and Stepped Planning Hulls - Graphs for Performance Prediction and Design*. Research and Development Report, David Taylor Model Basin, USN, 1961.
- [24] Clement, Eugene P., and Joseph G. Jr. Koelbel. "Progress During the Past Century Toward the Development of Efficient, Load-Carrying, Stepped Planing Boats." *SNAME Fifth Biennial Power Boat Symposium*. 1993.
- [25] Clement, Eugene P., and Peter M. Kimon. *Comparative Resistance Data for Four Planing Boat Designs*. Research and Development Report, David Taylor Model Basin, USN, 1957.
- [26] Clement, Eugene P., John Hollingsworth, and Robert Scher. "The Dynaplane Planing Motorboat Design." *Clean Technology*, 2008: pp 471-474.
- [27] Cohen, Steven H., and Donald L. Blount. "Research Plan for the Investigation of Dynamic Instability of Small High-Speed Craft." *SNAME Transactions*. 1986: pp 197-214.
- [28] Faltinsen, Odd M. *Hydrodynamics of High-Speed Marine Vehicles*. New York, NY: Cambridge University Press, 2005.
- [29] Gillmer, Thomas C., and Bruce Johnson. *Introduction to Naval Architecture*. Annapolis, MD: United States Naval Institute, 1982.

- [30] Gray, Harry P., Raymond G. Allen, and Robert R. Jones. *Prediction of Three-Dimensional Pressure Distributions on V-Shaped Prismatic Wedges During Impact or Planing*. Research and Development Report, Washington, DC.: Naval Ship Research and Development Center, 1972.
- [31] Kapryan, Walter J., and George M. Jr. Boyd. *Hydrodynamic Pressure Distributions Obtained During A Planing Investigation of Five Related Prismatic Surfaces*. Technical Note 3477, Langley Field, VA: National Advisory Committee for Aeronautics, Langley Aeronautical Laboratory, 1955.
- [32] Kinnas, Spyros A. *Supercavitating 2-D Hydrofoils: Prediction of Performance and Design*. Lecture, Brussels, Belgium: von Karman Institute, RTO AVT Lecture Series, 2001.
- [33] Koelbel, Joseph G. Jr. *Guide to Power Boat Design*. Final Report, Naval Ship Systems Command, Office of Naval Research, 1971.
- [34] Lawler, Clinton T., Mitchell, Gregory R., Suh, Il H. *Combat Craft – Riverine*. Course 2.705 Projects in New Construction and Naval Ship Design, MIT, May 2007.
- [35] Metcalf, Bryson J., Lisa Faul, Elissa Bumiller, and Jonathan Slutsky. *Resistance Tests of a Systematic Series of U.S. Coast Guard Planing Hulls*. Research and Development Report, West Bethesda, MD: Carderock Division, Naval Surface Warfare Center, December 2005.
- [36] Milburn, Darrell E. *Technical Characteristics Verification of the Prototype 47 FT MLB*. Final Report, Groton, CT: U.S. Coast Guard Research and Development Center, 1991.
- [37] Newman, John N. *Marine Hydrodynamics*. Cambridge, MA: The Massachusetts Institute of Technology Press, 1977.
- [38] Ranzenbach, Dr. Robert. "Froude for Thought: Getting Semi-Planing Hull Resistance Right." *The Yacht Report*, n.d.: pp 195-202.
- [39] Savitsky, Daniel. "Hydrodynamic Design of Planing Hulls." *Marine Technology* 1, no. 1 (1964): pp 71-95.
- [40] Savitsky, Daniel, and Michael Morabito. "Surface Wave Contours Associated with the Forebody Wake of Stepped Planing Hulls." New York Metropolitan Section, SNAME Meeting, March 10, 2009.
- [41] Savitsky, Daniel, and P. Ward Brown. "Procedures for Hydrodynamic Evaluation of Planing Hulls in Smooth and Rough Water." *Marine Technology* 13, October, 1976: pp 371-400.
- [42] Schleicher, Dean. *Breaking New Water*. Donald L. Blount Associates, Inc., April, 2003.
- [43] Versteeg, H. K., and W. Malalasekera. *An Introduction to Computational Fluid Dynamics: The Finite Volume Method*. London: Longman Group Ltd, 1995.